Competing Orders in URu2Si2 : from ordered magnetism to spin liquid phases

Carlene Paula Silva de Farias

Université de bordeaux
Laboratoire Ondes et Matière d'Aquitaine

T H È S E

pour obtenir le titre de

Docteur en Sciences

en cotutelle avec

Universidade Federal do Rio Grande do Norte – Brasil

Présentée et soutenue par

Carlene Paula Silva de Farias

Competing Orders in URu_2Si_2: from Ordered Magnetism to Spin Liquid Phases

soutenue le 10 Avril 2017

Jury :

Directeur :	Sébastien Burdin	-	Université de Bordeaux
Codirecteur:	Alvaro Ferraz	-	IIP- IFRN
Président :	Chaterine Pepin	-	CEA- Saclay
Rapporteurs :	Sergio Magalhães	-	UFRGS
	Idranil Paul	-	Université Paris 7 - CNRS
Examinateurs :	Pascoal Pagliuso	-	Unicamp
	Rodrigo Pereira	-	IIP-UFRN
	Tommaso Macri	-	DFTE-UFRN

Acknowledgements.

This thesis is the result of a work developed in these last four years. Many things have happened since then, and I take this opportunity to thank everybody who helped throughout this period.

First of all, I would like to thank my family, my parents and my sisters, who have always encouraged me to pursuit the best with my studies, even if that meant that I have to be away from home most of the time.

I thank my physics colleagues from DFTE, especially my friends from the César Lattes office, Leonardo, Jânio, Madson, Francis, Gislana and Mateus. I also thank the LOMA staff in Bordeaux, where I spent a year and a half developing part of this work. I also thank the staff of the International Institute of Physics, who offered me very good support and helped me to clarify all bureaucratic issues related with my *cotutelle* doctorate

I also thank friends I made outside physics, who gave me support during these years I have been living in Natal, especially Gloria, Isabella, Rodolfo, Ryanne and Rysa. I Thank the "Brazuca" friends I made in France, Jeane and Carolina, who were fundamental in those moments I felt homesick, and arouse my interest in sociology.

Thanks also to my supervisor, Prof. Álvaro Ferraz, who has been with me since my M.Sc. degree and always inspired me with his passion for Physics, as well as about the subjects that involve Politics. To my co-advisor prof. Sébastien Burdin, who gave me great support in my period in Bordeaux and taught me to work with discipline and pushed me to work more independently in my research.

Finally, I thank the financial support of CAPES for the first two years of my Ph.D. and also for my internship in Bordeaux as part of the CAPES/Cofecub program and, finally, I thank the CNPq for the financial support in my last year.

Competing Orders in URu_2Si_2: from Ordered Magnetism to Spin Liquid Phases.

Abstract: The main objective of this thesis is to investigate the competing ordered phases in the metallic heavy fermion compound URu_2Si_2, which displays a body-centered tetragonal lattice. We first provide a study case of the competition between antiferromagnetic (AF) and spin liquid phases. The antiferromagnetic state is study with spin-wave theory. Whereas the spin liquid analysis has been carried out in an algebraic spin liquid representation. In the second part, we describe an effective theory for Raman scattering experiments at these particular phases. We provide insight about the hidden order phase displayed by the heavy fermion compound URu_2Si_2.

Keywords: Antiferromagnetism, Spin Liquid, Hidden Order, Raman scattering, BCT lattice, Point Group Symmetry.

Ordres en compétition dans URu_2Si_2: de l'ordre magnétique aux phases de liquide de spin.

Résumé: L'objectif central de cette thèse est d'étudier des phases ordonnées en compétition dans des matériaux magnétiques présentant une structure cristalline tétragonale centrée. Ce travail est divisé en deux parties principales. Dans la première, nous présentons les résultats de notre étude de la compétition entre des états ordonnés antiferromagnétiques et des phases liquides de spin. Nous montrons comment ces dernières peuvent être stabilisées par la frustration géométrique et par une généralisation de la symétrie de spin au groupe SU(n). Les états antiferromagnétiques sont décrits par une théorie d'onde de spin et l'analyse de liquide de spin est effectuée par une représentation fermionique des opérateurs de spin. Dans la deuxième partie, nous décrivons une théorie effective pour dércrire des expériences de diffusion Raman. Nous fournissons un aperçu de la phase d'ordre caché affichée par le composé de fermions lourds URu_2Si_2.

Mots clés: Antiferromagnétisme, Liquide de Spin, Ordre Caché, Diffusion Raman, Réseau BCT , Groupe de Symétrie ponctuel.

List of Figures

List of Abbreviations

AF	Antiferromagnetic.
BCT	Body-centered Tetragonal.
HO	Hidden Order.
HP	Holstein–Primakoff.
SL	Spin Liquids.
ST	Simple Tetragonal.
SW	Spin Wave.

Contents

Prologue.

In this thesis, we analyze the competing magnetic phases of systems with a three dimensional lattice structure. Our main object are the body-centered tetragonal (BCT) lattices, whose structure is shown in Fig(1(b)). This is one of the 14 three-dimensional Bravais lattices types [Ashcroft 1976] and this crystalline structure is realized in several strongly correlated electrons materials with unusual magnetic and transport properties. It belongs to the point group D_{4h} (space group No. 139 $I4/mmm$). Among these transformations we can mention reflection, inversion and rotations of $2\pi/n$ around a specific axis, in which n can be an integer. Different examples of materials, including the heavy fermion systems [Stewart 1984] and rare earth atoms, display the BCT lattice structure and have been intensively studied for the last decades.

In URu_2Si_2, a still mysterious hidden order (HO) phase was discovered in 1986, that appears below the critical temperature $T_0 \approx 17$ K close to a pressure-induced antiferromagnetic (AF) transition [Palstra 1985, Maple 1986, Mydosh 2011]. The compounds $YbRh_2Si_2$ and $CeRu_2Si_2$ display non-Fermi liquid properties that are observed in the vicinity of the antiferromagnetic quantum phase transitions and are still poorly understood [Custers 2003, Friedemann 2009]. The $CeCu_2Si_2$ was the first heavy fermion material in

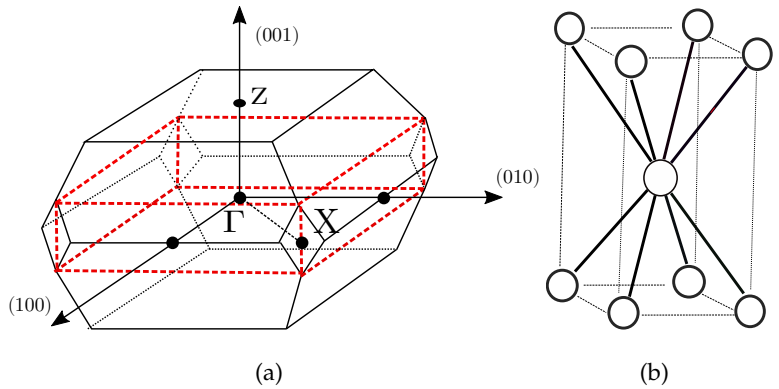

Figure 1: **(a)** Corresponding structure in reciprocal space, Brillouin zone, of the BCT, and the main points and directions. **(b)** The bct lattice structure.

which unconventional superconductivity was discovered in 1979 close to an AF transition [Steglich 1979]. The $CePd_2Si_2$ exhibits unconventional superconductivity which is related to an AF transition [Mathur 1998].

We will particularly focus on the problem of the hidden order phase in URu_2Si_2. We begin by reviewing the current state of research of the hidden order in URu_2Si_2.

The problem of the HO phase in the heavy fermion compound URu_2Si_2.

After thirty years of intense investigations, the origin of the mysterious hidden order (HO) phase of URu_2Si_2 is still unrevealed despite strong preliminary experimental indications [Palstra 1985, Maple 1986] confirming the phase transition from a metallic state to a newly ordered phase. The properties of this particular system comes from the Uranium element, which is from the actinide family in the periodic table. The URu_2Si_2 can display puzzling features in which the unusual properties derive directly from the U open $5f$ shell.

The systems is also known as a moderate heavy fermion with a Sommerfeld coefficient of ~ 180 m J/mol K^2. The mobile electrons, at low temperatures, behave as if their masses were a hundred times heavier than the mass of an electron in silicon or in a simple metal. Such systems exhibit a great variety of interesting phenomena like anomalies in electrical and thermal conductivities, quantum phase transitions between magnetically ordered state, superconductivity and, finally, the emergence and dissociation of local magnetic moments.

URu_2Si_2, represented in Fig(2), has a body-centered-tetragonal (BCT) crystal structure at high temperatures, with lattice parameters $a = 4.121$ $\mathring{A}$ and $c = 9.681$ $\mathring{A}$. Its first Brillouin zone is shown in figure (1(a)). The transition at $T_0 \approx 17.5$ K is a second order phase transition to a new phase well characterized by bulk thermodynamic and transport measurements [Broholm 1987, Maple 1986, Palstra 1985]. The order parameter and the elementary excitations of the newly ordered phase are still unknown, i.e., they cannot be determined directly from experiments. This fascinating new phase is at the center of considerable discussion concerning the origin of the mechanism that is governing it.

The phase diagram (Fig.3) obtained for the URu_2Si_2 is very interesting [Hassinger 2008, Villaume 2008]. In ambient pressure, the system undergoes by a second-order phase transition at $T_0 = 17.5$ K to a new hidden order phase with a small magnetic moment $\mu \approx 0.02$ μB. At very low temperature, a superconducting phase is found below $T \approx 1.5$ K. In the PM phase, the lattice structure is BCT, which belongs to the space group No 139 ($I4/mmm$).

When entering on the HO phase, the structure becomes simple tetragonal (ST) , which belongs to the point group symmetry No 136 ($P4_2/mnm$)[Harima 2010]. The possibility that HO displays a lower point group symmetry, with a subgroup of No 136 will be discussed in chapter 3 of this thesis.

Magnetic measurements reported an Ising like magnetic response along the c axis [Palstra 1985]. Transport and thermodynamic measurements suggest a considerable Fermi surface reconstruction occurring at the HO transition [Palstra 1985, Maple 1986]. The measured specific heat and the jump in the resistivity at the transition are consistent with the opening of an energy gap over a substantial part of the Fermi surface.

Over the years, different proposals have been put forward to explain the hidden order phase, which can be roughly classified as itinerant and localized. To mention some of them: There have been proposals in terms of the emergence of local currents [Haule 2009], multipolar order [Harima 2010, Kusunose 2011], spin liquids [Pépin 2011, Thomas 2013], unconventional density waves [Riseborough 2012], hastatic and nematic order [Chandra 2013, Okazaki 2011]. Moreover, it is well known that a second-order phase transition is always accompanied by some symmetry breaking, such as the time-reversal case in antiferromagnets or U(1) gauge symmetry breaking in superconductors. The order parameter is introduced to describe the ordered state with reduced symmetries. The manifestation of the HO should not be different. In this respect, however, if the OP is unknown the question of what symmetry is effectively broken remains uncertain.

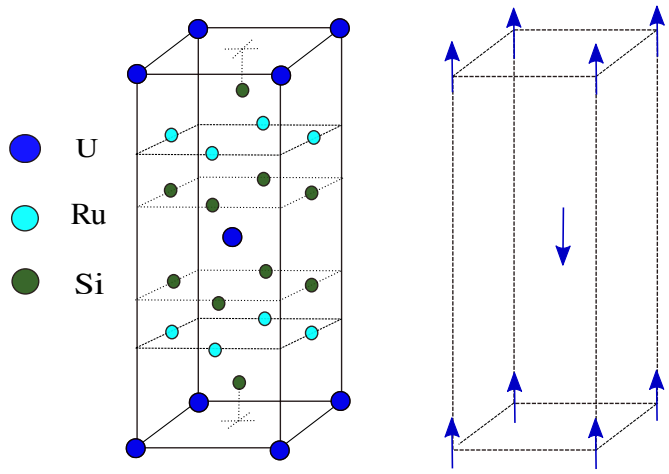

Figure 2: (Left) Crystal structure of body-centered tetragonal lattice for URu_2Si_2. The corresponding space group is the $I4/mmm$. (Middle) The antiferromagnetic pattern for the spin alignment of U moments. (Right) Corresponding structure in reciprocal space, Brillouin zone, of the BCT, with its the main symmetry points and directions.

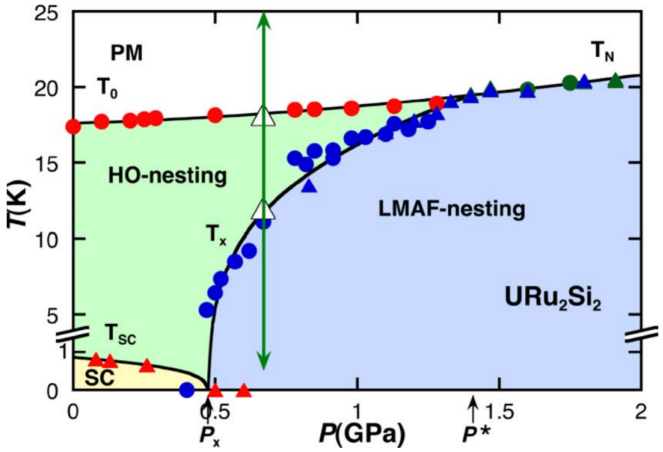

Figure 3: Temperature versus pressure phase diagram for URu_2Si_2 from [Villaume 2008]. At zero pressure a phase transition occurs from the paramagnetic (PM) phase to the so called hidden-order (HO), at T_0 ≈17.5 K. The phase diagram exhibits also data from resistivity (circles) and ac calorimetric (triangles measurements). At low pressure, the HO phase is dominant and there is a first order phase transition to a AF phase when a pressure ≈ 0.5 GPa is applied.

There is a consensus about the change in the lattice periodic structure when passing from the paramagnetic (PM) phase - in which the system has a body centered tetragonal (BCT) lattice structure - to the HO regime - a simple tetragonal structure (ST). This is manifested by the folding in the Brillouin zone along the c axis of the BCT lattice [Buhot 2014, Boariu 2013, Hassinger 2010], see Fig.(1). Hence, the suggestion arises that the HO transition breaks BCT translational symmetry. It is also argued that the change in lattice structure can cause an instability on the Fermi surface. As a consequence of that, there is a large Fermi surface gap in some regions in k space [Maple 1986, Elgazzar 2009, Boariu 2013, Tonegawa 2012].

A complementary approach was introduced by Harima-Miyake-Flouquet [Harima 2010]. They present a point group analysis of the URu_2Si_2 crystal structure. Thereby it is possible to associate the HO transition as a change of crystal point group symmetry. They claim that a second-order structural transition occurs from the "mother" space group $I4/mmm$ to $P4_2/mnm$ based on a systematic analysis of various scattering data [Saitoh 2005].

Some of these questions do call for further investigation, new theoretical proposals and also modern experimental technique investigations. It is not our intention here to solve all these questions. However, we try to provide some explanations using a simpler case. The

next sections are devoted to present briefly the methodology employed in this work and to give a general overview before engaging ourselves in a detailed analysis.

Overview.

The previous section serves as an introduction to the problem of the exciting competing ordered phases in the Heavy fermion compound URu_2Si_2. We want to establish connections between our results and the question of HO phase.

In the fist part of this work, we provide a case study of the competition between antiferromagnetic (AF) and spin liquid (SL) phases. The AF is represented in a spin-wave theory, while the spin liquid analysis is carried out in an algebraic spin liquid representation.

In **Chapter 1**, we start with an introduction on the phenomenon of Frustration in antiferromagnets. We give an overview about frustrated systems, with frustration being a result of competing interactions that are not fully predominating against each other or with symmetries which lack a clear geometrical definition. In particular, the BCT structures possess those two characteristics. We introduce the Heisenberg Hamiltonian to deal with localized spins in an antiferromagnetic system and we also introduce the concept of spin wave, to motivate our analysis of the collective excitations that are featured in these systems. We describe two experimental techniques that can probe this type of collective excitations.

In **Chapter 2**, we consider a model with localized spins. We show how frustration in the BCT lattice can enhance the critical value of S. This opens new possibilities for the realization of unconventional electronic quantum ordering in a 3-dimensional system. To see that clearly, we use a fermionic SU(n) symmetric representation of the Heisenberg model. We identify three spin liquid phases that can be stabilized if n is bigger than a critical value. These spin liquid states are then tested as possible candidates for the HO in URu_2Si_2.

For the second part, we use our model to develop an effective theory to describe Raman scattering experiments performed in materials with these particular structures.

In **Chapter 3**, we develop an effective theory to incorporate the varieties of states present in chapter 3. Our starting point is a non interacting model that is able to generate the different phases under investigation by systematic variation of a small number of parameters. The aim is to relate our effective theory directly to the Raman scattering experiments performed in the hidden-order phase of URu_2Si_2. To do that, we present numerical results and we make comparisons with Raman scattering data for URu_2Si_2.

Chapter 4. We present an overview of the whole work, draw conclusions about the

relevance of this work and point out futures perspectives which might be object of future work.

Chapter 1

Introduction.

1.1 Frustrated systems.

The phenomenon of frustration is present in spin systems when there is competition between interactions of magnetic degrees of freedom or incompatibilities with the lattice structure [Lacroix 2011, Balents 2010, Gingras 2009, Starykh 2015, Ramirez 1994]. In particular, frustrated quantum antiferromagnets have been at the center of intense experimental and theoretical investigations for many years. Frustration leads the way to a highly degenerate ground state and opens a window for novel states of matter. Perhaps the easiest way to visualize this is to consider a triangular lattice [Fazekas 1974]. Here frustration results from the impossibility of consistently establishing an AF ordering in the underlying lattice. We can construct an array of spins placing each one of them at each corner of the triangle lattice. This lattice exhibits frustration because if an up- and down-spin occupy two corners of the triangle, the spin on the third corner will necessarily break the AF arrangement with one of its two neighbors. In spite of the presence of frustration, neighboring spins in a triangular lattice still manage to order at a 120^o angle and exhibiting a AF Néel order. Other examples of frustrated lattice are the 2D Kagomé [Han 2012, Helton 2007] and the 3D pyrochlore [Bramwell 2001] or the body-centered tetragonal (BCT) [Rastelli 1990]. As argued before, the last example will be the main object of study in this work.

Fluctuations, thermal or quantum, play a major role. They can order the system by selecting one specific ordered state out of the ground-state manifold of degenerate states [Rastelli 1987], but they can also destroy any kind of magnetic long-range order [Chandra 1988]. This opens the way to new types of ground states such as the spin nematic [Andreev 1984], in which the order parameter is not the local spin but a more complicated object; valence-bond crystals [Anderson 1973, Iqbal 2012] that are completely

non-magnetic states with a broken translational symmetry; spin ice or spin liquid phases [Anderson 1973, Anderson 1987], in which both the rotational SU(2) symmetry in spin space and the translation symmetry in real space are preserved .

1.1.1 The Heisenberg Hamiltonian.

To understand the features of frustration it is usual to consider a simple Hamiltonian that accounts for interactions between nearest neighbor spins placed at fixed sites in some specific lattice. The Heisenberg Hamiltonian is [Heisenberg 1928]

$$H = J \sum_{\langle i,j \rangle} \mathbf{S}_i \cdot \mathbf{S}_j. \tag{1.1}$$

The exchange coupling J is defined as the interaction between the nearest neighbors and the $\mathbf{S}$ is the spin operators, labeled by the indices i and j indicating their positions in the lattice. The sum is taken over the nearest-neighbor pairs. Each spin operator $\mathbf{S}$ satisfy the usual commutation relations $[S_i^x, S_i^y] = i\hbar S_i^z$ of the SU(2) algebra. The spin operators all have spin S, i.e. the operators $\mathbf{S}_i^2$ have eigenvalue $S(S+1)$ where S is either an integer or half-integer. Each spin has a mean polarization oriented along some easy direction.

The ordering displayed by the system depends on the sign of the exchange coupling J, dimensionality and lattice structure. If $J < 0$ the ground state of the systems assumes a ferromagnetic configuration, i.e. all the spins point out along the same direction, choosing a specific orientation and breaking spontaneously the rotational symmetry of the Heisenberg Hamiltonian. If $J > 0$, the exchange coupling favors the antiparallel alignment of the spins and the ground state now favors the system to an antiferromagnetic (AF) configuration. In both cases there is the breaking of the rotational symmetry of the Heisenberg Hamiltonian. [Fazekas 1999]. In the case of antiferromagnets, there is the emergency of bipartite lattices, in which the next-nearest neighbors of one sub-lattice A belong to the other sub-lattice B, allowing the system to reach a configuration of a Néel state in the classical limit. The presence of frustration also results in degenerate manifold of ground states rather than a single stable ground-state configuration at the classical level.

When the quantum fluctuation are present, they interfere with the average direction in which the spin are aligned in the ground state. It is common to use the theory of spin wave (SW) to incorporate these fluctuations. Before entering in discussions about fluctuations, let us see the application of Heisenberg model to one simple and widely studied example. The Heisenberg model on the square lattice in the classical regime.

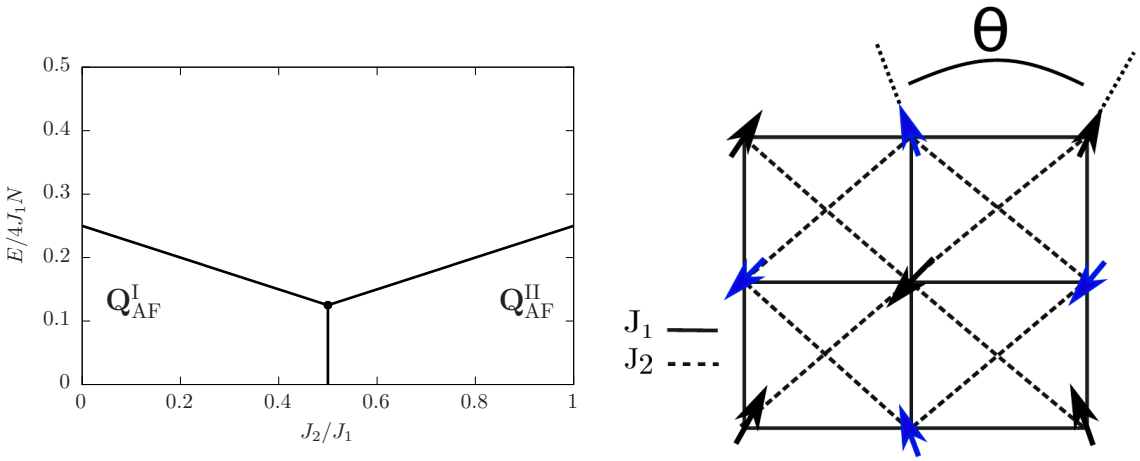

(a) (b)

Figure 1.1: **(a)** Ground-state energy per site N, for J_1-J_2 Heisenberg model. The two ground states regions are indicated with respect $\mathbf{Q}^{\mathrm{I}}_{\mathrm{AF}} = \{\pi, \pi\}$ and $\mathbf{Q}^{\mathrm{II}}_{\mathrm{AF}} = \{\pi, 0\}$. **(b)** The J_1-J_2 Heisenberg model. Each vertex indicates a spin and the parameter θ is indicated.

1.1.2 The Heisenberg model in a square lattice.

For a square lattice, the Heisenberg Hamiltonian is solved with a mean-field approach [Manousakis 1991]. This approach consists of classical spin in a lattice with nearest-neighbor coupling J_1 and next-nearest-neighbor coupling J_2, Fig.(1.1). The Fourier transform of the coupling constants is the classical spin-wave dispersion and is given by

$$J(\mathbf{Q}_{\mathrm{AF}}) = 2J_1(\cos(q_x a) + \cos(q_y a)) + 4J_2 \cos(q_x a)\cos(q_y a). \tag{1.2}$$

The Néel phase for small J_2 is characterized by an anti-parallel alignment of nearest neighbor spins, with a corresponding ordering wave vector $\mathbf{Q}_{\mathrm{AF}} = (\pi, \pi)$. The second kind of AF state for large J_2 is twofold degenerated and corresponds to the ordering wave vectors $\mathbf{Q}_{\mathrm{AF}} = (\pi, 0)$ and $\mathbf{Q}_{\mathrm{AF}} = (0, \pi)$.

These two states are characterized by a parallel spin orientation of nearest neighbors in vertical (horizontal) direction and an anti-parallel spin orientation of nearest neighbors in horizontal (vertical) direction and exhibit therefore Néel order. These two ordered phases are separated by a first-order transition. This remains true regardless of the relative angle θ between the spins of each sublattice, so that the ground-state manifold consists of all states with Néel-ordered sub-lattices. The ground state is thus infinitely degenerate, and the degeneracy is controlled by a continuous parameter, the angle θ between the sub-lattices.

In the linear spin-wave approach, which goes beyond the classical theory, quantum fluctuations destroy the magnetic order in the intermediate region of $0.4J_1 \lesssim J_2 \lesssim 0.6J_1$,

hence leading to a magnetically disordered state [Chandra 1988, Ren 2014]. However, the nature of this disordered phase is still elusive and several proposals have been raised, including spin-liquid states [Anderson 1973]. Two quantum phase transitions in the model are already known: the second-order transition from the Néel state to the spin liquid state at $(J_2/J_1) \approx 0.38$, and the first-order transition from the spin liquid state to the collinear state at $(J_2/J_1) \approx 0.60$ [de Oliveira 1991, Chandra 1988].

The next section is devoted to describe how quantum fluctuation can be incorporate to the problem by describing the theory of spin waves and also what these fluctuations can do with the degeneracy of the system.

1.2 Spin-wave theory.

The concept of spin-waves was first introduced by Bloch in 1930 [Bloch 1930]. These theories have enjoyed great popularity in the study of a wide variety of quantum magnets. In the beginning it was directed to the study of systems with simple ferromagnetic Hamiltonians [Oguchi 1960] and after that it has been applied to antiferromagnetic models [Anderson 1952, Kubo 1952], including frustrated ones [Xu 1991, Oguchi 1990]. In recent years it has reached such a state of refinement that it can deal with disordered systems [Mucciolo 2004, Castro 2006] and quasicrystals [Wessel 2005]. Its application is straightforward and its physical interpretation is clear, such that it is now a widely used tool since the last decades.

1.2.1 The Holstein-Primakoff approach.

The basic idea of semiclassical spin-wave theories is that quantum fluctuations only slightly perturb the long-range ordered state of the classical limit of the model. Spin waves are the low energy excitations in a standard magnetic system. This approach treats the mean value of the spin operator $\mathbf{S}$ as being of big magnitude (semi-classical limit), which characterizes the spins as rotating around their positions of equilibrium. The collective behavior is equivalent to rotations of the classical magnetic moment. In the large S limit and at low excitations, it is natural to describe the ordered state in terms of small fluctuations of these spins around their expected values.

The Heisenberg Hamiltonian has a global spin rotation symmetry. When the ground state of the Hamiltonian is magnetically ordered (either ferromagnetically for $J < 0$ or antiferromagnetically for $J > 0$), so that $\langle \mathbf{S}_i \rangle \neq 0$, this ground state is not invariant under a global spin rotation. We say that the ground state"spontaneously" breaks the

global spin rotation symmetry of the Hamiltonian. In this situation, we expect that gapless modes of the spectrum of energy associated to the spontaneous symmetry breaking of global spin rotation emerge. This is a consequence of the Goldstone's theorem [Goldstone 1962, Nambu 1960]. The theorem states that when the ground state breaks a continuous symmetry of the Hamiltonian, gapless bosonic excitations will exist in the energy spectrum. Bring it to our context, a quantized spin wave is called a "magnon" and they are the Goldstone modes of magnetic systems.

The effect of quantum fluctuations are conveniently represented in terms of spin raising and lowering operators, with $S^{\pm} = S_x \pm iS_y$. The most general quantum-mechanical way to set up spin waves follows the Holstein-Primakoff (HP) [Holstein 1940] transformations. Since we are in the limit of low excitations, this transformations replace the $S^{\pm}$ for bosonic creation and annihilation operators $a^{\dagger}$ and a, respectively [Manousakis 1991]. This reads,

$$S_i^+ = (2S - a_i^\dagger a_i)^{1/2} a_i \quad S_i^- = a_i^\dagger (2S - a_i^\dagger a_i)^{1/2} \quad S_i^z = (S - a_i^\dagger a_i). \tag{1.3}$$

The function $\phi(\hat{n}_i) = (2S - \hat{n}_i)^{1/2}$, where $\hat{n}_i = a_i^\dagger a_i$, is expanded as

$$\phi(\hat{n}_i) =: \sqrt{2S}\left(1 - \frac{\hat{n}_i}{4S} - \frac{\hat{n}_i^2}{32S^2} - ...\right) \tag{1.4}$$

Where $\hat{n}_i$ is the number operator.

The leading term of this expansion is proportional to $1/S$ and if we truncate the series at this stage we define the linear spin wave theory, which means that all corrections to the Hamiltonian and magnetization will be proportional to S. Terms of high order in this expansion take into account the interaction between magnons[1]. The purpose here is to calculate physical properties like the staggered sub-lattice magnetization and see how quantum fluctuations are able to modify significantly the classical spectrum of elementary excitations or if they could destabilize such ordered phases.

There are some well established results for two-dimensional systems. For example, in the square lattice [Oguchi 1990] (This model was first solved by Anderson in a semi-classical approximation to determine the ground state energy and the wave function [Anderson 1952]) and in the triangular lattice [Chubukov 1994]. Particularly, for the square lattice, the model considers the Heisenberg Hamiltonian with nearest neighbor coupling

[1] In linear spin wave approximation the Hamiltonian describes a system of uncoupled harmonic oscillators. If we take into account higher order terms, we are introducing interaction between the harmonic oscillators. However, the effect of these interactions can be suppressed at least by a factor $1/S$ compared to the $\mathcal{O}(S)$ noninteracting term and one can expect that their effects are small for a large S. Therefore, they can either be neglected to a first approximation or be treated as weak perturbations on the noninteracting theory.

(J_1) and next-nearest neighbor (J_2). It was pointed out that quantum fluctuation can destabilize the classical ordered states even at large S. When $p = J_2/J_1$ tends to $1/2$, leading quantum fluctuation become very soft, driving the system away from the classical fixed point. The instability can generate a spin liquid, at the ground state [Chandra 1988].

1.2.2 Order by disorder mechanism.

The phenomenon of frustration gives us a plethora of ground states indicating that the system is plausibly disordered. However, these degenerate ground states may be situated in very different regimes: they experience different thermal and quantum fluctuations. The fluctuations have a special role in these systems because they may partially lift the degeneracy and so make systems more ordered [Rastelli 1987, Buhrandt 2014]. The system, instead of having a disorder degeneracy, is finally ordered due to the new minimum energy selection at the classical or quantum level. This is recognized as "order by disorder mechanism". It was first proposed by Villain *et al.* [Villain 1980] for studying classical Ising systems, while the order by quantum disorder scenario was first considered by Shender [Shender 1982]. We take into account only those quantum fluctuation and leaving the questions of thermal apart, by referring only to the work of Villain. [Villain 1980].

Let us see how this concept of order by disorder works in practice, with quantum fluctuations. By looking back to the quantum Heisenberg model itself, the linear spin waves approximation only considers in the expansion the linear S corrections. In terms of the Holstein-Primakoff transformations, we end up with a Hamiltonian

$$H = E_0 + \sum_{\mathbf{k}} \left[A_{\mathbf{k}}\, a^\dagger_{\mathbf{k}} a_{\mathbf{k}} + \frac{B_{\mathbf{k}}}{2}(a^\dagger_{\mathbf{k}} a^\dagger_{-\mathbf{k}} + a_{\mathbf{k}} a_{-\mathbf{k}}) \right] \tag{1.5}$$

With E_0 being the zero point energy which is proportional to S^2. The $A_{\mathbf{k}}$ and $B_{\mathbf{k}}$ are proportional to S and they also depend on the exchange couplings J. Since the Hamiltonian acquires this non-trivial non-diagonal form, we perform a canonical transformation to new operators $\alpha_{\mathbf{k}}$. Such procedure is also known as a Bogoliubov transformation [Bogoljubov 1958, Ohara 1989], like

$$\alpha_{\mathbf{k}} = u_{\mathbf{k}} a_{\mathbf{k}} + v_{\mathbf{k}} a^\dagger_{-\mathbf{k}}. \tag{1.6}$$

With that, the Hamiltonian is written in the diagonal form

$$H = E_0 + \sum_{\mathbf{k}} \hbar\omega_{\mathbf{k}} \left[\alpha^\dagger_{\mathbf{k}} \alpha_{\mathbf{k}} + \frac{1}{2} \right] \tag{1.7}$$

The elementary excitations above the ground state are spin waves of one flavor and they are created by the action of $\alpha^\dagger$ on the ground state. The energy of these states is given by

$\omega_{\mathbf{k}} = \sqrt{A_{\mathbf{k}}^2 - B_{\mathbf{k}}^2}$. The condition for the functions $u_{\mathbf{k}}$ and $v_{\mathbf{k}}$ are

$$u_{\mathbf{k}} = \cosh\theta_{\mathbf{k}} \qquad v_{\mathbf{k}} = -\sinh\theta_{\mathbf{k}}, \tag{1.8}$$

in which $\theta_{\mathbf{k}} = \arctan(B_{\mathbf{k}}/A_{\mathbf{k}})$.

The energy of the quantum state is obtained by taking these quantum fluctuations. Therefore

$$E = E_0 + \frac{1}{2}\sum_{\mathbf{k}} \hbar\omega_{\mathbf{k}} \tag{1.9}$$

It is worth to say that the system will choose some states inside the manifold that minimize this expression. The mechanism of order by disorder was investigated in two-dimensional square lattices [Danu 2016], while, in the three-dimensional versions, we can mention the face-centered cubic (fcc) [Sinkovicz 2016] and BCT lattices [Rastelli 1989, Rastelli 1987].

In the next section we will see that in the Heisenberg model, when frustration together with a low spin quantum number is present, the situation where long-range magnetic order and breaking of SU(2) symmetry is not the most common one. Down to zero temperature they tend to form states with spins paired into rotationally invariant singlets or "valence bonds". They constitute an alternative to the long range magnetic order.

1.3 Alternatives to long-range magnetic ordering in Heisenberg models.

Up to now we have seen that the degeneracy in the ground state together with fluctuations does not favor magnetic ordering. These two main features cause the presence of additional zero frequency modes at the spin wave dispersion rather than those that can be expected on general grounds with the ordering wave vector $\mathbf{Q}_{\mathrm{AF}}$. In the limit of small k these additional zero modes may lead to divergences and to corrections of the local magnetization Δm [Chandra 1988, Chandra 1990].

This correction of the local magnetization can be calculated from the sub-lattice magnetization through the relation 1.3 at the leading order in large S expansion, i.e.

$$\langle S_i^z \rangle = S - \langle a_i^\dagger a_i \rangle. \tag{1.10}$$

This implies that

$$\Delta m = \langle a_i^\dagger a_i \rangle = S - \langle S_i^z \rangle = \frac{1}{N}\sum_{\mathbf{k}} \langle a_{\mathbf{k}}^\dagger a_{\mathbf{k}} \rangle, \tag{1.11}$$

where N is the number of lattice sites. If long-range magnetic order is maintained, high-order terms will have to open a gap at these accidental zero modes to restore the finite value of the correction. The correction has to be smaller than the mean value of the spin S, which is not often the case. This is an indication that we must look for alternatives to magnetic long-range order. We divided these new states into two groups: the ones capable of breaking the SU(2) symmetry and the ones that preserve the SU(2) symmetry. The spin-liquids are in the last group.

The concept of SL was first proposed by Anderson [Anderson 1973] in order to describe an Antiferromagnet system with spin-1/2 in triangular lattice with odd total spin value per unit cell. For instance a product of spin singlet dimers has to break the lattice symmetry. They are allowed to go through quantum mechanical fluctuations. Therefore the ground state is a superposition of all possible singlet dimers describing a Resonating Valence Bond (acronym RVB) state. This suggestion was for spins placed in a triangular lattice having in mind the physics behind the high-temperature superconductors [Anderson 1987].

The SL phase can be interpreted as a fluid-like state of matter in which the constituents spins are highly correlated though the fluctuations are very strong down to temperatures near the absolute zero [Balents 2010]. In theory, it represents a new state of matter. Unlike conventional magnetic states, the fluctuations give rise to the emergent collective behavior which could be mediated by gauge fields or fractional particles excitations. Low dimensionality might be as well one of the foremost ingredients for the formations of SL. Unlike the ferromagnetic state with parallel spins or the antiferromagnetic Néel state with antiparallel spins, a quantum SL never enters into a long range ordered phase with a static arrangement of spins. The presence of singlet dimers necessarily breaks the spatial translation symmetry. For RVB states the ground state is a superposition of all possible singlet dimers. It is a non magnetic state although spin are highly correlated with one another and they do not break the SU(2) symmetry.

Although, there has been much effort in verifying the existence of RVB states, they are difficult to be realized. Numerical studies using quantum Monte Carlo simulations [Foulkes 2001, Santos 2003, Troyer 2005] cannot be performed for frustrated magnets because they cannot handle the so called minus sign problem associated with the anti-commutation of the fermions, which makes the analysis intractable up to this date. Theoretically, the quantum dimer models [Moessner 2011] have been demonstrated the possibility of realizing an RVB state. It is not our intention here to stress on all aspects of spin liquids. However we would also like to mention a different kind of spin liquids, known as algebraic spin liquids.

1.3.1 Algebraic spin liquids

Algebraic spin liquids have this name because of the algebraically decay of their spin-spin correlations functions. They comprehend half-integer spin chains, in contrast to integer spin chains, in which the correlation decay exponentially. They can be extended to 2D frustrated systems, where we can implement a fermionic representation of spin-1/2 operators, sometimes known as Abrikosov fermions [Baskaran 1988, Affleck 1988b, Dagotto 1988]. Basically we replace the spin variable by

$$\mathbf{S}_i = \frac{1}{2}\sum_{\alpha,\alpha'} c^{\dagger}_{i,\alpha}\boldsymbol{\sigma} c_{i,\alpha'} \tag{1.12}$$

where the $c^{\dagger}_{i,\alpha}$ and $c_{i,\alpha}$ are fermionic creation and annihilation operators, respectively, satisfying the local single-particle occupation constraint $\sum_{\alpha} c^{\dagger}_{i,\alpha}c_{i,\alpha} = 1$, and $\boldsymbol{\sigma} \equiv (\sigma_x, \sigma_y, \sigma_z)$ denotes the Pauli matrices.

In most cases the Heisenberg Hamiltonian is non quadratic and a simple and approximate mean-field decoupling is required for the four-fermion operator [Wen 1996, Wen 2002]. By introducing a bond operator $\chi_{ij} = \sum_{\alpha} c^{\dagger}_{i,\alpha}c_{j,\alpha}$ the Hamiltonian can be decoupled by defining the order parameter $\chi^0_{ij} = \langle\chi_{ij}\rangle$. Thus, the solutions are obtained by the self-consistent equations. We know that the self-consistency of equation leads to many possibilities of ground-states, but we would like to stress two of them. The first solution for $\chi^0_{ij} = \chi^0$ leads to a set of bonds that covers the full lattice resulting in the dimerized state, while $\chi^0_{ij} = 0$ to other bonds, see Fig.(1.2 (a)). The second is $\chi^0_{ij} = \chi^0 e^{i\theta_{ij}}$ with θ chosen such that it provides a π-flux phase per plaquete [Affleck 1988a, Marston 1989], see Fig.(1.2 (b)). The order parameter χ_{ij} is invariant under the gauge transformation $c^{\dagger}_{i,\sigma} \rightarrow e^{i\theta}c^{\dagger}_{i,\sigma}$, where θ can take any value. This characterizes U(1) gauge symmetry in the problem, and this type of spin liquid is sometimes referred to as a U(1) spin liquid.

1.3.2 Chiral and Modulated spin liquids: two examples of spatially ordered spin liquids.

Recently, another kind of mean-field approximation has been proposed for a different spin liquid state, known as modulated spin liquid (MSL) [Pépin 2011], where the order parameter is defined as $\chi^0_{ij} = \chi^0 \pm \Delta$, with Δ being real. The real spatial modulations break translational symmetry where the value of the bond acquires an oscillating sign from site to site see Fig.(1.2 (c)). The phase on the bond is not oriented and consequently there is no flux generated there.

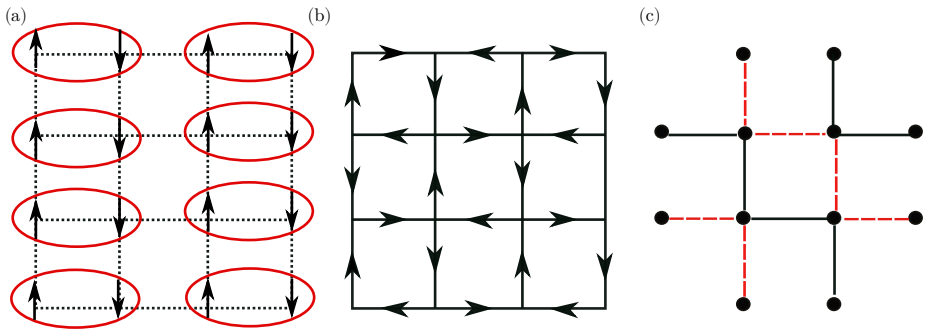

Figure 1.2: **(a)-(b)** The dimerized state and the Affleck-Marston π-flux phase on square lattice with θ is equal to $\pi/4$ [Affleck 1988a]. **(c)** The modulated spin liquid [Pépin 2011]. The sign plus or minus makes the distinction between solid or dashed bonds.

Another different alternative to the long range magnetic order in Heisenberg models is the case in which besides the SU(2) symmetry breaking there is also time-reversal (T) and parity symmetry (P) breaking. So far, the models that we have considered preserve the time-reversal symmetry. Another family of quantum spin liquids was suggested whose states might be stabilized by the presence of frustration and the breaking of time-reversal and of parity symmetries. They are known as chiral spin liquids [Wen 1989, Khveshchenko 1994]. A possible order parameter is the spin chirality $\mathbf{S}_1 \cdot (\mathbf{S}_2 \times \mathbf{S}_3)$, defined in a triad of spins placed at the site 1, 2 and 3. In the context of mean field approximation, the state is described by an ansatz χ_{ij}, where χ_{ij} is complex and generate a flux that is neither equal to 0 nor to π [Wen 2004].

The best evidences so far in favor of such ground states have been obtained for extensions of the Heisenberg model on the Kagome lattice [Bauer 2014, He 2015]. By introducing term of the form $\mathbf{S}_i \cdot (\mathbf{S}_j \times \mathbf{S}_k)$ on each plaquete which explicitly breaks the T and P symmetries.

1.4 Probing Frustrated Magnets.

In this section, we are going to discuss two main experimental techniques that are largely used to investigate magnetic systems. The first subsection is dedicated to present the basics concepts behind neutron scattering technique, while the second part is devoted to optical spectroscopy, more precisely, Raman electronic scattering. These are two very useful experimental tools used to probe the nature of of excitations of disordered and highly degenerate states that occur in frustrated magnets.

1.4.1 Inelastic Neutron Scattering.

Inelastic neutron scattering is used to study the spin-spin correlations in magnetic frustrated systems. It provides direct information of the existing magnetic order as well as the existing magnetic interactions [Hutchings 1972]. Taking a paramagnetic system in comparison with a system where the spins are ordered, like ferromagnetic or antiferromagnetic systems, the response given by neutron scattering is undoubtedly different for these two cases. For paramagnetic systems the spin-spin correlations decrease with the distance which leads to a continuous or diffuse patterns. While for spin ordered systems the correlations have one component with periodic symmetry that gives rise to discrete scattering in the form of Bragg peaks [Bramwell 2011]. Therefore, neutron scattering reflects the different symmetries underlying the physical system.

In an inelastic neutron experiment, an incident beam of neutrons of known wave vector $\mathbf{k}_i$ is scattered by the sample into an outgoing neutron of wave vector $\mathbf{k}_f$. It is possible to measure the change in both the direction and magnitude of the neutron wave vector, or equivalently, the changes in the momentum and energy when the neutrons interact with the sample [Bramwell 2011]. The magnetic field produced by the spins in the sample scatters the neutrons. It is also possible that the spin field can vary in space and time. Second order dynamical perturbation theory shows that the scattering is essentially proportional to the dynamical structure factor $\mathbf{S}(\mathbf{q},\omega)$ of two-spin correlation function of the sample:

$$S^{\alpha,\beta}(\mathbf{q},\omega) = \frac{1}{2\pi}\sum_{\mathbf{R}}\int_{-\infty}^{+\infty} dt\; e^{i(\mathbf{q}\cdot\mathbf{R}-\omega t)}\langle S_0^{\alpha}(0)S_{\mathbf{R}}^{\beta}(t)\rangle \tag{1.13}$$

The partial differential cross section measures the number of neutrons scattered in a solid angle $d\Omega$ within a range of energy between E and $E+dE$. The spin-spin correlation function $S(\mathbf{q},\omega)$ is the quantity directly associated with inelastic neutron scattering. The momentum $\mathbf{q}$ represents the difference between the initial momentum ($\mathbf{k}_i$) and the final momentum ($\mathbf{k}_f$) and the final momentum and is defined as scattering vector.

Particularly it has been used to study the properties of strongly correlated magnetic systems with large application for studying the spin excitation spectrum in the overdoped regime of the high temperature superconductors [Bourges 1996], itinerant antiferromagnetism [Liu 1970, Sokoloff 1969] and spin-spin correlation in magnetic frustrated systems [Mirebeau 2014, Lee 2000].

1.4.2 Optical spectroscopy.

The coupling between light and matter can be seen as a source of information for describing and understanding the physical properties of a particular system. The system can be either a molecule or a crystal structure. The different process in which light interact with matter can be divided in some categories such as absorption, photo-emission or diffusion [Baym 1990]. In our case we are interested in process where there is diffusion of light. The system will be irradiated by a monochromatic light with frequency ω_i and will diffuse part of this light in a different direction with frequency ω_f. Part of this diffused light will have the same frequency as the initial one ($\omega_f = \omega_i$). This process is known as elastic diffusion or Rayleigh scattering. Another part of the scattered light will have a different frequency from the initial one ($\omega_f \neq \omega_i$). This process is known as inelastic diffusion or Raman diffusion [Duyne 2003]. The Rayleigh diffusion is caused by spatial inhomogeneity (molecules, individual atoms, gases, etc) and the Raman diffusion is caused by temporal fluctuations (molecular vibration, lattice vibrations, magnetic excitation). Since our interest here is the Raman diffusion we can also predict what are the elementary or collective excitations of the system (phonon, exciton, magnons, etc) [Devereaux 2007].

The Raman diffusion is a second order process which involve two photons, one incident photon with frequency ω_i and momentum wave vector $\mathbf{q}_i$ and the diffused photon with frequency ω_f and momentum wave vector $\mathbf{q}_f$. The Raman displacement is the difference of the initial and final frequencies of the photons $\omega = \omega_i - \omega_f$. The frequency difference ω is a result of the energy exchange process between light and matter. This can be translated into a process of absorption (anti-Stokes) or creation (Stokes) of collective elementary excitations or individual ones (phonon, magnons, electron-hole pairs) in the material. We illustrate this schematically in fig(1.3).

In the fig(1.4) we describe the creation of a phonon (a) and of a electron-hole pair (b). In these processes one electron is initially excited to a higher energy level. The process of excitation can occur in the same band or in different bands, in this last case the energy of light beam is close the excitation one and we can observe the enhancement of diffusion, knowing the resonant process. Electrons that are excited to intermediate states can be diffused by the lattice, later on creating a phonon excitation and then relaxing to the original state by emitting a photon of energy different from that one from incident electromagnetic wave (see Fig.1.4 (a)). In the case of an electronic Raman process, the electron in its excited state relaxes to a different final state creating an electron-hole pair around the Fermi level (see Fig. 1.4 (b)). In the next section we will present the general concepts about Raman

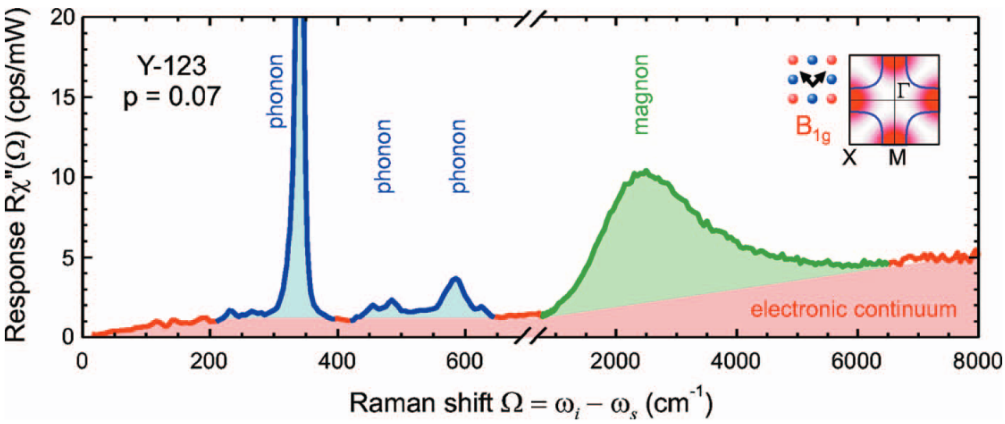

Figure 1.3: The Raman-scattering spectrum taken on $(Y_{0.92}Ca_{0.08})Ba_2Cu_3O_{6.3}$. The inset shows the photon polarization in the CuO_2 plane. From this picture it is possible to conclude that Raman scattering can give us lot of information from the systems, as phonon and magnons. [Devereaux 2007].

scattering.

1.5 Quantum mechanical description of Raman scattering.

The aim of this section is to present the quantum mechanical description for inelastic light scattering in general. For sake of simplification, by now, we set $\hbar$ and c equals to unity. It is by no means as detailed as other reviews available for consultation [Garmire 2013, Devereaux 2007, Devereaux 1997]. However, it explains the main features about this process.

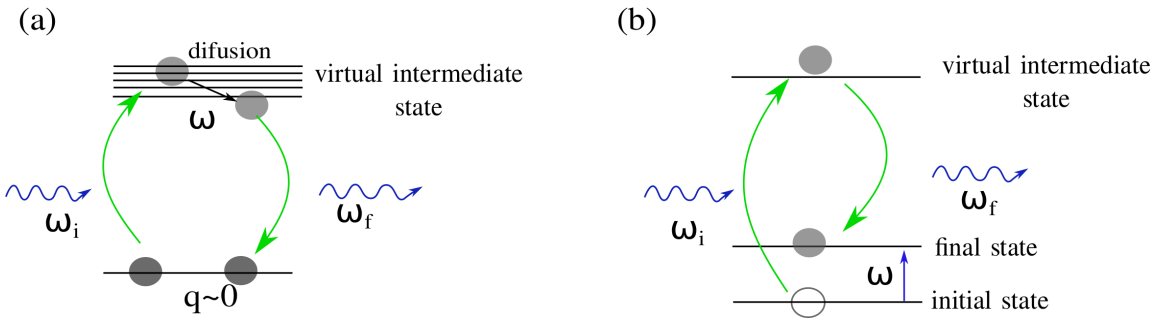

Figure 1.4: (a) The creation process of a phonon with frequency ω. (b) Creation process of a pair particle-hole of frequency ω.

1.5.1 General approach.

We consider a Hamiltonian for N electrons coupled to the electromagnetic field. It can be written as

$$H = \sum_i^N \frac{(\hat{\mathbf{p}}_i + (-e/c)\hat{\mathbf{A}}(\mathbf{r}_i))^2}{2m} + H_{Coulomb} + H_{fields}. \tag{1.14}$$

Where $\hat{\mathbf{p}} = -i\nabla$ is the momentum operator, $-e$ is the magnitude of electronic charge and c the speed of light. The quantity $\hat{\mathbf{A}}(\mathbf{r}_i)$ is the vector potential of the electromagnetic field at space-time $\mathbf{r}_i$ and m is the electron mass. Also we define $\mathcal{H}_{Coulomb}$ as being the Coulomb interaction and $\mathcal{H}_{fields}$ is the free electromagnetic part. If we develop the quadratic term , we can rewrite the Hamiltonian in a more compact form as

$$H = H' + H_{int}, \tag{1.15}$$

where now $H' = H_0 + H_{fields}$, with the usual definition of $H_0 = \frac{1}{2m}\sum_i^N (\hat{\mathbf{p}}_i)^2 + H_{Coulomb}$ and $H_{int} = H_A + H_{AA}$ where

$$H_A = -\frac{e}{2mc}\sum_i^N (\hat{\mathbf{p}}_i \cdot \hat{\mathbf{A}}(\mathbf{r}_i) + \hat{\mathbf{A}}(\mathbf{r}_i) \cdot \hat{\mathbf{p}}_i) \tag{1.16}$$

and

$$H_{AA} = \frac{e^2}{2mc^2}\sum_i^N \hat{\mathbf{A}}(\mathbf{r}_i)^2 \tag{1.17}$$

Here we use the Coulomb gauge $\nabla \cdot \hat{\mathbf{A}}(\mathbf{r}_i) = 0$, that guarantees that $\mathbf{A}$ is purely transverse.

Since we are dealing with a many body problem, we can use the second quantization formalism. In this approach, the interacting Hamiltonian can be written as

$$H_{int} = -\frac{e}{c}\int d^3r\, \hat{\mathbf{j}}(\mathbf{r}) \cdot \hat{\mathbf{A}}(\mathbf{r}) + \frac{e^2}{2mc^2}\int d^3r\, \rho(\mathbf{r})\hat{\mathbf{A}}(\mathbf{r}) \cdot \hat{\mathbf{A}}(\mathbf{r}). \tag{1.18}$$

It is also appropriate to use the representation of the density and current operators

$$\rho(\mathbf{r}) = \psi^\dagger(\mathbf{r})\psi(\mathbf{r}), \tag{1.19}$$

$$\mathbf{j}(\mathbf{r}) = \frac{1}{2m}[\psi^\dagger(\mathbf{r})(\hat{\mathbf{p}}\psi(\mathbf{r})) - (\hat{\mathbf{p}}\psi^\dagger(\mathbf{r}))\psi(\mathbf{r})], \tag{1.20}$$

where the operators $\psi(\mathbf{r})$ and $\psi^\dagger(\mathbf{r})$ are respectively fermionic operators which annihilate and create particles at a point $\mathbf{r}$. They can be expanded in momentum space as

$$\psi(\mathbf{r}) = \sum_{\mathbf{k},m} \phi(\mathbf{r}, m) c_{\mathbf{k},m} \tag{1.21}$$

$$\psi^\dagger(\mathbf{r}) = \sum_{\mathbf{k},n} \phi^*(\mathbf{r}, n) c^\dagger_{\mathbf{k},n} \tag{1.22}$$

The functions $\phi^*(\mathbf{r}, n)$ and $\phi(\mathbf{r}, n)$ are eigenstates of the Hamiltonian H_0, which may be simply plane waves corresponding to position $\mathbf{r}$. The indices n and m specify other quantum number associated with the state, like band index or spin for example. Electron states with momentum $\mathbf{k}$ are created or annihilated by $c^\dagger_{\mathbf{k},n}$, $c_{\mathbf{k},n}$, respectively, and the indices n or m referring to the quantum number associated with the state, such as the momenta and/or spin states.

In second quantization, the vector potential $\mathbf{A}$ is a linear combination of creation and annihilation operators for photons. The nonvanishing matrix elements produced by the action of this operator depend entirely of the initial and final states in question. The operator $\hat{\mathbf{A}}(\mathbf{r})$ is written as

$$\hat{\mathbf{A}}(\mathbf{r}) = \sum_{\mathbf{q},\mu} A^0(\omega_\mathbf{q})[a_{\mathbf{q},\mu}\ \boldsymbol{\varepsilon}^{\boldsymbol{\mu}}_{\mathbf{q}}\ e^{i\mathbf{q}\cdot\mathbf{r}} + a^\dagger_{\mathbf{q},\mu}\ \boldsymbol{\varepsilon}^{*\boldsymbol{\mu}}_{\mathbf{q}}\ e^{-i\mathbf{q}\cdot\mathbf{r}}], \tag{1.23}$$

where $A^0(\omega_\mathbf{q}) = \sqrt{\frac{c^2\hbar}{2\omega_\mathbf{q} V}}$. The bosonic operators $a_\mathbf{q}$ and $a^\dagger_\mathbf{q}$ annihilate or create photons with wave vector $\mathbf{q}$ and polarization $\boldsymbol{\varepsilon}^{\boldsymbol{\mu}}_{\mathbf{q}}$. The volume V define the box for the periodic boundary conditions of $\mathbf{A}$. By using this representation of $\mathbf{A}$ in second quantization as well as eq(1.19) and eq(1.20), we rewrite the terms of H_{AA} and H_A as

$$\begin{aligned} H_{AA} = \frac{e^2}{2mc^2} \sum_{\substack{\mathbf{k},n;\mathbf{k}',m \\ \mathbf{q}_1,\mu_1;\mathbf{q}_2,\mu_2}} & A^0(\omega_{q_1})A^0(\omega_{q_2})c^\dagger_{\mathbf{k},n}c_{\mathbf{k}',m} \\ & \times [\langle n|e^{i\mathbf{q}_1\cdot\mathbf{r}}|m\rangle a_{\mathbf{q}_1,\mu_1}\ \boldsymbol{\varepsilon}^{\boldsymbol{\mu_1}}_{\mathbf{q_1}} + \langle n|e^{-i\mathbf{q}_1\cdot\mathbf{r}}|m\rangle a^\dagger_{\mathbf{q}_1,\mu_1}\ \boldsymbol{\varepsilon}^{*\boldsymbol{\mu_1}}_{\mathbf{q_1}}] \\ & \times [\langle n|e^{i\mathbf{q}_2\cdot\mathbf{r}}|m\rangle a_{\mathbf{q}_2,\mu_2}\ \boldsymbol{\varepsilon}^{\boldsymbol{\mu_2}}_{\mathbf{q_2}} + \langle n|e^{-i\mathbf{q}_2\cdot\mathbf{r}}|m\rangle a^\dagger_{\mathbf{q}_2,\mu_2}\ \boldsymbol{\varepsilon}^{*\boldsymbol{\mu_2}}_{\mathbf{q_2}}] \end{aligned} \tag{1.24}$$

and

$$\begin{aligned} H_A = -\frac{e}{m} \sum_{\substack{\mathbf{k},n;\mathbf{k}',m \\ \mathbf{q}_1,\mu_1}} & A^0(\omega_{q_1})c^\dagger_{\mathbf{k},n}c_{\mathbf{k}',m} \\ & \times [\langle n|\mathbf{p}e^{i\mathbf{q}_1\cdot\mathbf{r}}|m\rangle a_{\mathbf{q}_1,\mu_1}\ \boldsymbol{\varepsilon}^{\boldsymbol{\mu_1}}_{\mathbf{q}} + \langle n|\mathbf{p}e^{-i\mathbf{q}_1\cdot\mathbf{r}}|m\rangle a^\dagger_{\mathbf{q}_1,\mu_1}\ \boldsymbol{\varepsilon}^{*\boldsymbol{\mu_1}}_{\mathbf{q_1}}], \end{aligned} \tag{1.25}$$

with

$$\langle n|e^{i\mathbf{q}\cdot\mathbf{r}}|m\rangle = \int d^3r\phi^*(\mathbf{r}, n)e^{i\mathbf{q}\cdot\mathbf{r}}\phi(\mathbf{r}, m), \tag{1.26}$$

$$\langle n|\mathbf{p}\cdot e^{i\mathbf{q}\cdot\mathbf{r}}|m\rangle = \int d^3r\phi^*(\mathbf{r}, n)\mathbf{p}\cdot e^{i\mathbf{q}\cdot\mathbf{r}}\phi(\mathbf{r}, m). \tag{1.27}$$

The first term H_{AA} gives rise to intraband electronic transitions from the two-photon scattering in first-order perturbation theory. While H_A is related to intraband or interband electronic transitions from the single-photon scattering at second order via intermediate states. It does not contribute at first order since the average of the momentum operator is zero.

1.5.1.1 The probability transition and effective density operator.

The electronic Raman scattering cross section is proportional to the probability transition between one initial state and one final state of the system. This transition rate can be calculated by the Fermi's golden rule.

$$\mathbf{\Gamma}_{I\to F} = 2\pi|\langle F|H_{int}|I\rangle|^2\delta(E_F - E_I) \tag{1.28}$$

The scattering tensor $|\langle F|H_{int}|I\rangle|^2$ is calculated by perturbation theory in H_{int}. It will involve contributions from both H_A at second order and H_{AA} at first order. The term H_A involves the coupling between current and H_{AA} is the contribution from charge. Later on we will see that this produces the charge and current sector of our Raman analysis in the next chapter.

Let us first discuss the effect of H_{AA}. We have as initial and final state

$$|I\rangle=|\mathbf{k},m\rangle|n_{\mathbf{q}_1,\mu_1},n_{\mathbf{q}_2,\mu_2}=0\rangle \tag{1.29}$$

$$|F\rangle=|\mathbf{k}+\mathbf{q},n\rangle|n_{\mathbf{q}_1,\mu_1}-1,n_{\mathbf{q}_2,\mu_2}=1\rangle. \tag{1.30}$$

We have two possible processes. The photon matrix element can be non-zero if the $\mathbf{A}$ on the right annihilates a $\mathbf{q}_1,\mu_1$ photon and the $\mathbf{A}$ on the left creates a $\mathbf{q}_2,\mu_2$ photon, or vice versa. These two possibilities give us

$$\langle F|H_{AA}|I\rangle=\frac{e^2}{mV}\sqrt{\frac{n_i}{\omega_q\omega_{-q}}}\sum_{\substack{\mathbf{k},n,m\\ \mu_1,\mu_2}}\langle\mathbf{k}+\mathbf{q},m|c^\dagger_{\mathbf{k},m}c_{\mathbf{k}-\mathbf{q},m}|\mathbf{k},m\rangle(\boldsymbol{\varepsilon}^{\boldsymbol{\mu_1}}_{\mathbf{q}}\cdot\boldsymbol{\varepsilon}^{*\boldsymbol{\mu_2}}_{-\mathbf{q}}) \tag{1.31}$$

At second order, we compute the expectation value of H_A but now we have an intermediate state, with two possible process. They represent the destruction of an incident photon and the creation of an diffused photon, or vice versa.

$$|M_1\rangle=|\mathbf{k}+\mathbf{q_2},l\rangle|n_{\mathbf{q}_1,\mu_1}-1,n_{\mathbf{q}_2,\mu_2}=0\rangle \tag{1.32}$$

$$|M_2\rangle=|\mathbf{k}-\mathbf{q_1},l\rangle|n_{\mathbf{q}_1,\mu_1},n_{\mathbf{q}_2,\mu_2}=1\rangle \tag{1.33}$$

At second order, the probability amplitude for H_A is

$$\langle F|H_A|I\rangle^{(2)}=\sum_M\left[\frac{\langle F|H_A|M_1\rangle\langle M_1|H_A|I\rangle}{E_I-E_{M_1}}+\frac{\langle F|H_A|M_2\rangle\langle M_2|H_A|I\rangle}{E_I-E_{M_2}}\right]. \tag{1.34}$$

By using the definitions of $|F\rangle$, $|I\rangle$ and $|M\rangle$, we end up with

$$\langle F|H_A|I\rangle^{(2)} = \frac{e^2}{2m^2V}\sqrt{\frac{n_i}{\omega_1\omega_2}}\sum_{\substack{\mathbf{k},n,m,l\\ \mu_1,\mu_2}} \times \left[\frac{\langle n,\mathbf{k}+\mathbf{q}|\mathbf{p}\cdot\boldsymbol{\varepsilon}^{*\mu_2}_{\boldsymbol{q_2}} c^\dagger_{\mathbf{k},n}c_{\mathbf{k}-\mathbf{q}_2,m}|\mathbf{k}+\mathbf{q}_2,l\rangle\langle l,\mathbf{k}+\mathbf{q}_2|\mathbf{p}\cdot\boldsymbol{\varepsilon}^{\mu_1}_{\boldsymbol{q_1}} c^\dagger_{\mathbf{k},n}c_{\mathbf{k}+\mathbf{q}_1,m}|\mathbf{k},m\rangle}{\varepsilon_{\mathbf{k},n}-\varepsilon_{\mathbf{k}+\mathbf{q}_2,l}-\omega_2} + \frac{\langle n,\mathbf{k}+\mathbf{q}|\mathbf{p}\cdot\boldsymbol{\varepsilon}^{\mu_1}_{\boldsymbol{q_1}} c^\dagger_{\mathbf{k},n}c_{\mathbf{k}+\mathbf{q}_1,m}|\mathbf{k}-\mathbf{q}_1,l\rangle\langle l,\mathbf{k}-\mathbf{q}_1|\mathbf{p}\cdot\boldsymbol{\varepsilon}^{*\mu_2}_{\boldsymbol{q_2}} c^\dagger_{\mathbf{k},n}c_{\mathbf{k}-\mathbf{q}_2,m}|\mathbf{k},m\rangle}{\varepsilon_{\mathbf{k},n}-\varepsilon_{\mathbf{k}-\mathbf{q}_1,l}+\omega_1}\right]. \quad (1.35)$$

The momentum transferred during the process is defined as $\mathbf{q} = \mathbf{q}_1 - \mathbf{q}_2$ and the difference in energy is given by $\omega = \omega_1 - \omega_2$.

In this way, we end up with the final expression for the probability rate

$$\boldsymbol{\Gamma}_{I\to F} = \frac{\pi e^4 n_i}{2m^2V^2\omega_i\omega_f}|\langle n,\mathbf{k}+\mathbf{q}|\hat{\tilde{\rho}}(\mathbf{q})|\mathbf{k},m\rangle|^2\delta(\varepsilon_{\mathbf{k}+\mathbf{q},n}-\varepsilon_{\mathbf{k},m}-\omega) \quad (1.36)$$

Where we have introduced the effective density operator [Hayes 2012]

$$\hat{\tilde{\rho}}(\mathbf{q}) = \sum_{\mathbf{k},n}\boldsymbol{\gamma}_{\mathbf{k},\boldsymbol{n}}(\boldsymbol{\varepsilon^i},\boldsymbol{\varepsilon^f})c^\dagger_{\mathbf{k}+\mathbf{q},n}c_{\mathbf{k},n} \quad (1.37)$$

In experiments, the selection of the symmetries of excitations observed by Raman are selected by the orientation of the sample and the polarizations of photons. Since the momentum transferred to electrons $\mathbf{q}$ is much less than the momentum scale of order k_F, the Fermi momentum in metallic systems, the limit $q \to 0$ is a good approximations in practically all

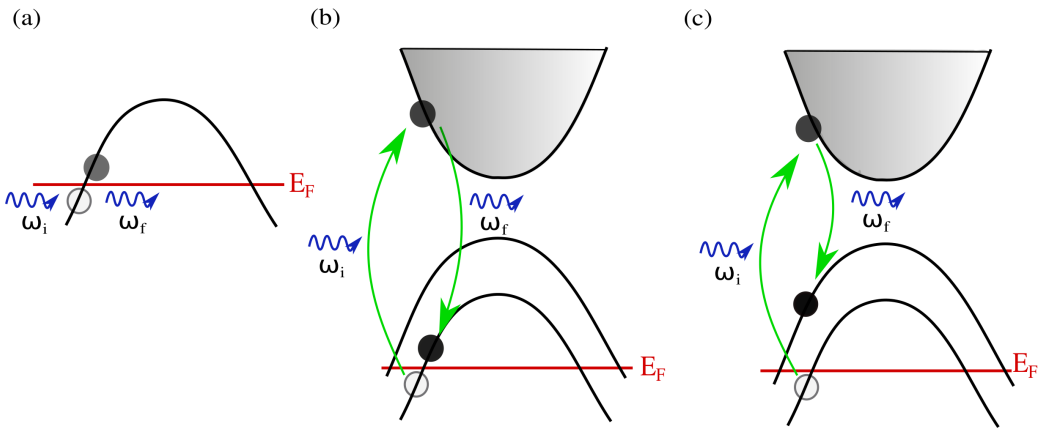

Figure 1.5: Some process that can occur in Raman electronic diffusion. At first order in perturbation theory we have the intraband process (a). At second order in perturbation theory. we have intraband (b) and interband (c) process.

cases. Therefore,

$$\gamma_{\mathbf{k},n}(\boldsymbol{\varepsilon^i},\boldsymbol{\varepsilon^f}) = \sum_{\mu_i,\mu_f} \boldsymbol{\varepsilon^{\mu_i}}\cdot\boldsymbol{\varepsilon^{*\mu_f}} + \frac{1}{m}\sum_{\mu_i,\mu_f,l}\left[\frac{\langle n,\mathbf{k}|\mathbf{p}\cdot\boldsymbol{\varepsilon^{*\mu_f}}|\mathbf{k},l\rangle\langle l,\mathbf{k}|\mathbf{p}\cdot\boldsymbol{\varepsilon^{\mu_i}}|\mathbf{k},m\rangle}{\varepsilon_{\mathbf{k},n}-\varepsilon_{\mathbf{k},l}-\omega_f} + \frac{\langle n,\mathbf{k}|\mathbf{p}\cdot\boldsymbol{\varepsilon^{\mu_i}}|\mathbf{k},l\rangle\langle l,\mathbf{k}|\mathbf{p}\cdot\boldsymbol{\varepsilon^{*\mu_f}}|\mathbf{k},m\rangle}{\varepsilon_{\mathbf{k},n}-\varepsilon_{\mathbf{k},l}+\omega_i}\right]. \quad (1.38)$$

In Fig.(1.5) we represent these two cases considered here, using perturbation theory. At first order, the Raman scattering produce a creation of an electron-hole pair at the same band by promoting the electron to a level of energy above the Fermi level. At second order we have creation of a electron-hole pair at different bands which involve virtual intermediate states.

1.5.2 The importance of light polarization.

In the previous section 1.5.1.1, we saw that the effective density operator has two contributions, one generated by the coupling of electron's charge to the two photons and the other by the coupling of electron's current to a single photon. However, to evaluate the Raman scattering matrix of effective density operator $\hat{\tilde{\rho}}(\mathbf{q})$ is a difficult task, since we cannot always specify the quantum numbers of the electronic many body state.

However, applying symmetry arguments we are able to view what types of excitations can be created. The charge density fluctuations, due to light scattering, are modulated in the directions determined by the polarization of incident and scattered photons involved on the process. Thus, these density fluctuations have the symmetry imposed on them by the way in which light is oriented [Devereaux 2007]. This can be seen on the dependence of Raman matrix elements on the initial and final fermion state. Basically the Raman matrix elements can be decomposed in into basis functions of the irreducible point group symmetry of the crystal [Shastry 1990, Hayes 2012].

Another important consequence is the fact that we are able to map the Brillouin zone (BZ). The analysis is based in the representative basis functions $\Phi(\mathbf{k})$ from the complete set of BZ harmonics from the crystal's pint group symmetry. Consequently we are able to map excitations in different regions of the Brillouin zone by just choosing the polarization direction of incident photon.

1.5.3 The Correlation functions.

The Raman scattering cross section is the quantity accessible in the experiments and can be written in terms of the transition probability of Fermi's golden rule.

$$R(\mathbf{q},\omega) = r_0^2 \frac{\omega_f}{\omega_i} \mathbf{\Gamma}_{I\to F} \tag{1.39}$$

where $\mathbf{\Gamma}_{I\to F}$ is given by the probability transition in Eq.(1.36) and $r_0 = e^2/mc^2$ is the Thompson radius. For weakly interacting systems, the Raman scattering cross section reduces to a correlation function $\tilde{S}$ of an effective charge density $\hat{\tilde{\rho}}(\mathbf{q})$.

$$R(\mathbf{q},\omega) = r_0^2 \frac{\omega_f}{\omega_i} \tilde{S}(\mathbf{q}, i\omega \to \omega + i0), \tag{1.40}$$

where $\tilde{S}(\mathbf{q}, i\omega)$ is defined as

$$\tilde{S}(\mathbf{q}, i\omega) = \sum_n \frac{e^{-\beta E_n}}{Z} \int d\tau \; e^{i\omega\tau} \langle n | T_\tau (\hat{\tilde{\rho}}(\mathbf{q},\tau)\hat{\tilde{\rho}}(-\mathbf{q},0)) | n \rangle \tag{1.41}$$

with T_τ being the time ordering operator and $Z = \sum_n e^{-\beta E_n}$ is the partition function for the system, with $\beta = 1/k_B T$. The effective density $\hat{\tilde{\rho}}$ will be defined as

$$\hat{\tilde{\rho}}(\mathbf{q},\tau) = \sum_{\mathbf{k},n} \boldsymbol{\gamma}_{\mathbf{k},\boldsymbol{n}}(\boldsymbol{\varepsilon^i}, \boldsymbol{\varepsilon^f}) c^\dagger_{\mathbf{k}+\mathbf{q},n}(\tau) c_{\mathbf{k},n}(\tau) \tag{1.42}$$

The operators are time dependent in the Heisenberg picture. We also introduced the scattering amplitudes $\boldsymbol{\gamma}_{\mathbf{k},\boldsymbol{n}}(\boldsymbol{\varepsilon^i}, \boldsymbol{\varepsilon^f})$, as in Eq.(1.38).

The dynamical effective density-density correlation function or the Raman response $\tilde{S}$ can be written in terms of a dynamical effective density susceptibility $\tilde{\chi}$ via the fluctuation dissipation theorem

$$\tilde{S}(\mathbf{q},\omega) = -\frac{1}{\pi}[1 + n_B(i\omega, T)]\tilde{\chi}''(\mathbf{q},\omega) \tag{1.43}$$

where $n_B(i\omega, T)$ is the Bose distribution function. At finite temperature, the susceptibility is define as a correlation function of the effective density operator

$$\tilde{\chi}(\mathbf{q}, i\omega) = -\frac{1}{\mathcal{V}} \int_0^\beta d\tau e^{i\omega\tau} \langle T_\tau (\tilde{\rho}(\mathbf{q},\tau)\tilde{\rho}(-\mathbf{q},0)) \rangle. \tag{1.44}$$

The effective density operator $\hat{\tilde{\rho}}$ is given by Eq.(1.42). Thus, for noninteracting electrons the Raman scattering is given by a two-particle effective density correlation function. There are several methods to calculate this correlation function, e.g. diagrammatic perturbation theory [Devereaux 1999, Devereaux 1997, Perkins 2013], dynamical mean field theory (DMFT) [Freericks 2001].

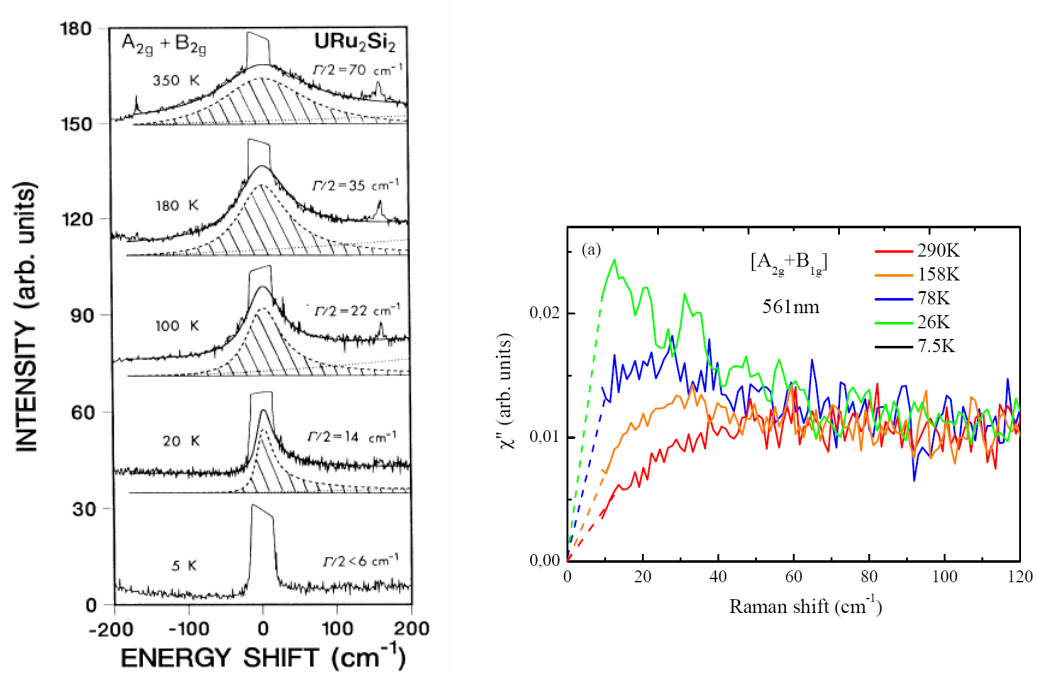

Figure 1.6: The Raman spectra for URu_2Si_2 in a pure A_{2g} symmetry at paramagnetic phase and hidden order phase. In both cases, the quasielastic spin scattering in the paramagnetic phase. Data in (**a**) is from [Cooper 1987] while (**b**) is from [Buhot 2015].

1.5.4 Raman spectroscopy in URu_2Si_2.

The first Raman spectroscopy experiments were performed on URu_2Si_2 in 1987 by Cooper *et al*. [Cooper 1987] and in 2006 Lampakis *et al.* [Lampakis 2006]. The measurements carried out by Cooper *et al.* (Fig.1.6(a)) have revealed the presence of signal for symmetry A_{1g}, which is associated with the presence of phonons. The intensity of the Raman response has a dependence on temperature. Hence, suggesting that at low temperatures, the electron-phonon coupling is strengthened. The responses to the symmetry A_{2g} are associated with the quasielastic spin scattering in the paramagnetic phase. Due to the limitations of the experimental resolution at that time, these studies reveal no evidence for the hidden order phase. Lampakis' work tells us about the temperature dependence of the phonon that can be accessible by Raman spectroscopy. The response, in this case, is associated with the languishing of the curve related to the symmetry A_{1g} for temperatures near the transition temperature T_0. Although, in this case also, no evidence is presented for the hidden order phase.

New experiments with Raman spectroscopy were performed precisely in the hidden order phase [Buhot 2014]. They had shown that the phase transition from PM to HO state

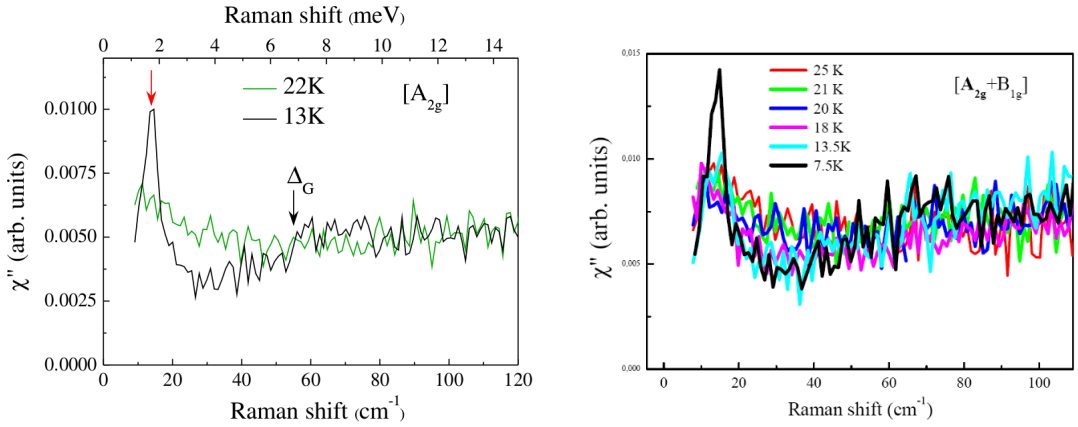

(a) (b)

Figure 1.7: The Raman spectra for URu_2Si_2 in a pure A_{2g} symmetry at paramagnetic phase and hidden order phase, adapted from [Buhot 2015].

is characterized by two Raman signatures of pure A_{2g} symmetry. In the paramagnetic phase the signal show a quasi-elastic response for this particular symmetry, Fig.(1.6(b)). In the HO phase, it exhibits precisely an electronic gap below $\Delta_G \sim 55$ cm^{-1} (6.8 meV) and a sharp excitation deep inside the gap at 14 cm^{-1} (1.7 meV) that matches the neutron resonance at $\mathbf{Q}$, Fig(1.7(a)). These two signatures were confirmed only in the A_{2g} precisely at the HO phase, as shown in Fig.(1.7(b)).

They proposed that the gap is due to quasiparticle excitations near the Fermi level, that accounts for the Fermi surface reconstruction at the HO transitions. Different Raman results, at the HO phase, were obtained by Kung et al. [Kung 2015]. They found that beyond the signal in A_{2g} there is also A_{1g} signatures exactly at the same energy. These signals come from the transitions in the crystalline field environments from partially delocalized levels. Both experimental results have shown a direct connection between the HO and A_{2g} symmetry. Although an explanation among his connections still requires theoretical investigations.

Chapter 2

Spin liquid versus long-range magnetic order.

In this chapter we present our studies related to the competition of the spin liquid states against the onset of long range magnetic order in a body centered tetragonal (BCT) lattice. It was discussed earlier on that in the presence of frustration the classical magnetic order can be unstable against spin liquid states. It was also pointed out that low dimensionality is a key ingredient for the emergence of a SL ordering.

Contradicting this low dimensionality idea, in this chapter we will analyze the effect of frustration in the 3D BCT lattice[1]. We begin by describing the classical ground states of the system. After that, we develop a spin-wave theory in order to study the quantum fluctuations. The BCT lattice displays full frustration induced by its own lattice structure. We define three kinds of exchange couplings between the spins located at the center and the spins sitting on the corner of the lattice, fig(2.1). We know that frustration is a key ingredient to destabilize classical magnetic order. However, in this 3D case we will see that in the framework of the spin wave theory the magnetic states are stable against quantum fluctuation at the lowest order.

The other approximation that can be carried out is to consider the effect of the fermionic excitations in the large-N limit. In this limit it is possible to destabilize the classical ordered state and observe the emergence of SL phases. Recently, the fermionic approach of the Heisenberg model has been carried out in order to investigate the formation of spin liquid states in a 2d [Pépin 2011] and 3d system [Thomas 2013]. The emergence of spin-liquid states motivates the analyses presented in the next chapter for Raman scattering.

[1]One version of this chapter has been published. C. Farias, C. Thomas, C. Pépin, A. Ferraz, C. Lacroix and S. Burdin. [Farias 2016]

2.1 Ground state for $J_1 - J_2 - J_3$ model.

The spin waves in modulated magnetic structures display certain interesting aspects which are not shared by simple ferromagnetic structures. However, this same feature makes their experimental study considerably more difficult. The structures can be defined as *incommensurate* with the lattice periodicity, when the original translational symmetry in the direction of the wave-vector is totally destroyed, and *commensurate* structures, in the case this symmetry is only modified, though possibly quite drastically. In this system a rotational symmetry is already spontaneously broken by the ground state. In this case, Goldstone theorem (1961) [Nolting 2009] predicts the existence of collective modes with energies approaching zero as their wavelengths go to infinity. Let us see how these two kinds of structures emerge in our model.

Let us derive the possible classical antiferromagnetic states from the Heisenberg model in a BCT lattice. Before performing our standard spin-wave approach, we first consider the classical limit, $S \to \infty$. The 3d version of the Heisenberg Hamiltonian that describes this system is

$$\mathcal{H} = J_1 \sum_{\langle i,j \rangle} \mathbf{S}_i \cdot \mathbf{S}_j + J_2 \sum_{\langle\langle i,j \rangle\rangle} \mathbf{S}_i \cdot \mathbf{S}_j + J_3 \sum_{\langle\langle i,j \rangle\rangle} \mathbf{S}_i \cdot \mathbf{S}_j, \tag{2.1}$$

where J_1-J_2-J_3 are the interactions on the BCT lattice, as showed in figure (2.1). The exchange couplings are the antiferromagnetic interlayer coupling J_1 and the intra-layer nearest and the next-nearest neighbors J_2 and J_3, respectively.

The possible emergent classical ordered states are derived by writing down the Fourier transforms for the spin operators as

$$\mathbf{S}_i = \frac{1}{\sqrt{N}} \sum_q e^{-i\mathbf{q}\cdot\mathbf{R}_i} \mathbf{S}_q, \tag{2.2}$$

and minimizing the classical energy

$$J(\mathbf{q}) = 8J_1\gamma_1(\mathbf{q}) + 2J_2\gamma_2(\mathbf{q}) + 4J_3\gamma_3(\mathbf{q}). \tag{2.3}$$

The γ expressions are, respectively

$$\gamma_1(\mathbf{q}) = \cos\left(\frac{q_x a}{2}\right) \cos\left(\frac{q_y a}{2}\right) \cos\left(\frac{q_z c}{2}\right), \tag{2.4}$$

$$\gamma_2(\mathbf{q}) = \cos(q_x a) + \cos(q_y a), \tag{2.5}$$

$$\gamma_3(\mathbf{q}) = \cos(q_x a) \cos(q_y a). \tag{2.6}$$

The wave vector $\mathbf{Q}_{\mathrm{AF}}$ is written in reduced notation as

$$\mathbf{Q}_{\mathrm{AF}} = 2\pi \left(\frac{l}{a}, \frac{m}{b}, \frac{n}{c}\right), \tag{2.7}$$

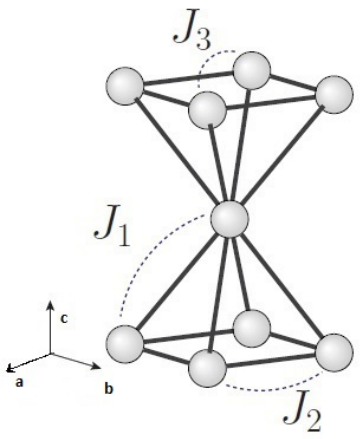

Figure 2.1: The BCT lattice with the J_1-J_2-J_3 interactions underlined. The lattice constants are set to $a = b = c = 1$

where a, b and c are the lattice constants for the BCT lattice. For simplicity, let us consider that the lattice constants are $a = b = c = 1$. The values considered for $\mathbf{Q}_{\rm AF} = 2\pi\,(l, m, n)$ will be those that minimize the classical energy $J(\mathbf{q})$, given by eq(2.3). We introduce the dimensionless parameters $p_2 = J_2/J_1$ and $p_3 = J_3/J_1$. We derive the saddle point equation that minimize the dispersion $J(\mathbf{q})$ in appendix A. The trivial solutions for these equations give us the commensurate states, $\mathbf{Q}^{\rm I}_{\rm AF} = (1, 1, 1)$ and $\mathbf{Q}^{\rm II}_{\rm AF} = (1/2, 1/2, \nu)$. This phases correspond to the regimes in which J_1 and J_2 dominate, respectively. The degeneracy ν indicates the underlying tow-dimensionality.

There are other two possible states, given by the incommensurate wave vector that characterize helical states. One of them is $\mathbf{Q}^{\rm III}_{\rm inc} = (0, \Upsilon_3, 0)$ which is degenerate with $\mathbf{Q}^{\rm III}_{\rm inc} = (1, \Upsilon_3, 1)$, $\mathbf{Q}^{\rm III}_{\rm inc} = (\Upsilon_3, 0, 0)$ and $\mathbf{Q}^{\rm III}_{\rm inc} = (\Upsilon_3, 1, 1)$, where $\Upsilon_3 = \frac{1}{\pi}\arccos\left(\pm\frac{1}{p_2+2p_3}\right)$. The second one is $\mathbf{Q}^{\rm II}_{\rm inc} = (\Upsilon_2, \Upsilon_2, 1)$, which is degenerate with $\mathbf{Q}^{\rm II}_{\rm inc} = (\Upsilon_2, \Upsilon_2 \pm 1, 0)$, with $\Upsilon_2 = \frac{1}{2\pi}\arccos\left(\frac{1-p_2}{2p_3}\right)$. Another possibility of an ordering wave-vector $\mathbf{Q}^{\rm III}_{\rm AF} = (0, 1/2, \nu)$ was proposed [Sugiyama 1990] in case J_3 dominates. This corresponds to the commensurate order in a purely bi-dimensional square lattice. However the state with modulation $\mathbf{Q}^{\rm III}_{\rm inc}$ is energetically more stable than $\mathbf{Q}^{\rm III}_{\rm AF}$. The classical phase diagram is displayed in fig.(2.2) and it shows each of the antiferromagnetic orders associated with each wave vector. The ordering wave vectors are continuous along each critical line (see appendix A) with the exception of the transition between $\mathbf{Q}^{\rm II}_{\rm inc} - \mathbf{Q}^{\rm III}_{\rm inc}$. The next step is to check the large-S corrections at a giving ground state with a specific $\mathbf{Q}$. The presence of two incommensurate states requires a generalization of the spin wave approach in order to take into account those kind of states.

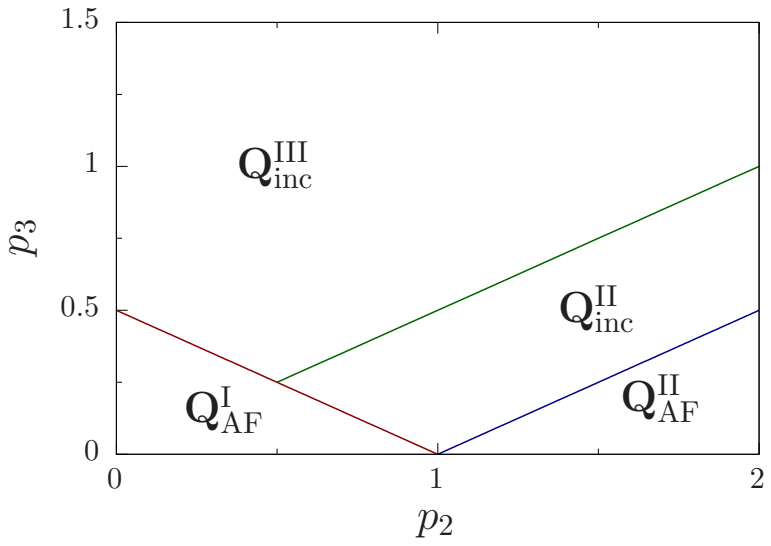

Figure 2.2: The classical phase diagram of J_1-J_2-J_3 model on BCT lattice. The coordinates p_2 and p_3 are defined as the ratio between J_2/J_1 and J_3/J_1 respectively. Solid lines indicate transitions between the stable magnetic orders with the modulation wave-vector $\mathbf{Q}$ defined previously.

2.2 Large S expansion and possible instabilities of the SW excitations.

Since we have derived the classical phase diagram for J_1-J_2-J_3, let us now investigate the stability of magnons excitations against quantum fluctuations with the framework of the spin wave (SW) analysis. We find that this fluctuation can either increase or decrease the value of S_c (critical value of S). This magnitude is related with the maximum value of S for which the elementary excitations, i.e. the spin waves are still stable. Our approach consists essentially in doing the large S expansion [Chubukov 1994].

We can write the Heisenberg Hamiltonian 2.1 in short for this approach as

$$\mathcal{H} = \sum_{\langle i,j \rangle} J_{ij} \mathbf{S_i} \cdot \mathbf{S_j} \tag{2.8}$$

We use the generalized form of the Holstein-Primakoff (see section 1.2.2) transformations taking into account helical states [Diep 1989, Chubukov 1984]

$$S_i^x = \sqrt{\frac{S}{2}}(a_i + a_i^\dagger), \tag{2.9}$$

$$\begin{pmatrix} S_i^z \\ S_i^y \end{pmatrix} = \begin{pmatrix} \cos\theta_i & \sin\theta_i \\ -\sin\theta_i & \cos\theta_i \end{pmatrix} \begin{pmatrix} S - a_i^\dagger a_i \\ -i\sqrt{\frac{S}{2}}\left(a_i - a_i^\dagger\right) \end{pmatrix}, \tag{2.10}$$

with a and $a^\dagger$ being boson annihilation and creation operators, respectively. The angle $\theta_i = \mathbf{Q}\cdot(\mathbf{R}_i - \mathbf{R}_o)$, where z is the easy axis that characterizes the site at $\mathbf{R}_o$ in some reference position. The scalar product $\mathbf{S}_i \cdot \mathbf{S}_j$ is rewritten using these transformation as

$$\begin{aligned}\mathbf{S}_i \cdot \mathbf{S}_j = & \frac{S}{2}(a_i + a_i^\dagger)(a_j + a_j^\dagger) + \cos\theta_{j-i}(S - a_i^\dagger a_i)(S - a_j^\dagger a_j) \\ & -\frac{S}{2}\cos\theta_{j-i}(a_i - a_i^\dagger)(a_j - a_j^\dagger) + i\sqrt{\frac{S}{2}}\sin\theta_{j-i}(a_i - a_i^\dagger)(S - a_j^\dagger a_j) \\ & -i\sqrt{\frac{S}{2}}\sin\theta_{j-i}(S - a_i^\dagger a_i)(a_j - a_j^\dagger),\end{aligned} \tag{2.11}$$

where we use the notation $\theta_j - \theta_i = \theta_{j-i} = \mathbf{Q}\cdot(\mathbf{R}_j - \mathbf{R}_i)$. We keep the bilinear terms of the product since it is a generalization of the linear spin wave theory. These are terms of order S^2 and S that are relevant in the large S series. We find the following expression

$$\begin{aligned}\mathbf{S}_i \cdot \mathbf{S}_j = & S^2\cos\theta_{j-i} - S\cos\theta_{j-i}(a_i^\dagger a_i + a_j^\dagger a_j) \\ & +\frac{S}{2}(1 - \cos\theta_{j-i})(a_i a_j + a_i^\dagger a_j^\dagger) + \frac{S}{2}(1 + \cos\theta_{j-i})(a_i a_j^\dagger + a_i^\dagger a_j).\end{aligned} \tag{2.12}$$

Therefore, the Hamiltonian is

$$\begin{aligned}\mathcal{H} = & \sum_{\langle i,j\rangle} J_{ij}[S^2\cos\theta_{j-i} - S\cos\theta_{j-i}(a_i^\dagger a_i + a_j^\dagger a_j) \\ & +\frac{S}{2}(1 - \cos\theta_{j-i})(a_i a_j + a_i^\dagger a_j^\dagger) + \frac{S}{2}(1 + \cos\theta_{j-i})(a_i a_j^\dagger + a_i^\dagger a_j)].\end{aligned} \tag{2.13}$$

By invoking the Fourier transforms of a_i and $a_i^\dagger$

$$a_i = \frac{1}{\sqrt{N}}\sum_{\mathbf{k}} e^{i\mathbf{k}\cdot\mathbf{R_i}} a_{\mathbf{k}} \qquad a_i^\dagger = \frac{1}{\sqrt{N}}\sum_{\mathbf{k}} e^{-i\mathbf{k}\cdot\mathbf{R_i}} a_{\mathbf{k}}^\dagger, \tag{2.14}$$

and considering that $\mathbf{R}_j = \mathbf{R}_i + \delta$, we split the sum in the Hamiltonian such that

$$\begin{aligned}\mathcal{H} = & \frac{S^2 N}{2}\sum_\delta J_\delta\cos(\mathbf{Q}\cdot\delta) - S\sum_\delta J_\delta\cos(\mathbf{Q}\cdot\delta)\sum_{\mathbf{k}} a_k^\dagger a_k \\ & + \frac{S}{4}\sum_{i\delta} J_\delta(1 - \cos(\mathbf{Q}\cdot\delta))\left(\frac{1}{N}\sum_{\mathbf{k},\mathbf{k}'} e^{i(\mathbf{k}+\mathbf{k}')\cdot\mathbf{R}_i} e^{i\mathbf{k}'\cdot\delta} a_{\mathbf{k}} a_{\mathbf{k}'} + h.c.\right) \\ & + \frac{S}{4}\sum_{i\delta} J_\delta(1 + \cos(\mathbf{Q}\cdot\delta))\left(\frac{1}{N}\sum_{\mathbf{k},\mathbf{k}'} e^{i(\mathbf{k}-\mathbf{k}')\cdot\mathbf{R}_i} e^{-i\mathbf{k}'\cdot\delta} a_{\mathbf{k}} a_{\mathbf{k}'}^\dagger + h.c.\right)\end{aligned} \tag{2.15}$$

Since $\sum_i e^{i(\mathbf{k}-\mathbf{k}')\cdot\mathbf{R}_i} = N\delta_{\mathbf{k},\mathbf{k}'}$, we rearrange the terms and get the usual expansion of the Hamiltonian in terms of the spin eigenvalue S.

$$\begin{aligned}\mathcal{H}=& \frac{S^2NJ(\mathbf{Q})}{2} - SJ(\mathbf{Q})\sum_{\mathbf{k}} a^\dagger_{\mathbf{k}}a_{\mathbf{k}} \\ &+ \frac{S}{4}\sum_{\mathbf{k}}\sum_{\delta} J_\delta(1-\cos(\mathbf{Q}\cdot\delta))(e^{-i\mathbf{k}\cdot\delta}a_{\mathbf{k}}a_{-\mathbf{k}} + e^{i\mathbf{k}\cdot\delta}a^\dagger_{\mathbf{k}}a^\dagger_{-\mathbf{k}}) \\ &+ \frac{S}{4}\sum_{\mathbf{k}}\sum_{\delta} J_\delta(1+\cos(\mathbf{Q}\cdot\delta))(e^{-i\mathbf{k}\cdot\delta}a_{\mathbf{k}}a^\dagger_{\mathbf{k}} + e^{i\mathbf{k}\cdot\delta}a^\dagger_{\mathbf{k}}a_{\mathbf{k}}).\end{aligned} \tag{2.16}$$

We use the following Fourier transform

$$J(\mathbf{k})=\sum_{\delta} J_\delta e^{-i\mathbf{k}\cdot\delta} \tag{2.17}$$

$$\tag{2.18}$$

and, finally, we end up with the expression

$$\begin{aligned}\mathcal{H}=& \frac{S^2NJ(\mathbf{Q})}{2} - SJ(\mathbf{Q})\sum_{\mathbf{k}} a^\dagger_{\mathbf{k}}a_{\mathbf{k}} \\ &+ \frac{S}{4}\sum_{\mathbf{k}}\left[J(\mathbf{k}) - \frac{J(\mathbf{k}+\mathbf{Q})+J(\mathbf{k}-\mathbf{Q})}{2}\right](a_{\mathbf{k}}a_{-\mathbf{k}} + a^\dagger_{\mathbf{k}}a^\dagger_{-\mathbf{k}}) \\ &+ \frac{S}{4}\sum_{\mathbf{k}}\left[J(\mathbf{k}) + \frac{J(\mathbf{k}+\mathbf{Q})+J(\mathbf{k}-\mathbf{Q})}{2}\right](a_{\mathbf{k}}a^\dagger_{\mathbf{k}} + a^\dagger_{\mathbf{k}}a_{\mathbf{k}}).\end{aligned} \tag{2.19}$$

If we split the sums into "positive" and "negative" values of $\mathbf{k}$ and if we make a change of variable $\mathbf{k} \to -\mathbf{k}$ in the sum where k is negative, it follows that

$$\begin{aligned}\mathcal{H}=& \frac{S^2NJ(\mathbf{Q})}{2} \\ &+S\sum_{\mathbf{k}}\left[\frac{J(\mathbf{k})}{2} + \left(\frac{J(\mathbf{k}+\mathbf{Q})+J(\mathbf{k}-\mathbf{Q})}{4}\right) - J(\mathbf{Q})\right]\left(a^\dagger_{\mathbf{k}}a_{\mathbf{k}} + a^\dagger_{-\mathbf{k}}a_{-\mathbf{k}}\right) \\ &+S\sum_{\mathbf{k}}\left[\frac{J(\mathbf{k})}{2} - \left(\frac{J(\mathbf{k}+\mathbf{Q})+J(\mathbf{k}-\mathbf{Q})}{4}\right)\right]\left(a^\dagger_{\mathbf{k}}a^\dagger_{-\mathbf{k}} + a_{\mathbf{k}}a_{-\mathbf{k}}\right)\end{aligned} \tag{2.20}$$

We see that this expression is a perturbative expansion in decreasing powers of S. We keep only the leading terms $\mathcal{O}(S^2)$ and the first order term. Another point that can be seen from this is that it provides a generalized expression for no matter what phase we take into account. In the next section we will see how we can diagonalize this Hamiltonian and find important relations in order to determine the S critical.

2.2.1 Diagonalization of the Hamiltonian.

The difficulty in dealing with such a Hamiltonian is obvious. We must diagonalize it first. What we have to do is to use an unitary transformation that allow us to rewrite it in that way. Let us use the following transformations

$$\begin{pmatrix} a_{\mathbf{k}} \\ a^{\dagger}_{-\mathbf{k}} \end{pmatrix} = \begin{pmatrix} \cosh(\theta_{\mathbf{k}}) & -\sinh(\theta_{\mathbf{k}}) \\ -\sinh(\theta_{\mathbf{k}}) & \cosh(\theta_{\mathbf{k}}) \end{pmatrix} \begin{pmatrix} \alpha_{\mathbf{k}} \\ \alpha^{\dagger}_{-\mathbf{k}} \end{pmatrix} \tag{2.21}$$

Of course, the operators $\alpha_{\mathbf{k}}$ and $\beta_{\mathbf{k}}$ must obey the same commutation relations of $a_{\mathbf{k}}$ and $b^{\dagger}_{\mathbf{k}}$. This is in the same spirit of the Bogoliubov quasiparticles in superconductivity theory. We can see that the Hamiltonian has the following matrix form

$$\mathcal{H} = E_0 + S\sum_{\mathbf{k}} \begin{pmatrix} a^{\dagger}_{\mathbf{k}} & a_{-\mathbf{k}} \end{pmatrix} \begin{pmatrix} A_{\mathbf{k}} & B_{\mathbf{k}} \\ B_{\mathbf{k}} & A_{\mathbf{k}} \end{pmatrix} \begin{pmatrix} a_{\mathbf{k}} \\ a^{\dagger}_{-\mathbf{k}} \end{pmatrix}, \tag{2.22}$$

with

$$A_{\mathbf{k}} = \frac{J(\mathbf{k})}{2} + \left(\frac{J(\mathbf{k}+\mathbf{Q}) + J(\mathbf{k}-\mathbf{Q})}{4}\right) - J(\mathbf{Q}) \tag{2.23}$$

$$B_{\mathbf{k}} = \frac{J(\mathbf{k})}{2} - \left(\frac{J(\mathbf{k}+\mathbf{Q}) + J(\mathbf{k}-\mathbf{Q})}{4}\right) \tag{2.24}$$

The eigenvalues of this matrix are given by $\lambda_k = \sqrt{\Omega^{+}_{\mathbf{k}}\Omega^{-}_{\mathbf{k}}}$, where $\Omega^{+}_{\mathbf{k}} = A_{\mathbf{k}} + B_{\mathbf{k}}$ and $\Omega^{-}_{\mathbf{k}} = A_{\mathbf{k}} - B_{\mathbf{k}}$, are the dispersion frequencies obtained for Bogoliubov quasiparticles. Therefore, we find that

$$\begin{aligned} \mathcal{H} = E_0 &+ S\sum_{\mathbf{k}} \left[A_{\mathbf{k}}(\cosh 2\theta_{\mathbf{k}} - 1) - B_{\mathbf{k}}\sinh 2\theta_{\mathbf{k}}\right] \\ &+ S\sum_{\mathbf{k}} \left[A_{\mathbf{k}}\cosh 2\theta_{\mathbf{k}} - B_{\mathbf{k}}\sinh 2\theta_{\mathbf{k}}\right]\left(\alpha^{\dagger}_{\mathbf{k}}\alpha_{\mathbf{k}} + \alpha^{\dagger}_{-\mathbf{k}}\alpha_{-\mathbf{k}}\right). \end{aligned} \tag{2.25}$$

with $B_{\mathbf{k}}\cosh 2\theta_{\mathbf{k}} - A_{\mathbf{k}}\sinh 2\theta_{\mathbf{k}} = 0$ or equivalently $\tanh 2\theta_{\mathbf{k}} = \frac{B_{\mathbf{k}}}{A_{\mathbf{k}}}$. These expressions in terms of hyperbolic functions will be used later on to write the corrections for S_c. Finally, the energy of the ground state is expressed as

$$E = E_0 + S\sum_{\mathbf{k}} \left(\sqrt{\Omega^{+}_{\mathbf{k}}\Omega^{-}_{\mathbf{k}}} - \frac{\Omega^{+}_{\mathbf{k}} + \Omega^{-}_{\mathbf{k}}}{2}\right) \tag{2.26}$$

By using this expression, it is possible to compute the corrections for the energies for each of the classical ground states derived in the previous section. We will investigate how quantum fluctuations can stabilize a particular order for $\mathbf{Q}^{\mathrm{II}}_{\mathrm{AF}}$ in the next section. .

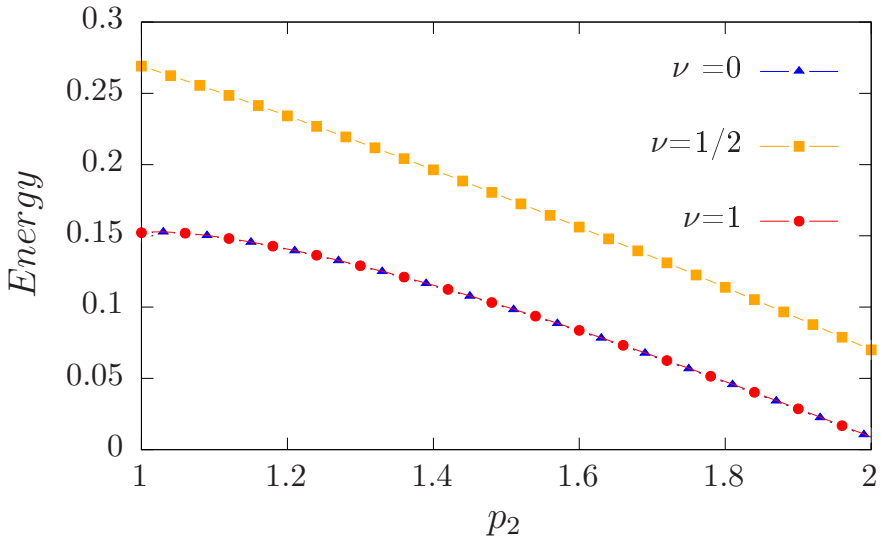

Figure 2.3: Energy as a function of p_2, for $S = 1/2$. Including the first corrections we are able to lift the degeneracy in favor of ν=0 or ν=1, which means q_z=0 or 2π.

2.2.2 Order by disorder and the degeneracy of the modular vector $\mathbf{Q}_{\mathrm{AF}}^{\mathrm{II}}$.

In solving the classical phase diagram of our model, we saw that because of the presence of frustration we ended up with one particular state that exhibits degeneracy. For the $\mathbf{Q}_{\mathrm{AF}}^{\mathrm{II}}$, the value of q_z can take any value which leads to a manifold of possible configurations along z. This indicate that the system is most likely degenerate and almost 2D, without correlations along the c axis. However, as we mention before, these degenerate ground states may be situated in very different regimes: they experience thermal and quantum fluctuations. The fluctuations have a special role in these systems because they may partially lift this degeneracy and induce in this way the onset of an ordered state [Rastelli 1987, Buhrandt 2014]. Let us see what happens when the degeneracy present is associated with $\mathbf{Q}_{\mathrm{AF}}^{\mathrm{II}}$. Let us verify what happens with the fluctuations produced by those S corrections.

Here again the presence of quantum fluctuations is the mechanism to lift some of this degeneracy. The determination of the appropriate $\mathbf{Q}_{\mathrm{AF}}^{\mathrm{II}}$ automatically selects one precise state from the available manifold of states. We take the expression (2.26) and compute numerically the energy for specific values of ν as a function of p_2. In Fig. (2.3), we plot the values of E for three values of ν. The degeneracy is lifted in favor of $\nu = 0$ that gives the

same result of $\nu = 1$. For other values between the interval $0 < \nu < 1$ the selected values of ν are therefore ν =1/2, $\nu = 0$ or $\nu = 1$.

2.3 Fluctuation corrections to the magnetization.

Let us now consider the influence of the fluctuations on the stability of the antiferromagnetic ordered states. We have in mind Anderson's idea [Anderson 1973] that strong quantum fluctuations may generate novel spin liquid ground states. Since we have derived the classical phase diagram and specified the possible ordered states by a given ordering wave vector $\mathbf{Q}$, we can analyze the zero-point fluctuations around those ordered states. We can derive the sub-lattice magnetization per spin and include the effects of fluctuations by taking

$$\langle S_i^z \rangle = S - \langle a_i^\dagger a_i \rangle \tag{2.27}$$

or equivalently,

$$\langle m \rangle = S - \frac{1}{N} \sum_{\mathbf{k}} \langle a_{\mathbf{k}}^\dagger a_{\mathbf{k}} \rangle \tag{2.28}$$

We can use the relation (2.21), and write down the product of operators. In the linear spin wave approximation, the quasiparticles created by $\alpha_{\mathbf{k}}$ and $\alpha_{-\mathbf{k}}$ represent a fully decoupled system in which the particle number is conserved. That means that we have $\langle \alpha_{\mathbf{k}} \alpha_{-\mathbf{k}} \rangle = \langle \alpha_{\mathbf{k}}^\dagger \alpha_{-\mathbf{k}}^\dagger \rangle = 0$. If we do this, we end up with one expression like

$$\langle a_{\mathbf{k}}^\dagger a_{\mathbf{k}} \rangle = \sinh^2 \theta_{\mathbf{k}} + \langle \alpha_{\mathbf{k}}^\dagger \alpha_{\mathbf{k}} \rangle \cosh^2 \theta_{\mathbf{k}} + \langle \alpha_{-\mathbf{k}}^\dagger \alpha_{-\mathbf{k}} \rangle \sinh^2 \theta_{\mathbf{k}}. \tag{2.29}$$

The $\alpha_{\mathbf{k}}$ and $\alpha_{-\mathbf{k}}$ quasiparticles are non-interacting Bosons. Therefore, the expectation values of their occupation number operators are the Bose–Einstein distribution functions. To calculate the magnetization, we convert the sum in eq.(2.28) into an integral over the Brillouin zone for the BCT lattice and perform the corresponding numerical calculation. In Fig.(2.4), we present the respective result for m for each AF phase, at T $\simeq 0$ and for $S = 1/2$, as a function of p_2, when p_3 is a given value on the critical line. For $p_2 < 0.93$ the magnetization is a decreasing function and above this point it becomes negative, suggesting the possible existence of a disordered phase. However, the existence of the AF phase $\mathbf{Q}_{\rm inc}^{\rm II}$ in this region prevents the formation of this disordered state.

The next step is the calculation of the S_c, that is the S value at which the spin wave excitation starts to become unstable. We are interested in the T $\simeq 0$ limit and in the case in

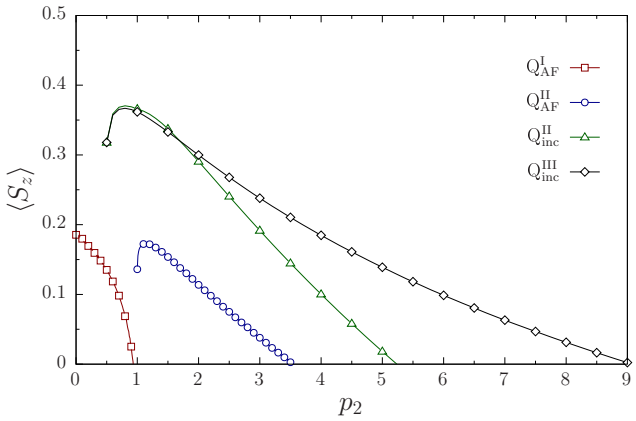

Figure 2.4: The magnetization phase diagram as a function of $p_2 = J_2/J_1$ for $S = 1/2$, when p_3 is defined in the critical lines. The quantum corrections to the magnetization diverges as $p_2 \to \infty$ for Q^{II}_{inc}. For values of $p_2 < 0.93$ the magnetization is a decreasing function and it becomes negative after this point. This suggest that the possibility of having a quantum disordered state, like spin liquids [Anderson 1973, Chandra 1988]. However, the presence of the incommensurate orders that are still AF, for values of $0.93 < p_2 < 1.0$ prevents the formation of such disordered state.

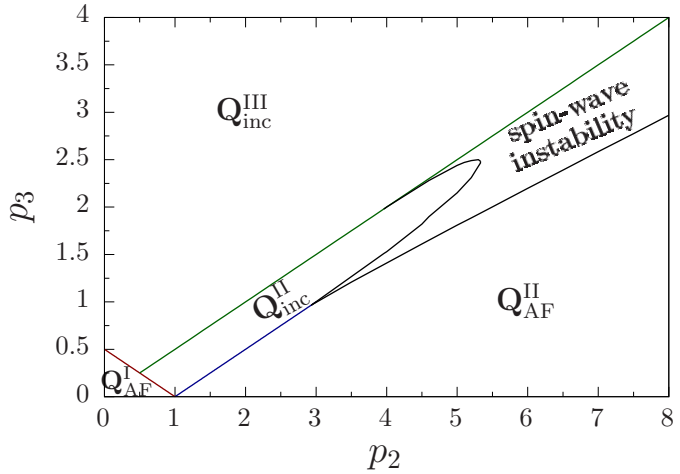

Figure 2.5: The classical phase diagram modified to show the region where spin wave theory becomes unstable for $S = 1/2$.

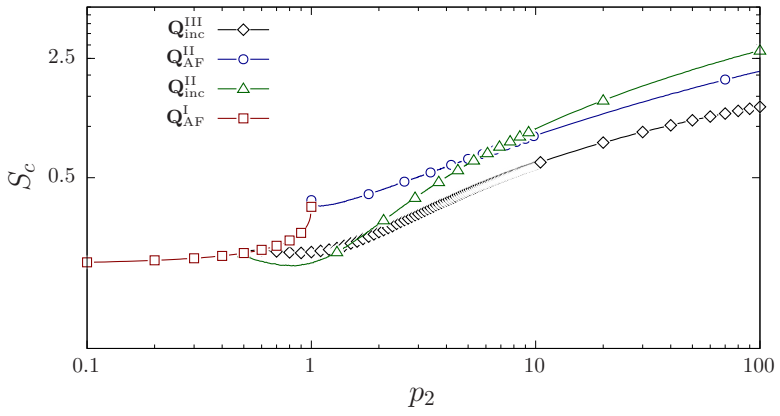

Figure 2.6: The critical value for S_c as a function of p_2, when p_3 is defined in the critical lines. The scale in the axis are logarithmic in order to see the asymptotic behaviour for large p_2.

which the magnetization vanishes. Therefore, it turns out that

$$S_c = -\frac{1}{2} + \int_{BCT} \frac{d^3k}{64\pi^3} \frac{\Omega^+_{\mathbf{k}} + \Omega^-_{\mathbf{k}}}{\sqrt{\Omega^+_{\mathbf{k}}\Omega^-_{\mathbf{k}}}} \tag{2.30}$$

Once again, by performing numerical calculations, we calculate S_c considering each phase as a function of p_2 when p_3 is approaching the critical line. The result is plotted in Fig.(2.6). Unlike the 2D case, the fluctuation corrections do not diverge [Chandra 1988]. We call attention to the fact that, in the 3D case, frustration can relatively increase the critical value of S below which the linear spin-wave correction cancels the staggered magnetization, i.e., $S_c \equiv \Delta m(p_2, p_3)$. Indeed, for a fixed p_2 , we find that S_c increases when p_3 approaches its critical value associated with the classical phase boundary. This maximal value is plotted in the inset of Fig(2.6) as a function of p_2 for the continuous $\mathbf{Q}^{\mathrm{II}}_{\mathrm{AF}}/\mathbf{Q}^{\mathrm{II}}_{\mathrm{inc}}$ transition and on each side of the discontinuous $\mathbf{Q}^{\mathrm{II}}_{\mathrm{inc}}/\mathbf{Q}^{\mathrm{III}}_{\mathrm{inc}}$ transition. On each of these critical lines, we find $S_c \sim \sqrt{p_2}$ for large p_2. Furthermore, a logarithmic $S_c \sim \ln(p_2/2 - p_3)$ and a power law $S_c \sim 1/\sqrt{p_3 - p_2/2}$ are respectively obtained at large p_2 in the vicinity of the $\mathbf{Q}^{\mathrm{II}}_{\mathrm{inc}} \to \mathbf{Q}^{\mathrm{III}}_{\mathrm{inc}}$ and of the $\mathbf{Q}^{\mathrm{III}}_{\mathrm{inc}} \to \mathbf{Q}^{\mathrm{II}}_{\mathrm{inc}}$ transitions. This results is consistent with the square lattice spin wave analysis present elsewhere [Chandra 1988].

These results tell us that the SW approach reveals some weaknesses of the present magnetic orders, but the three-dimensionality protects these states against small fluctuations at the lowest linear order. To go beyond this approach we must study the possible instabilities emerging from the next orders in the $1/S$ expansion and consider the interactions between the spin-wave bosonic excitations. However, it has been shown for a two-dimensional lat-

tice that the second-order correction can indeed increase considerably the magnitude of the sub-lattice magnetization, although first-order perturbation produce a decreases in the magnitude [Igarashi 2005]. It is thus possible that the series oscillates and this may be a general characteristic of SW expansion in our model. Therefore, stabilizing a spin-liquid state seems to require going beyond second order when invoking a perturbation approach from classical order. We leave this aside, and we now turn to the analysis of possible non-magnetic phases in our model using the algebraic spin liquid approximation.

2.4 Algebraic spin liquid.

2.4.1 Generalized SU(n) symmetric approach.

It was suggested by P. W. Anderson [Anderson 1987] that small spin values, low spatial dimensions, and large frustration are the three main ingredients for the melting of magnetic long range order and for the emergence of exotic spin liquid ground state. There is increasing evidence that quantum effects play a major role in the low-temperature properties of various classes of magnetic systems. In this section we analyze the possibility that the spin forms a resonating valence bond state with fermionic excitations and SL correlations [Fazekas 1974]

The physical motivations for this study are the unconventional physical phenomena exhibited by metallic systems with BCT structure. In several of these correlated systems, the magnetic degrees of freedom seems to be "deconfined " into fermionic modes that may actually contribute to the existing of the Fermi surface, unlike weakly coupled bosons. This situation, which also might occur in high-T$_c$ superconductors [Anderson 1987, Wen 1996], could be easily strengthened by a coupling of the Heisenberg spin of J_1-J_2-J_3 model to extra charge degrees of freedom. We study the possible fermionic "deconfinement" of spin operators as an intrinsic property of the Heisenberg model.

Once again, we take the Heisenberg Hamiltonian, for S = 1/2, and generalize it to its SU(n)-symmetric form[2].

$$H_n = \sum_{i,j} \frac{J_{ij}}{n} \sum_{\sigma,\sigma'} \chi^{\dagger}_{i,\sigma} \chi_{i,\sigma'} \chi^{\dagger}_{j,\sigma'} \chi_{j,\sigma}, \tag{2.31}$$

where $\chi^{\dagger}_{i,\sigma}$ and $\chi_{i,\sigma}$ are fermionic creation and annihilation operators in a site i and spin degeneracy $\sigma = 1, ..., n$, which are subject to the local constraints $\sum_{\sigma} \chi^{\dagger}_{i,\sigma} \chi_{i,\sigma} = n/2$. This is

[2]This work was carried out by C. Thomas in collaboration to [Farias 2016]. In this part, we do not driven much attention to specific calculations, and only concentrate in the results.

a standard SU(n) generalization [Affleck 1988a] of the fermionic representation developed by Abrikosov for $n = 2$. The scaling factor $1/n$ ensures that the energy remains finite at the large-n limit.

In order to take into account the SL correlations, the Hubbard-Stratonovich decoupling [Pépin 2011, Thomas 2013], is used to introduce two kinds of order parameters[3]:

- the local magnetization field:

$$m_i^\sigma = \langle \chi_{i,\sigma}^\dagger \chi_{i,\sigma} \rangle - \frac{1}{2}, \tag{2.32}$$

- the inter-site SL field:

$$\varphi_{ij} = -\frac{1}{n} \sum_\sigma \langle \chi_{i,\sigma}^\dagger \chi_{j,\sigma} \rangle. \tag{2.33}$$

The purely magnetic mean-field approximation is described by the staggered magnetization $m_i^\sigma = \pm S_{\mathbf{Q}}$ and which is completely equivalent to the one obtained in the large S limit. The corresponding ground state phase diagram is once again given by Fig.(2.2).

The stability of the various possible magnetic phases can be analyzed by testing different SL *ansätze* as possible alternatives for the ground state. Generalizing the modulated SL (MSL) order [Thomas 2013], we consider the nearest-neighbor inter-site correlations

$$\varphi_{ij}^1 = \frac{1}{2}[\Phi_1 + ie^{i\mathbf{Q}_{\mathrm{AF}}^{\mathrm{I}} \cdot \left(\frac{\mathbf{R}_i + \mathbf{R}_j}{2}\right)} \Phi_M], \tag{2.34}$$

$$\varphi_{ij}^2 = \Phi_2, \tag{2.35}$$

$$\varphi_{ij}^3 = \Phi_3, \tag{2.36}$$

with a bond index definition similar to that exhibited in Fig.(2.1). The three kinds of spin liquid patterns are shown in Fig.(2.7).It depicts Φ_2 and Φ_3 as two-dimensional correlations as in square lattice. Finally, we also have the interplane correlation ϕ_{ij}^1, represented by dashed lines which $\phi_{ij}^1 = \Phi_1 + \Phi_M$ and $\phi_{ij}^1 = \Phi_1 - \Phi_M$ bond modulations represented by solid lines.

The free energy per spin component and per lattice site is written as

$$F = F_0 - \frac{k_B T}{32\pi^3} \int_{BCT} d^3k \sum_{s=\pm} \ln(1 + e^{-\frac{E_{\mathbf{k}}^s}{k_B T}}) - \frac{\lambda_0}{2} \tag{2.37}$$

[3]The detailed Mean field decoupling can be seen in A.3

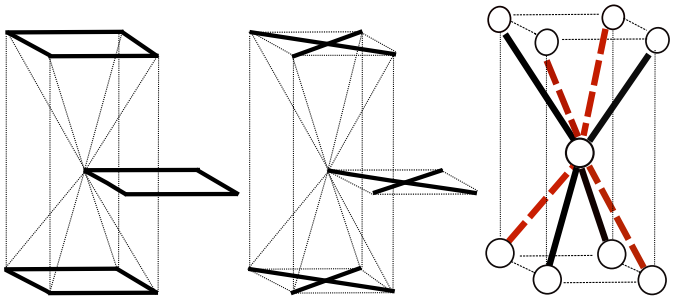

(a) Φ_2 (b) Φ_3 (c) MSL

Figure 2.7: The three kinds of inter-site spin liquids correlations on the BCT structure. (**a-b**) For Φ_2 and Φ_3, have two-dimensional character as in square lattice. Φ_3 is a long-range ordered modulation. (**c**) The inter-plane correlation. Dashed lines represent $\Phi^1_{ij} = \Phi_1 + \Phi_M$ and solid lines represent $\Phi^1_{ij} = \Phi_1 - \Phi_M$ the bond modulation.

Where λ_0 denotes the Lagrange multiplier that minimizes F in order to satisfy the fermionic occupation constraint. The mean field AF ordering state has $F_0 = -\frac{2J(\mathbf{Q})}{n}|S_\mathbf{Q}|^2$ with dispersion $E^\pm_\mathbf{k} = \lambda_0 \pm \frac{J(\mathbf{Q})}{n} S_\mathbf{Q}$. For the SL states we find, accordingly

$$\frac{F_0}{J_1} = |\Phi_1|^2 + |\Phi_M|^2 + 2p_2|\Phi_2|^2 + 2p_3|\Phi_3|^2, \tag{2.38}$$

and the dispersion

$$\frac{E^\pm_\mathbf{k} - \lambda_0}{J_1} = 2p_2\gamma_2(\mathbf{k})\Phi_2 + 4p_3\gamma_3(\mathbf{k})\Phi_3 \pm 4\sqrt{(\gamma_1(\mathbf{k})\Phi_1)^2 + (\gamma_\mathrm{M}(\mathbf{k})\Phi_\mathrm{M})^2}. \tag{2.39}$$

The real term Φ_M does not have the periodicity of the BCT lattice. The term $\gamma_\mathrm{M}(\mathbf{k}) = \sin(k_x/2)\sin(k_y/2)\sin(k_z/2)$[4] takes into consideration a possible spatial amplitude modulation of the SL field. The numerical analysis consists basically in solving self-consistently the mean-field parameters for each AF or SL state. The most stable solution is selected by the minimization of the free energy, eq.(2.37). The MSL phase is a BCT adaptation of the "kite" phase investigated in [Affleck 1988a] on a square lattice. We also tested another non-homogeneous "flux" phase with the SL character, i.e., a chiral state with complex $\varphi^1_{ij} = (\varphi^1_{ji})^*$ (see Fig.3.1(d)), that could be described using the same formalism, but with the replacement $\gamma_M(\mathbf{k}) \to \sin(q_x/2)\sin(q_y/2)\cos(q_z/2)$. This chiral SL was found to have a higher energy than the MSL.

[4]This expression is derived in appendix B. For the moment it will be sufficient to say that it can be obtained from the Fourier transform of the Hamiltonian H_n after the mean field decoupling.

2.4.2 The phase diagram for large n.

For $n \leqslant 3$ we find purely AF ground states, and for $n \geqslant 10$ the most stable states are SL characterized by finite values of either Φ_M, Φ_2, or Φ_3. At mean-field level, these three SL parameters do not coexist. Furthermore, we remark that the transition between the MSL and the Φ_2-dominated SL phases is first order. Beyond mean field, we expect that only the SL critical temperature associated with a non-zero Φ_M still corresponds to a phase transition signalled by the translation symmetry breaking. For $4 \leqslant n \leqslant 9$, we find a rich phase diagram exhibiting AF and SL quantum phase transitions that are controlled by J_1-J_2-J_3 parameters, as illustrated in (phase diagram of large n). Increasing n, the AF-SL instability shows up first within the $\mathbf{Q}^{\text{II}}_{\text{inc}}$ phase. Furthermore, comparing the large-S phase diagram in Fig.(2.8) obtained for $n = 4$ (phase diagram of large n), one observes that the $S_c = 1/2$ spin-wave instability is located in the same region where the 2-dominant state becomes stabilized. Moreover, going beyond the specificity of the associated order parameters, the phase diagram of large n indicates that the SL instability "propagates" from large-p_2 (Φ_2) to smaller-p_2 (MSL) areas if we increase the value of n.

2.4.3 The modulated spin liquid phase.

An interesting feature also appears for the MSL solution: with a relatively high numerical accuracy the modulation field Φ_M is found to be always equal to the homogeneous field Φ_I. This leads to a very extreme situation for the interlayer $\varphi^1_{ij} = \frac{1}{2}[\Phi_1 \pm \Phi_M]$ which vanishes on half of the bonds while it keeps its finite value $\Phi_1 = \Phi_M$ on the other bonds. Introducing the probability $p^{singlet}_{ij}$ that a given bond $\mathbf{R}_i\mathbf{R}_j$ forms a singlet, the formation of the MSL state can be interpreted here as follows: first, for all the interlayer bonds such that $\mathbf{Q}^{\text{I}}_{\text{AF}} \cdot (\mathbf{R}_i + \mathbf{R}_j)/2 = \pi/2$, the interaction terms are effectively decoupled at mean-field level, leading to $p^{singlet}_{ij} = 1/4$ and $\langle \mathbf{S}_i \cdot \mathbf{S}_j \rangle = 0$. Then the SL with $\langle \mathbf{S}_i \cdot \mathbf{S}_j \rangle \neq 0$ is formed on the other interlayer bonds, with $\mathbf{Q}^{\text{I}}_{\text{AF}} \cdot (\mathbf{R}_i + \mathbf{R}_j)/2 = -\pi/2$, that remain effectively coupled. Using the numerical value $\Phi_1 = \Phi_M \approx 0.45$ computed at T = 0 in the MSL, we find that $p^{singlet}_{ij} \approx 0.60$ on these effectively coupled bonds. This value has to be compared with the value $\ln(2) \approx 0.69$ that is predicted for a one-dimensional Heisenberg chain by using exact methods, like Bethe ansatz or DMRG [Schollwöck 2005]. We may thus interpret the MSL as a crystal of interacting filaments formed by the connected effectively coupled bonds (2.8.d). In this picture, spin excitations are deconfined fermions moving along these filaments. This may generalize the usual concept of valence-bond crystal [Lacroix 2011] where localized spin-1 excitations correspond to confined fermions.

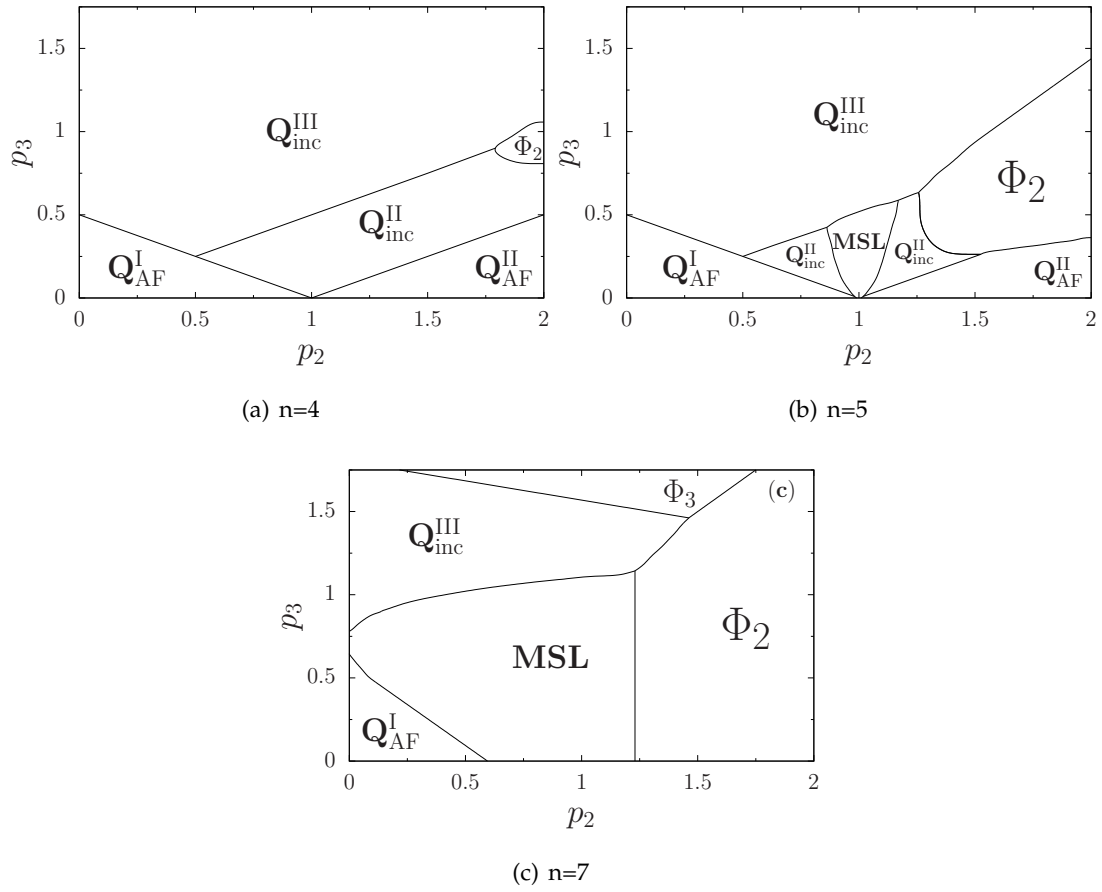

Figure 2.8: **(a-c)** Ground-state phase diagram of the $J_1 - J_2 - J_3$ model in coordinates (p_2, p_3) computed self-consistently for different values of n.

2.5 Summary.

In conclusion, we considered a model with only localized spins. However, charge fluctuations play a crucial role in destabilizing AF states in heavy fermions and cuprates. In the context of the cuprates, the AF phase of the insulating parent compounds corresponds to $\mathbf{Q}^{\mathrm{II}}_{\mathrm{AF}}$. The SL phase introduced by Anderson *et al.* [Fazekas 1974, Anderson 1987, Baskaran 1987] corresponds to the homogeneous correlated state associated here with Φ_2. Stabilizing a SL state in 3D is commonly thought to be more tricky in view of the fact that the corresponding linear SW correction remains finite within a large-S approach. Nevertheless, we show how frustration in the BCT lattice can enhance the critical value S_c that, in some sense, characterizes the weakness of AF order against SW fluctuations. In connection with this weakening, we could identify various SL phases that can be stabilized when n is larger than a relatively small critical value.

We also notice the possible emergence of stable SL phases in cubic lattices that has also

been proposed recently [Laubach 2016, Farnell 2016]. This opens new perspectives for the realization of unconventional electronic quantum orderings in 3D systems. In particular, our results suggest that materials, like URu_2Si_2, with BCT-lattice structure, have the feature of manifesting themselves in numerous different phases. Indeed, the very phase diagram depicted in Fig.(2.2) and phase diagram of large n could provide a unifying framework for the understanding and for the analysis of the rich phase diagram of URu_2Si_2.

With respect to the large n analysis, the number n may be considered as an effective parameter related to the electronic orbital degeneracy, which could be phenomenologically increased or decreased by charge fluctuations or crystal-field effects. Considering a given compound, n might also be effectively decreased by applying an external magnetic field. Similarly, a tuning of the model parameters p_2 and p_3 may phenomenologically account for some effects of applied pressure [Thomas 2013]. This scenario could explain two different AF instabilities of the HO phase that are observed experimentally in URu_2Si_2: assuming that the HO is a MSL order and applying a finite pressure this corresponds to increasing J_1 for a fixed n (see Fig. 2.8), leading to a commensurate AF instability characterized by $\mathbf{Q}^{\mathrm{I}}_{\mathrm{AF}}$, as observed experimentally [Palstra 1985, Mydosh 2011]. Alternatively, applying a magnetic field without pressure corresponds to lowering the effective value of n for fixed p_2 and p_3: the MSL (HO) is destabilized to an incommensurate AF. Interestingly, by using different numerical values of J_1, J_2 , and J_3 obtained from different fits of inelastic-neutron-scattering data, our scenario predicts an instability from MSL to $\mathbf{Q}^{\mathrm{III}}_{\mathrm{inc}} = (\Upsilon_3, 0, 0)$ with $\Upsilon_3 \approx 0.69$ [Broholm 1991], 0.66 [Kusunose 2012]. This scenario could be tested experimentally since it predicts that the AF order $\mathbf{Q}^{\mathrm{III}}_{\mathrm{inc}}$ could be continuously tuned to $\mathbf{Q}^{\mathrm{I}}_{\mathrm{AF}}$ by applying pressure on URu_2Si_2 under a high magnetic field.

This SL mechanism driven by frustration on the BCT lattice may also be tested for the heavy-fermion URu_2Si_2. The possible formation of a MSL could also give rise to a commensurately ordered pairing that would break the BCT symmetry down to simple tetragonal. Such a modulated pairing scenario could be tested with the superconducting instability observed for this compound inside the HO phase. Alternatively, even if the chiral SL order was found here to be less stable than the MSL, an opposite result could occur if we include charge fluctuations.

Chapter 3

Raman signatures of electronic states in URu_2Si_2.

In the last chapter, we saw that spin liquids states may arise as an alternative to the long-range magnetic order in BCT structures. We also made clear that the presence of frustration is a key ingredient to stabilize those new kinds of phases. Our aim now is to develop an effective theory which incorporates these varieties of states. Our starting point is a two band effective Hamiltonian that it is able to generate the phases of interest by systematic variation of a small number of parameters [Das 2012, Das 2014, Oppeneer 2011]. Afterwards, we want to relate our effective theory with Raman scattering experiments performed at the hidden-order phase of URu_2Si_2 [Buhot 2014]. The effective theory describes the possible emergent phases in a BCT lattice without making any assumption about the specific order parameter. Instead, we assume that the HO phase has something to do with a particular choice of space group.

In this context we follow Harima-Miyake-Flouquet [Harima 2010] who have suggested earlier on that the second order phase transition from the PM phase to the HO is directly related to a change in the point group symmetry. In the PM phase, the BCT lattice belongs to the space group No 139 ($I4/mmm$), with a local point group D_{4h}. When entering the HO phase, the ST lattice belongs to the new space group No 136 ($P4_2/mnm$, D_{2h}). This leads to the loosing of C_4 rotation (rotation by $\pi/2$) at the U site. This lower of symmetry is a consequence of the Coulomb interaction between the localized $5f$ electrons and it does not require any lattice distortion, but the charge distortion at the U site. As a consequence, the charge distribution inside the HO phase also changes, although this is difficult to be detected by the existing experimental techniques.

This consensual change in the lattice structure when passing from the PM phase to the

HO regime reflects itself in other physical properties. The folding in the Brillouin zone along the c axis of the BCT was observed in several experiments [Buhot 2014, Boariu 2013, Hassinger 2010]. It places the Z point on top of the Γ point of the Brillouin zone as expected when a transition from a BCT to an ST lattice takes place. By changing the lattice structure, one instability on the Fermi surface develops, and this produces a pseudogap in some regions of k-space [Maple 1986, Elgazzar 2009, Boariu 2013, Tonegawa 2012].

When dealing with space group or point group symmetry representation, sometimes it is convenient to work with its irreducible representation of the lattice symmetry group. This feature is applicable as soon as optical investigations are under consideration, specifically in the context of Raman scattering experiments [Devereaux 2007]. Here the emphasis is given to the types of space groups that represent the spin liquid order introduced before, i.e., the modulated spin liquid. The effect of the breaking of lattice symmetry is implicit in the periodic modulation in the density of electronic spins. We also discuss the possible existence of a second kind of spin liquid, the so-called chiral spin liquid. Each state is associated with a particular space group signaled by some specific parameter. All of these possible ordered phases break the lattice translation symmetry in the same way, which is also a remarkable feature of the phase transition from PM to HO phase of the URu_2Si_2. The next section is devoted to describe the Hamiltonian of our model and to explain how we incorporate all those different phases into it.

3.1 The Hamiltonian of effective model.

In order to construct a model which displays different ordering phases as candidates for hidden order in URu_2Si_2, we have to take into account experimental features that are well established.

First, the low-pressure experiments performed at the HO phase show clearly that it is not an AF phase, but at pressures above $P_x \sim 0.5$ GPa, the HO suffers a first-order transition and the long-range antiferromagnetic order is established with wave vector $\mathbf{Q}_{\mathrm{AF}} = \{0, 0, 1\}$ that corresponds to a lattice doubling along c-axis. Inelastic neutron scattering experiments performed at the HO phase characterized this state by the presence of a sharp resonance at wave-vector $\mathbf{Q}_0 = \{1, 0, 0\}$, which is equivalent to $\mathbf{Q}_0 = \{0, 0, 1\}$ [Villaume 2008]. Going through the AF phase leads to the collapse of the resonance and to the observation of an inelastic neutron magnetic signal at $\mathbf{Q}_{\mathrm{AF}}$ [Harima 2010]. Thus, it is reasonable to search for a model that accounts for this change in the lattice structure while, switching from the HO to the AF by applying pressure, induces supplementary time-reversal

symmetry breaking, as is the case for an onset of antiferromagnetic ordering.

Angle-resolved photo-emission spectroscopy (ARPES) demonstrated that there is a Fermi surface instability of the itinerant quasiparticles taking part in the PM to HO transition. The HO phase is also accompanied by a remarkable symmetry change of the electronic structure and this is consistent with the periodicity characterized by the commensurate vector $\mathbf{Q}_0$ [Bareille 2014]. Density-functional theory (DFT) calculations investigate the Fermi surface properties of URu_2Si_2. Their results conclude that there is a strong nesting between portions of the Fermi surface which are linked to each other by wave vector $\mathbf{Q}_0$ [Oppeneer 2011]. Effects of interaction between two FS sectors leads to hybridization, FS gaping and lattice symmetry breaking.

Here, we construct a two band effective theory that is based on a simple tight-binding-like Hamiltonian of spinless fermions which can be used to characterize the HO phase. A similar two-band model was recently used to describe the Raman signatures in iron-arsenide based superconductors with strong Fermi surface nesting [Yang 2014]. A tight-binding effective model was also proposed for a spin-orbit density wave as a candidate to explain the HO in URu_2Si_2 [Das 2014, Oppeneer 2011].

One crucial ingredient to building an effective model for URu_2Si_2 is the underlying lattice symmetry. In the PM phase, the lattice structure is BCT symmetric, but the HO lowers the symmetry to simple tetragonal (ST). This lowering of symmetry can be characterized by a nesting of the BCT Fermi surface with $\mathbf{Q}_0 = \{0, 0, 1\}$

With this assumption, we write the Hamiltonian as

$$H = \sum_i (E_0 + me^{i\mathbf{Q}\cdot\mathbf{R}_i}) c_i^\dagger c_i + \sum_{\langle i,j \rangle} t_{ij} c_i^\dagger c_j. \tag{3.1}$$

The operators $c_i^\dagger$ and c_i are the creation and annihilation of spinless fermions at a given site i with position $\mathbf{R}_i$. The parameter E_0 adjust the chemical potential. The hopping t_{ij} connects nearest neighbors on the BCT lattice, but they may break BCT lattice symmetry down to simple tetragonal lattice symmetry.

We start in the framework of a regular paramagnetic state where the system has its structure defined by the space group No 139 ($I4/mmm$, D_{4h}). We assume that it can pass from this regular state to a new phase defined with three different space groups symmetries which could be associated with the No 123 ($P4/mmm$, D_{4h}), the No 126 ($P4/nnc$, D_4) or the No 128 ($P4/mnc$, C_{4h}). Also those point symmetry groups D_4 and C_{4h} have the same selection rules and also they are subgroups of point group D_{4h} [Harima 2010]. We introduce appropriate parameters that capture the characteristics of these ordered states.

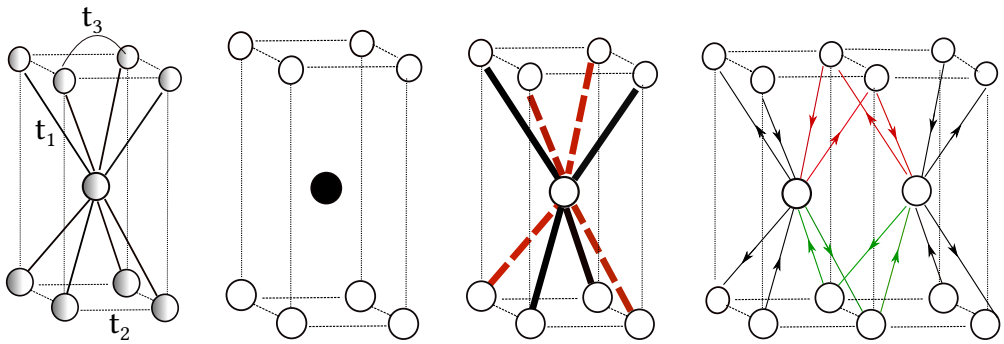

Figure 3.1: The four possible ordered states that are considered in our model. Figure (**a**) shows the paramagnetic phase, that displays the full BCT lattice structure with space group No 139. In Fig.(**b**) we represent an states that breaks lattice translation symmetry and results in to two sub-lattices that reduces the BCT down to ST lattice. This phase is characterized by the space group symmetry No 123. Figure(**c**), we represent the modulated SL phase, associated with the space group No 126. Figure (**d**), the chiral SL phase, that is related to the space group No 128.

1. The space group No 123 ($P4/mmm$), with $\mathbf{Q}$ being an ordering wave vector characterizing one modulation

$$me^{i\mathbf{Q}\cdot\mathbf{R}_i}, \tag{3.2}$$

   This parameter can account for some local Kondo hybridization or a charge-density wave or, in the last case, an staggered magnetization.

2. The space group No 128 ($P4/mnc$) characterizes a chiral spin liquid phase:

$$t_{ij} = t_1 \pm i\Delta_c. \tag{3.3}$$

3. The space group No 126 ($P4/nnc$) characterizes a modulated spin liquid phase:

$$t_{ij} = t_1 \pm \Delta_M. \tag{3.4}$$

Since the c's operators here represent fermions, the magnetic states, specified for the parameter m, is justified by the fact that fermions here are like spinons in a deconfined phase which have an intrinsic magnetic moment. This also leads to the formation of SL phases because the spinons can be seem as the elementary excitations in this phase which posses the character of being fractionalized [Kitaev 2006].

We have seen in the previous chapter that the various wave vectors characterize different magnetic ordered ground states on the BCT lattice. Here, we consider only $\mathbf{Q} = \mathbf{Q}^{\mathrm{I}}_{\mathrm{AF}}$

because of the experimental evidence from INS [Bourdarot 2010] that both AF and HO phases break BCT lattice symmetry to the simple tetragonal lattice symmetry with an wave vector $\mathbf{Q}_0 = \mathbf{Q}^{\mathrm{I}}_{\mathrm{AF}}$. By using $me^{i\mathbf{Q}\cdot\mathbf{R}_i}$, to characterize a given phase that breaks the lattice translation symmetry, we assume that the fermions at $\mathbf{k}$ band are coupled to fermions at $\mathbf{k}+\mathbf{Q}$ band by the particular wave vector $\mathbf{Q}$ [Yang 2014, Ványolos 2005].

The hopping parameter t_{ij} can be either complex or real. If it is complex, the imaginary part is associated with the parameter Δ_c. The choice of the sign relates itself to the orientation of the link between two sites. In approaching a site, we consider a plus sign in eq.(3.3) or if the link leaves the site is a minus, see Fig.3.1(d)). If t_{ij} is real, we add the term Δ_m for first inter-plane neighbors, which corresponds to the MSL phase that is schematically illustrated in Fig.3.1(c). The choice of the sign plus, in eq.(3.4), represents a full line and if it is the minus sign it represents a dotted line. The other real cases are $t_{ij} = t_2$ for first neighbors in-plane and $t_{ij} = t_3$, for the second neighbors in-plane, see Fig.3.1(a). Indeed in this work, we do not investigate the in-plane ordering.

Using the Fourier transforms for the creation and annihilation operators

$$c_i^{\dagger}=\frac{1}{\sqrt{N}}\sum_{\mathbf{k}} e^{-i\mathbf{k}\cdot\mathbf{R}_i}c_{\mathbf{k}}^{\dagger} \tag{3.5}$$

$$c_i=\frac{1}{\sqrt{N}}\sum_{\mathbf{k}} e^{i\mathbf{k}\cdot\mathbf{R}_i}c_{\mathbf{k}}, \tag{3.6}$$

where the sum in k runs over the first Brillouin zone of the BCT lattice, we write down the Hamiltonian in a matrix representation with a folded Brillouin zone from the BCT to the Simple Tetragonal (ST) lattice. The Hamiltonian in second quantized form becomes

$$\hat{H}=\sum_{\mathbf{k}} \Psi_{\mathbf{k}}^{\dagger} h_{\mathbf{k}} \Psi_{\mathbf{k}}, \tag{3.7}$$

with the sum over k now running over the first Brillouin zone of the tetragonal (T) lattice (see a more detailed calculation in appendix B). Using

$$\Psi_{\mathbf{k}}=\begin{pmatrix} c_{\mathbf{k}} \\ c_{\mathbf{k}+\mathbf{Q}} \end{pmatrix}, \tag{3.8}$$

$$h_{\mathbf{k}}=\begin{pmatrix} \varepsilon_{\mathbf{k}} & V_{\mathbf{k}}^{*} \\ V_{\mathbf{k}} & \varepsilon_{\mathbf{k}+\mathbf{Q}} \end{pmatrix}, \tag{3.9}$$

It follows that the $E_{\mathbf{k}}$ eigenvalues give us the dispersion in the form

$$E_k^{\pm}=\frac{\varepsilon_{\mathbf{k}}+\varepsilon_{\mathbf{k}+\mathbf{Q}}}{2} \pm \sqrt{|V_{\mathbf{k}}|^2+\left(\frac{\varepsilon_{\mathbf{k}}-\varepsilon_{\mathbf{k}+\mathbf{Q}}}{2}\right)^2}. \tag{3.10}$$

with the specific relations $\varepsilon_{\mathbf{k}} = E_0 + t_1\gamma^1_{\mathbf{k}} + t_2\gamma^2_{\mathbf{k}} + t_3\gamma^3_{\mathbf{k}}$ and $V_{\mathbf{k}} = m + i\Delta_{SL}f_{SL}(\mathbf{k})$, that are present in eq.(3.9), where Δ_{SL} can be Δ_m or Δ_c if we have a modulated or chiral spin liquid, respectively and $f_{SL}(\mathbf{k})$ being defined in the same fashion. The derivation of γ's factors is made in appendix B. The off-diagonal term V_k couples the two bands which are connected by the lattice wave vector $\mathbf{Q}$. As a result it turns out that

$$\gamma^1_{\mathbf{k}} = 8\cos\left(\frac{k_x a}{2}\right)\cos\left(\frac{k_y a}{2}\right)\cos\left(\frac{k_z c}{2}\right) \tag{3.11}$$

$$\gamma^2_{\mathbf{k}} = 2(\cos(k_x a) + \cos(k_y a)) \tag{3.12}$$

$$\gamma^3_{\mathbf{k}} = 4\cos(k_x a)\cos(k_y a) \tag{3.13}$$

$$f_c(\mathbf{k}) = 8\sin\left(\frac{k_x a}{2}\right)\sin\left(\frac{k_y a}{2}\right)\cos\left(\frac{k_z c}{2}\right) \tag{3.14}$$

$$f_m(\mathbf{k}) = 8\sin\left(\frac{k_x a}{2}\right)\sin\left(\frac{k_y a}{2}\right)\sin\left(\frac{k_z c}{2}\right). \tag{3.15}$$

The diagonalization of the Hamiltonian from eq.(3.7) can be performed by using one general representation of the Bogoliubov transformations (see B.2 in appendix). We define

$$\Psi_{\mathbf{k}} = \hat{P}_k \Psi^{diag}_k, \tag{3.16}$$

where

$$\Psi^{diag}_{\mathbf{k}} = \begin{pmatrix} \alpha_{\mathbf{k}} \\ \beta_{\mathbf{k}} \end{pmatrix} \tag{3.17}$$

and

$$\hat{P}_k = \begin{pmatrix} \cos\theta_k & e^{i\varphi}\sin\theta_k \\ -e^{-i\varphi}\sin\theta_k & \cos\theta_k \end{pmatrix} \tag{3.18}$$

The relations for $\cos(\theta_k)$ and $\sin(\theta_k)$ provide the conditions for the θ_k parameter. We find

$$\cos(2\theta_k) = \frac{\varepsilon_k - \varepsilon_{k+Q}}{\sqrt{|V_k|^2 + \left(\frac{\varepsilon_k - \varepsilon_{k+Q}}{2}\right)^2}} \tag{3.19}$$

$$\sin(2\theta_k) = \frac{|V_k|}{\sqrt{|V_k|^2 + \left(\frac{\varepsilon_k - \varepsilon_{k+Q}}{2}\right)^2}} \tag{3.20}$$

$$\tag{3.21}$$

In a similar way, we find that

$$\varphi_k = -(\arg(V_k) \pm \pi) \tag{3.22}$$

Consequently, the Hamiltonian in the diagonal basis is written as

$$\hat{H} = \sum_{\mathbf{k}} \begin{pmatrix} \alpha^\dagger_{\mathbf{k}} & \beta^\dagger_{\mathbf{k}} \end{pmatrix} \begin{pmatrix} E^+_{\mathbf{k}} & 0 \\ 0 & E^-_{\mathbf{k}} \end{pmatrix} \begin{pmatrix} \alpha_{\mathbf{k}} \\ \beta_{\mathbf{k}} \end{pmatrix} \tag{3.23}$$

In chapter 1, we saw that the light can couple either to charge or current degrees of freedom and this allows us to define the charge and current sectors, respectively. The charge sector is related to the density-density correlation function while the current sector is related to the current-current correlation function. To each sector, we can associate a specific vertex which is directly linked with the irreducible point group symmetry of the lattice. In order to clarify this association with point group symmetries and apply this concept in our analysis, let us describe the possible vertices for BCT lattice structure.

3.2 The correlation functions and Raman vertices for the BCT lattice.

Let us present the correlation functions that will be used to compute the Raman response. For simplicity, we assume the small moment transfer limit, which allows us to use the effective mass approximation to calculate Raman vertices for each specific sector with a defined symmetry.

3.2.1 The spinon density sector.

The physical quantity observed experimentally is the Raman scattering cross section. It is determined by the dynamical structure factor $\tilde{S}(\mathbf{q}, i\omega)$, which is directly related to the imaginary part of the Raman response $\tilde{\chi}$ through the fluctuation dissipation theorem

$$\tilde{S}^{\lambda}(\mathbf{q},\omega) = -\frac{1}{\pi}[1 + n_B(\omega)]\mathrm{Im}[\tilde{\chi}^{\lambda}(\mathbf{q},\omega)], \tag{3.24}$$

where $n_B(\omega)$ is the Bose distribution function and λ stands for the specific irreducible point group of the lattice in consideration. The Raman response for the electron system measures the "effective density" fluctuations by

$$\tilde{\chi}^{\lambda}(\mathbf{q}, i\omega_m) = -\frac{1}{\mathcal{V}}\int_0^{\beta} d\tau e^{i\omega_m\tau}\langle T_\tau(\tilde{\rho}^{\lambda}(\mathbf{q},\tau)\tilde{\rho}^{\lambda}(-\mathbf{q},0))\rangle, \tag{3.25}$$

where $\mathcal{V}$ is the volume of the system and $\tilde{\rho}^{\lambda}$ is the effective density operator. It is convenient to decompose this matrix element into basis functions of the irreducible point group of the lattice in accordance with the polarization of the incident and scattered light λ = B_{1g}, A_{1g}, etc [Devereaux 2007]. Using the effective polarization-dependent density [Valenzuela 2013]

$$\hat{\tilde{\rho}}^{\lambda}(\mathbf{q},\tau) = \sum_{\mathbf{k},\alpha,\alpha'} \gamma^{\lambda}_{\alpha,\alpha'}(\mathbf{k}) c^{\dagger}_{\mathbf{k}+\mathbf{q}/2,\alpha}(\tau) c_{\mathbf{k}-\mathbf{q}/2\alpha'}(\tau), \tag{3.26}$$

where $\gamma^{\lambda}_{\alpha,\alpha'}(\mathbf{k})$'s are matrix elements which originate from the second derivatives of the matrix $h_{\mathbf{k}}$. Then, it follows that the density-density correlation function (see appendix B.3) can be written as

$$\tilde{\chi}^{\lambda}(i\omega_m) = \frac{1}{\mathcal{V}}\sum_{\mathbf{k}}\frac{1}{\beta}\sum_{\omega_n}\mathrm{Tr}[\gamma^{\lambda}(\mathbf{k})G_{\mathbf{k}}(i\omega_n + i\omega_m)\gamma^{\lambda}(\mathbf{k})G_{\mathbf{k}}(i\omega_n)], \tag{3.27}$$

where $\mathcal{V}$ is the volume of the system, β is the inverse of temperature, and $\omega_m = 2m\pi/\beta$ and $\omega_n = (2n+1)\pi/\beta$ are bosonic and fermionic Matsubara frequencies, respectively.

For URu_2Si_2, by combining different incident and scattered light polarizations and sample geometries, the Raman scattering can extract informations of the A_{1g}, B_{1g}, B_{2g} and A_{2g} symmetries of the D_{4h} point group. For each one of these representations, we have to write an appropriate vertex. In the effective mass approximation this leads to

$$\gamma^{A_{1g}}(\mathbf{k}) = \frac{\partial^2 h_{\mathbf{k}}}{\partial k_x^2} + \frac{\partial^2 h_{\mathbf{k}}}{\partial k_y^2} \tag{3.28}$$

$$\gamma^{B_{1g}}(\mathbf{k}) = \frac{\partial^2 h_{\mathbf{k}}}{\partial k_x^2} - \frac{\partial^2 h_{\mathbf{k}}}{\partial k_y^2} \tag{3.29}$$

$$\gamma^{A_{2g}}(\mathbf{k}) = \frac{\partial^2 h_{\mathbf{k}}}{\partial k_x \partial k_y} - \frac{\partial^2 h_{\mathbf{k}}}{\partial k_y \partial k_x} \tag{3.30}$$

$$\gamma^{B_{2g}}(\mathbf{k}) = \frac{\partial^2 h_{\mathbf{k}}}{\partial k_x \partial k_y} + \frac{\partial^2 h_{\mathbf{k}}}{\partial k_y \partial k_x}. \tag{3.31}$$

Vertices like the A_{2g} cannot be accessed independently by linear polarizations. Only sums including circular polarizations allows the isolation of the corresponding A_{2g} components.The relation in 3.30 is identically zero. However if we take into account higer order derivatives with respect k-components we could have $\gamma^{A_{2g}}(\mathbf{k}) \neq 0$. The A_{2g} symmetry is usually associate with chiral excitations [Khveshchenko 1994, Devereaux 2007].

3.2.2 The spinon current sector.

Usually resonant contributions are associated with strong correlations, as is the case of the Heisenberg limit of the Hubbard model [Devereaux 2007]. When this is indeed the case, we need to go beyond first order in the perturbative expansion and consider the role of two, three and four point correlation functions. The definition of the current sector is based on the work of resonant features of Raman experiments for the insulating cuprates compounds [Khveshchenko 1994, Liu 1993]. The theory showed that the Raman spectroscopy is a direct tool to investigate electronic current algebra and the chirality of charged excitations which are believed to be important for various mechanisms for high-T_c superconductivity [Laughlin 1988].

However, here we simply compute the two particle correlation function for the current operator. The μ component of the current operator is

$$\hat{j}_\mu(\mathbf{q},\tau) = \sum_{\mathbf{k},\alpha,\alpha'} \tilde{\gamma}^{\mu}_{\alpha\alpha'}(\mathbf{k}) c^{\dagger}_{\mathbf{k}+\mathbf{q}/2,\alpha}(\tau) c_{\mathbf{k}-\mathbf{q}/2,\alpha'}(\tau), \tag{3.32}$$

where $\hat{j}_\mu = \hat{\mathbf{j}}\cdot\boldsymbol{\mu}$, with $\boldsymbol{\mu}$ being an unitary vector along some coordinate (x, y, z), and $\tilde{\gamma}^{\mu}(\mathbf{k}) = \partial h_{\mathbf{k}}/\partial k_\mu$. We can write down the current-current correlation function as

$$\tilde{\chi}_{\mu\nu}(\mathbf{q}, i\omega_m) = -\frac{1}{\mathcal{V}} \int_0^\beta d\tau e^{i\omega_m \tau} \langle T_\tau \hat{j}_\mu(\mathbf{q},\tau) \hat{j}_\nu(-\mathbf{q},0)\rangle \tag{3.33}$$

Although the vertices are different now, the procedure of calculate this correlation function follows what we did in the previous section. Once again we consider the effective mass approximation in which $\mathbf{q} \to 0$ and if we proceed with similar calculations of appendix B.3, we find that,

$$\tilde{\chi}_{\mu\nu}(i\omega_m) = \frac{1}{\mathcal{V}} \sum_{\mathbf{k}} \frac{1}{\beta} \sum_{\omega_n} \mathrm{Tr}[\tilde{\gamma}^{\mu}(\mathbf{k}) G_{\mathbf{k}}(i\omega_n + i\omega_m) \tilde{\gamma}^{\nu}(\mathbf{k}) G_{\mathbf{k}}(i\omega_n)] \tag{3.34}$$

In order to extract the signal of a particular symmetry we have to specify the components of all derivatives. For example for the BCT lattice the correlation function for the irreducible symmetries A_{1g}, B_{1g} and B_{2g} are, respectively

$$\tilde{\chi}^{A_{1g}}(i\omega_m) = \tilde{\chi}_{xx}(i\omega_m) + \tilde{\chi}_{yy}(i\omega_m) \tag{3.35}$$

$$\tilde{\chi}^{B_{1g}}(i\omega_m) = \tilde{\chi}_{xx}(i\omega_m) - \tilde{\chi}_{yy}(i\omega_m) \tag{3.36}$$

$$\tilde{\chi}^{B_{2g}}(i\omega_m) = \tilde{\chi}_{xy}(i\omega_m) + \tilde{\chi}_{yx}(i\omega_m) \tag{3.37}$$

We have only to specify which components of k_μ or k_ν we are taking in the derivatives and perform our calculations. However, in this approach we do not have any signal for A_{2g} symmetry. What we have to do is to consider a different correlation function.

If we define an operator that is proportional to the equal time current-current commutator, such that,

$$\hat{M}_{\mu\nu}(\mathbf{q},\tau) = [\hat{j}_\mu(\mathbf{q},\tau), \hat{j}_\nu(\mathbf{q},\tau)], \tag{3.38}$$

We can extract the signal for A_{2g} by computing the following correlation function

$$\tilde{\chi}^{A_{2g}}(\mathbf{q}, i\omega_m) = -\frac{1}{\mathcal{V}} \int_0^\beta d\tau\, e^{i\omega_m \tau} \langle T_\tau \hat{M}^{A_{2g}}(\mathbf{q},\tau) \hat{M}^{A_{2g}}(-\mathbf{q},0)\rangle, \tag{3.39}$$

where $\hat{M}^{A_{2g}}(\mathbf{q},\tau) = \hat{M}_{xy}(\mathbf{q},\tau) - \hat{M}_{yx}(\mathbf{q},\tau)$. If we consider the an effective mass approximation where $\mathbf{q} \to 0$, we get the following expression

$$\tilde{\chi}^{A_{2g}}(i\omega_m) = \frac{1}{\beta\mathcal{V}} \sum_{\mathbf{k},n} \mathrm{Tr}\left[\tilde{\gamma}^{A_{2g}}(\mathbf{k}) G_{\mathbf{k}}(i\omega_n + i\omega_m) \tilde{\gamma}^{A_{2g}}(\mathbf{k}) G_{\mathbf{k}}(i\omega_n)\right]. \tag{3.40}$$

The vertex for A_{2g} symmetry is defined as

$$\tilde{\gamma}^{A_{2g}}(\mathbf{k})=\frac{\partial h_{\mathbf{k}}}{\partial k_x}\frac{\partial h_{\mathbf{k}}}{\partial k_y}-\frac{\partial h_{\mathbf{k}}}{\partial k_y}\frac{\partial h_{\mathbf{k}}}{\partial k_x} \tag{3.41}$$

For this specific case of the A_{2g} symmetry, it looks as if this contribution will be zero. However, in the next section we will see that when writing down $h_{\mathbf{k}}$ in terms of the SU(2) basis, i.e. the Pauli's matrices, we pick up a nonvanishing result.

3.2.3 Extracting the A_{2g} response.

We will now show how to extract a non-zero signal for the symmetry A_{2g} in the current sector. Consider the expression for the vertex for A_{2g} before as

$$\tilde{\gamma}^{A_{2g}}(\mathbf{k}) = \frac{\partial h_{\mathbf{k}}}{\partial k_x}\frac{\partial h_{\mathbf{k}}}{\partial k_y}-\frac{\partial h_{\mathbf{k}}}{\partial k_y}\frac{\partial h_{\mathbf{k}}}{\partial k_x}, \tag{3.42}$$

this is analogous to the commutation

$$\tilde{\gamma}^{A_{2g}}(\mathbf{k}) = \left[\frac{\partial h_{\mathbf{k}}}{\partial k_x}, \frac{\partial h_{\mathbf{k}}}{\partial k_y}\right]. \tag{3.43}$$

We can make use of the Pauli's matrices together with an identity, and rewrite $h_{\mathbf{k}}$ as

$$h_{\mathbf{k}}=A_k\mathbf{1}+\mathbf{Re}(V_k)\boldsymbol{\sigma}_1+\mathbf{Im}(V_k)\boldsymbol{\sigma}_2+B_k\boldsymbol{\sigma}_3, \tag{3.44}$$

with

$$A_k = \frac{\varepsilon_k+\varepsilon_{k+Q}}{2}, \tag{3.45}$$

$$B_k = \frac{\varepsilon_k-\varepsilon_{k+Q}}{2}. \tag{3.46}$$

Using the notation, $\mathrm{Im}(V_k)=V_k''$ and $\mathrm{Re}(V_k)=V_k'$, the commutator becomes

$$\begin{aligned}\left[\frac{\partial h_{\mathbf{k}}}{\partial k_x}, \frac{\partial h_{\mathbf{k}}}{\partial k_y}\right] = &\left(\frac{\partial V_k'}{\partial k_x}\frac{\partial V_k''}{\partial k_y}-\frac{\partial V_k''}{\partial k_x}\frac{\partial V_k'}{\partial k_y}\right)[\boldsymbol{\sigma}_1,\boldsymbol{\sigma}_2]\\ &+\left(\frac{\partial V_k''}{\partial k_x}\frac{\partial B_k}{\partial k_y}-\frac{\partial B_k}{\partial k_x}\frac{\partial V_k''}{\partial k_y}\right)[\boldsymbol{\sigma}_2,\boldsymbol{\sigma}_3]\\ &+\left(\frac{\partial B_k}{\partial k_x}\frac{\partial V_k'}{\partial k_y}-\frac{\partial V_k'}{\partial k_x}\frac{\partial B_k}{\partial k_y}\right)[\boldsymbol{\sigma}_3,\boldsymbol{\sigma}_1]\end{aligned} \tag{3.47}$$

Using the commutation relations for the Pauli matrices, we have

$$\begin{aligned}\left[\frac{\partial E_{\mathbf{k}}}{\partial k_x}, \frac{\partial E_{\mathbf{k}}}{\partial k_y}\right] = &\left(\frac{\partial V_k''}{\partial k_x}\frac{\partial B_k}{\partial k_y}-\frac{\partial B_k}{\partial k_x}\frac{\partial V_k''}{\partial k_y}\right)2i\boldsymbol{\sigma}_1\\ &+\left(\frac{\partial B_k}{\partial k_x}\frac{\partial V_k'}{\partial k_y}-\frac{\partial V_k'}{\partial k_x}\frac{\partial B_k}{\partial k_y}\right)2i\boldsymbol{\sigma}_2\\ &+\left(\frac{\partial V_k'}{\partial k_x}\frac{\partial V_k''}{\partial k_y}-\frac{\partial V_k''}{\partial k_x}\frac{\partial V_k'}{\partial k_y}\right)2i\boldsymbol{\sigma}_3.\end{aligned} \tag{3.48}$$

In our model, we have explicitly defined the form of V_k. By doing so, all the terms that involve derivatives with respect to the real part of V_k vanish identically. The only term that survives is the fist one on the right hand side. Therefore, we have that

$$\tilde{\boldsymbol{\gamma}}^{A_{2g}}(\mathbf{k})=\left(\frac{\partial V_k''}{\partial k_x}\frac{\partial B_k}{\partial k_y}-\frac{\partial V_k''}{\partial k_y}\frac{\partial B_k}{\partial k_x}\right)2i\boldsymbol{\sigma}_1. \tag{3.49}$$

From this result, we can check if the $\gamma^{A_{2g}}(\mathbf{k})$ is invariant under time reversal symmetry or not. For spinless particles, the time reversal operator T is directly connected to the complex conjugation operator K, i.e., $T = K$. If a particular operator is invariant under time reversal symmetry, this means that

$$T\hat{A}T^{-1} = \hat{A} \tag{3.50}$$

For our operator $\gamma^{A_{2g}}(\mathbf{k})$ It follows that

$$T\tilde{\boldsymbol{\gamma}}^{A_{2g}}(\mathbf{k})T^{-1} = -\left(\frac{\partial V_k''}{\partial k_x}\frac{\partial B_k}{\partial k_y}-\frac{\partial V_k''}{\partial k_y}\frac{\partial B_k}{\partial k_x}\right)2i\boldsymbol{\sigma}_1 \tag{3.51}$$

However, time reversal operation also changes momentum from $\mathbf{k} \to -\mathbf{k}$. Here we keep in mind the definitions of $B_\mathbf{k}$ in Eq.(3.46) and $V_\mathbf{k} = m + i\Delta_{c/m}f_{c/m}(\mathbf{k})$. The function $B_\mathbf{k}$ is always even because of the dispersion $\varepsilon_\mathbf{k}$. For the imaginary part of $V_\mathbf{k}$, we have to consider the two spin liquid dispersions. For the chiral spin liquid $\gamma^c_\mathbf{k}$ is even, while for the modulate spin liquid $\gamma^m_\mathbf{k}$ is odd. Therefore

$$f_c(-\mathbf{k}) = f_c(\mathbf{k}) \tag{3.52}$$

$$f_m(-\mathbf{k}) = -f_m(\mathbf{k}) \tag{3.53}$$

These results show that, in terms of time reversal symmetry, only the modulated SL has a $\tilde{\boldsymbol{\gamma}}^{A_{2g}}(\mathbf{k})$ time reversal invariant, as it should be [Thomas 2013] if the HO does not break this symmetry. In contrast, for the chiral SL, there is a breaking of the time reversal symmetry [Wen 1989].

In the next section, we analyze our results based on the numerical calculations of the spinon density-density and spinon current-current correlation functions.

3.3 Numerical analysis.

In the following, we present our results for the effective theory of Raman scattering in URu_2Si_2. We compute the correlation functions numerically in each sector, using Eq.(3.27) in the spinon density sector and (3.35-3.37) for A_{1g}, B_{1g} and B_{2g} symmetries in the spinon current sector together with Eq.(3.40) for A_{2g} symmetry. Following that, we extract the imaginary part of these correlation functions as required by the Raman response. All the results are calculated at $T = 0$ K.

3.3.1 The spinon density sector.

We begin with the spinon density sector, by computing the density-density correlation function derived previously, namely

$$\tilde{\chi}^{\lambda}(i\omega_m) = \frac{1}{\beta\mathcal{V}} \sum_{\mathbf{k},n} \mathrm{Tr}[\gamma^{\lambda}(\mathbf{k}) G_{\mathbf{k}}(i\omega_n + i\omega_m)\gamma^{\lambda}(\mathbf{k}) G_{\mathbf{k}}(i\omega_n)]. \tag{3.54}$$

The $\gamma^{\lambda}(\mathbf{k})$ vertices are defined in eq.(3.28)-(3.30). We concentrate on the response provided by A_{1g}, B_{1g} and B_{2g}, since the A_{2g}, in this case, does not provide any Raman signature.

The Raman signal for the conventional PM state, which is associated to the space group No 139 ($I4/mmm$), is presented in fig.(3.2(a)). This metallic phase has the space group associated with the full BCT lattice. We observe a signal when we activate only the hopping t_1 for symmetries A_{1g} and B_{2g}. In contrast, for B_{1g}, we must have both t_1 and t_2 non zero. We also verify the effect of t_1 together with t_2 or t_3 for the symmetries A_{1g} and the B_{2g} (see Fig.(3.2(b))). In the A_{1g} case, it results in a modification of the shape of curve in a broader region around the quasi-elastic peak. For B_{2g} no significant change was observed. For all these three symmetries no Raman signal could be detected when either t_2 or t_3 are activated one at a turn or when they are turned on together.

We analyze now the other three possible states. The phase characterized by m parameter, which has space group No 123 ($I4/mmm$); the modulated spin liquid phase, associated with the No 126 ($P4/nnc$); and the chiral spin liquid, which is connected with

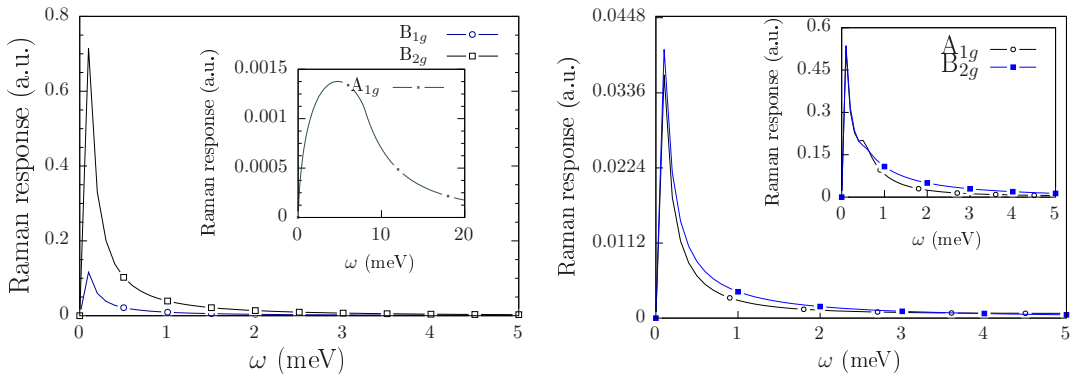

Figure 3.2: Raman signal in the spinon density sector for the paramagnetic state, with space group No 139. Figure **(a)** shows the response for the symmetries A_{1g} and B_{2g} when only t_1 is active. In the B_{1g} case, the signal is obtained when we turn both t_1 and t_2. **(b)** Raman response when t_1 is activated together with t_2 and in the inset t_1 and t_3.In this analysis, we use $t_1 = 1.0$ eV, and $t_2 = t_3 = 0.5$ eV. We added a small phenomenological scattering rate Σ= 3.5 meV in the imaginary part of the self-energy in the Green's function

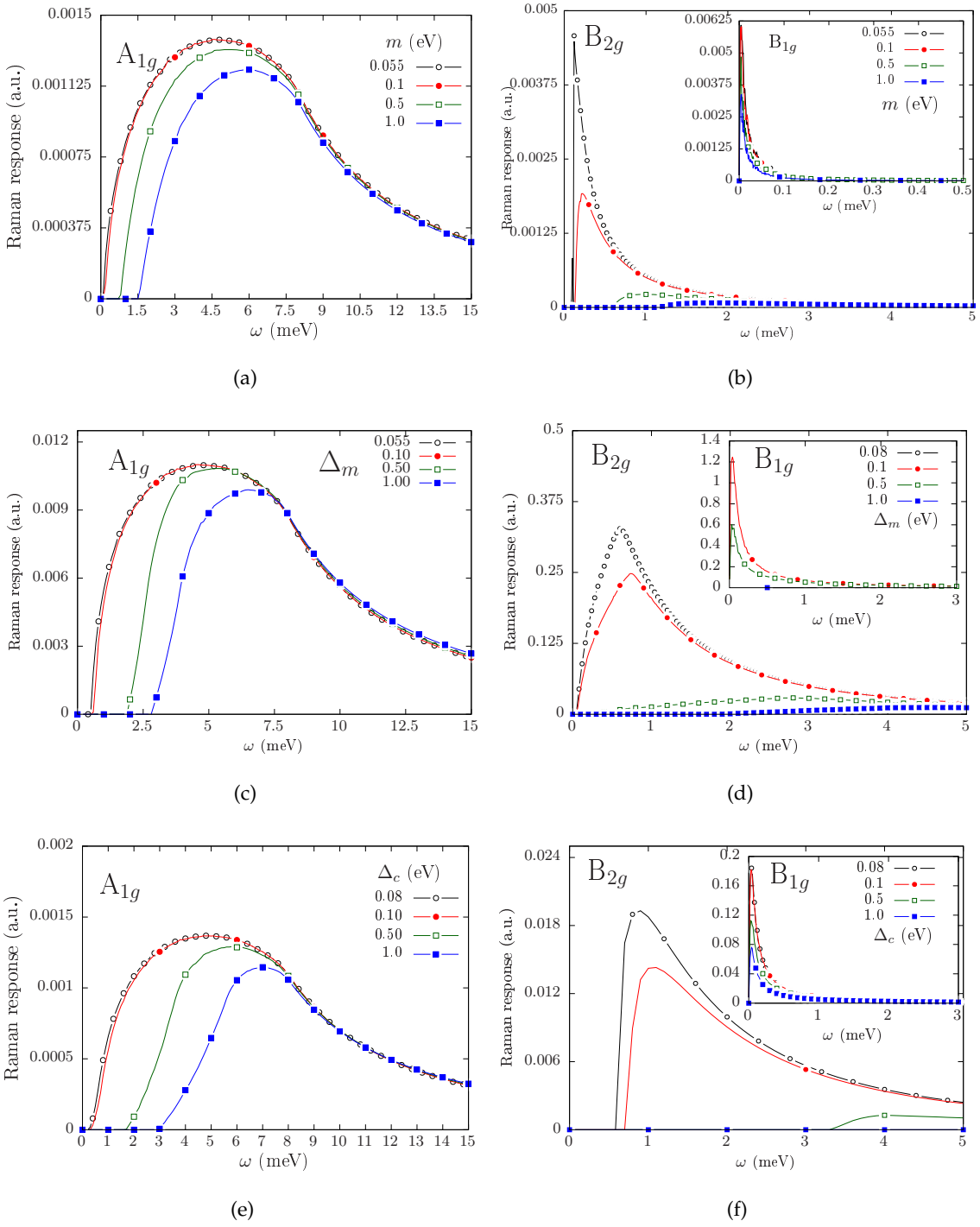

Figure 3.3: Raman response for the spinon density sector. Figures (**a-b**) display the response in the case of m activated. This state is related to the space group No 123 ($P4/mmm$). Figures (**c-d**) associated with the MSL phase, connected to the space group No 126 ($P4/nnc$). Figures (**e-f**) display the CSL phase, which corresponds to the space group symmetry No 128 ($P4/mnc$). There is a gap opening in the case of the A_{1g} and B_{2g} symmetries for all states signaling the effect of breaking the lattice translation symmetry. In the case of B_{1g}, insets (**b**),(**d**),(**e**), the signal does not present any change from the ordinary state described in (3.2). In this graphs we set $t_1 = 1.0$ eV for A_{1g} and B_{2g}, while $t_1 = 1.0$ and $t_2 = 0.5$ eV for B_{1g}. We use a small scattering rate $\Sigma = 3.5$ meV.

No 128 ($P4/mnc$). The tests consist in keeping t_1 activated for A_{1g} and B_{2g} symmetries when varying the parameters Δ_m, Δ_c and m. For the B_{2g} case, we keep t_1 and t_2 activated. These phases now display lattice translation symmetry breaking. The results are shown in Fig.(3.3). For A_{1g} and B_{2g}, a gap is opening for the three parameters. For B_{1g}, there is no difference with respect to the paramagnetic state. When t_1 and t_2 or t_1 and t_3 are activated together, the gap is lost for the A_{1g} and B_{2g} symmetries by performing variation of m. The effect of tuning the parameters Δ_c and Δ_m moves the peak but does not tell us much about what kind of states is truly manifested. The effect of the coexistence between m and the Δ's was also investigate. However, the only resulting effect is that, in this case, the gap is enhanced. Thus, It is not possible to predict with precision which state is actually being observed from Raman data in the spinon density sector.

The electronic Raman signal displays clear signatures of the opening a gap produced by the systematic variation of the different parameters which are related to the phases which are under test. The peaks observed in the A_{1g} and the B_{2g} symmetries disappear as we move towards higher frequencies. For the B_{1g} symmetry, we have only one Raman signal but no matter what parameter we tune this does not produce any considerable difference in the response. In particular, in the case when only t_1 is active, the phases exhibit the nesting condition $\varepsilon_{\mathbf{k}\pm\mathbf{Q}} = -\varepsilon_{\mathbf{k}}$, with ordering wave vector $\mathbf{Q} = \{1, 1, 1\}$. That is in agreement with recent studies of the Fermi surface properties the PM phase of URu_2Si_2 and has a direct relation with HO phase [Oppeneer 2011].

3.3.2 The spinon current sector.

The spinon current sector as we stated earlier on is described by the correlation functions in Eq.(3.35-3.36) for A_{1g}, B_{1g} and B_{2g} symmetries and Eq.(3.40) for A_{2g} symmetry. We start by describing the results for the first three symmetries, and in the next subsection we will present the results concerning A_{2g}. In the Fig.(3.4) we have the Raman responses at the PM phase, with respect the space group No 139 ($I4/mmm$), which is associated with the the A_{1g}, the B_{1g} and the B_{2g} symmetries. They are similar to the results of the spinon density sector. Now, A_{1g}, B_{1g} and B_{2g} display a signal when only t_1 is activated. Once again we consider the effect of turning on the parameters that break lattice translation symmetry, one by one. The first case is when m, connected with the space group No 123 ($P4/mmm$), is activated. There is a gap opening for A_{1g}, B_{1g} and B_{2g} symmetries (see Fig.(3.5(a)) and (3.5(b))). As soon as we move towards high values of m which are comparable with the hopping t_1, the signal decreases, even with the enhancement of the gap. A similar behavior

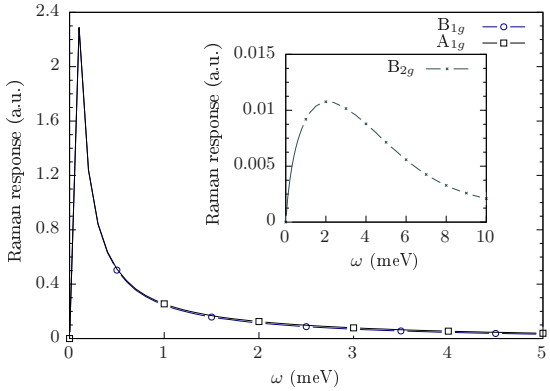

Figure 3.4: Raman signal in the the spinon current sector for paramagnetic state, with space group No 139. The A_{1g}, B_{1g} and B_{2g} symmetries can be observed when only t_1 is active.

occurs when we turn Δ_m for the modulated SL phase (space group No 126 ($P4/nnc$)), or turn instead Δ_c for the chiral SL phase (space group No 126 ($P4/mnc$)), in the A_{1g} and the B_{1g} symmetries (see Fig.(3.5(c)-3.5(f))). However in these two cases the gap is not present in A_{1g} or B_{1g} symmetries. In the B_{2g} case, the signal is increased and the gap is significantly enhanced by Δ_c (see insets of 3.5(d) and 3.5(f)). The effect of having a coexisting m and Δ is also shown to be relevant. However, as in the spinon density sector, the presence of Δ_m or Δ_c only increases the value of the gap, without revealing which parameter is responsible for producing this effect. If we include t_2 and t_3 simultaneously, the gap disappears in all symmetries.

The exhaustive analysis of the spinon current sector show us that the PM phase, the phase described by m, the modulated SL and the chiral SL phases display Raman signatures of the A_{1g}, B_{1g} and B_{2g} symmetries. The gap manifests itself simultaneously, for the three symmetries, in the case of m activated. We can distinguish between the spin liquid phases by looking at the specific response, that in the case of modulated SL presents itself as a quasielastic peak for the A_{1g} and the B_{1g} symmetries, while for the chiral SL it shows a structureless broader region with a peak. In the case of B_{2g}, the gap appears for the modulated and for the chiral SL phases for significant large values of Δ, with a significant increasing of the signal.

3.3.3 The case of A_{2g} symmetry.

The plots in Fig.(3.6) represent the results for the A_{2g} symmetry. In contrast with what happened in the spinon density sector, the symmetry A_{2g} does not vanishes in the spinon current sector. We need simply to activate t_1 together with m and with one of the Δ's in

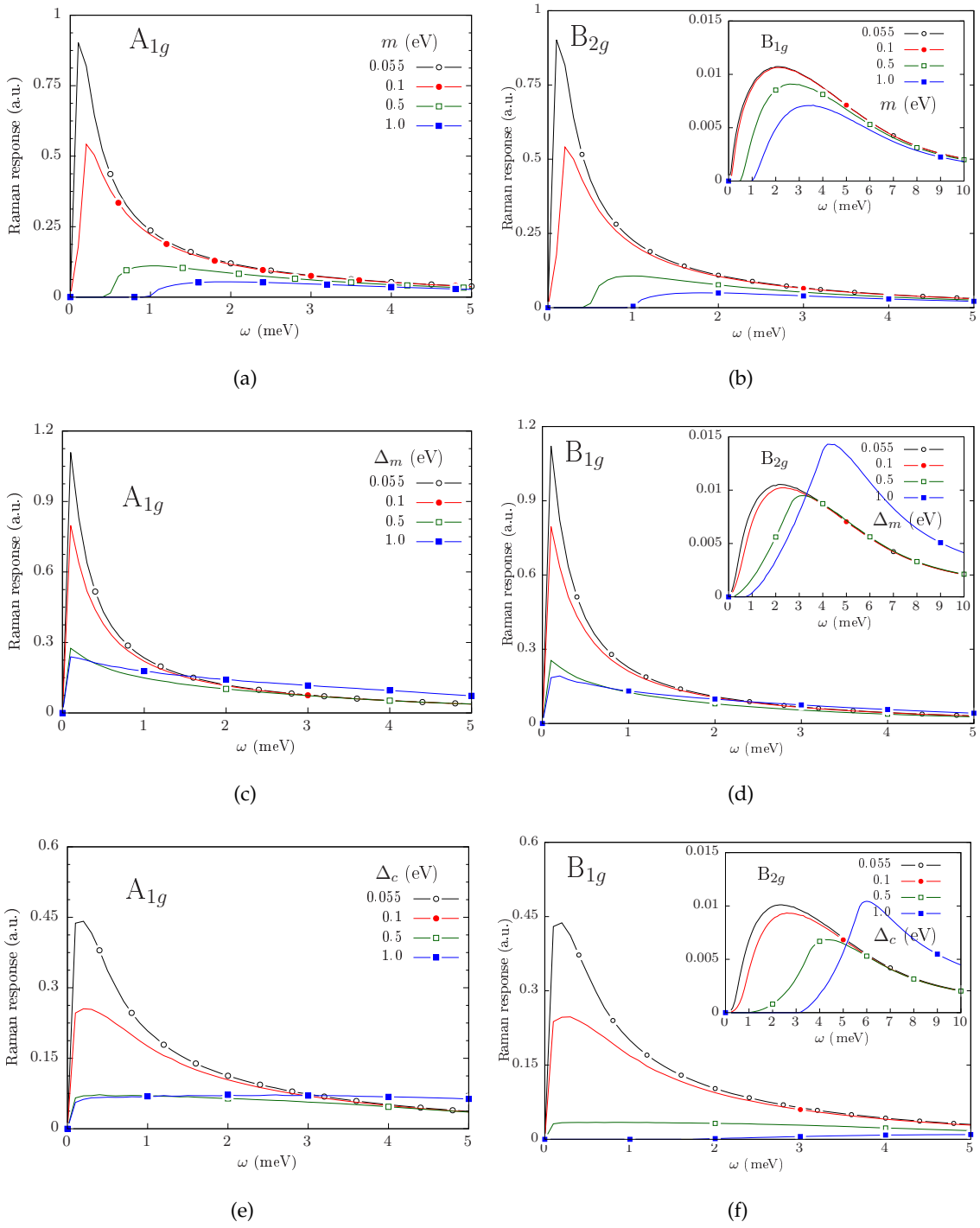

Figure 3.5: Raman response in the spinon current sector for the A_{1g}, the B_{1g} and the B_{2g} symmetries. Figure **(a)-(b)** display the phase characterized by m parameter, associated to the space group symmetry No 123 ($P4/mmm$). The gap is proportional to the value of m and as soon as we increase m the signal decreases. Figures **(c)-(d)** display the modulated SL phase, associated with the point space symmetry No 126 ($P4/nnc$). There is no gap for the A_{1g} and the B_{1g} symmetries. For B_{2g} symmetry, the gap appears when we go up to high values of Δ_m. Figures **(e)-(f)** display the chiral SL phase, which corresponds to space group No 128 ($P4/mnc$). There is a gap only for the B_{2g} symmetry. We set $t_1 = 1.0$ eV and use a small scattering rate $\Sigma = 3.5$ meV.

order to observe the signal.

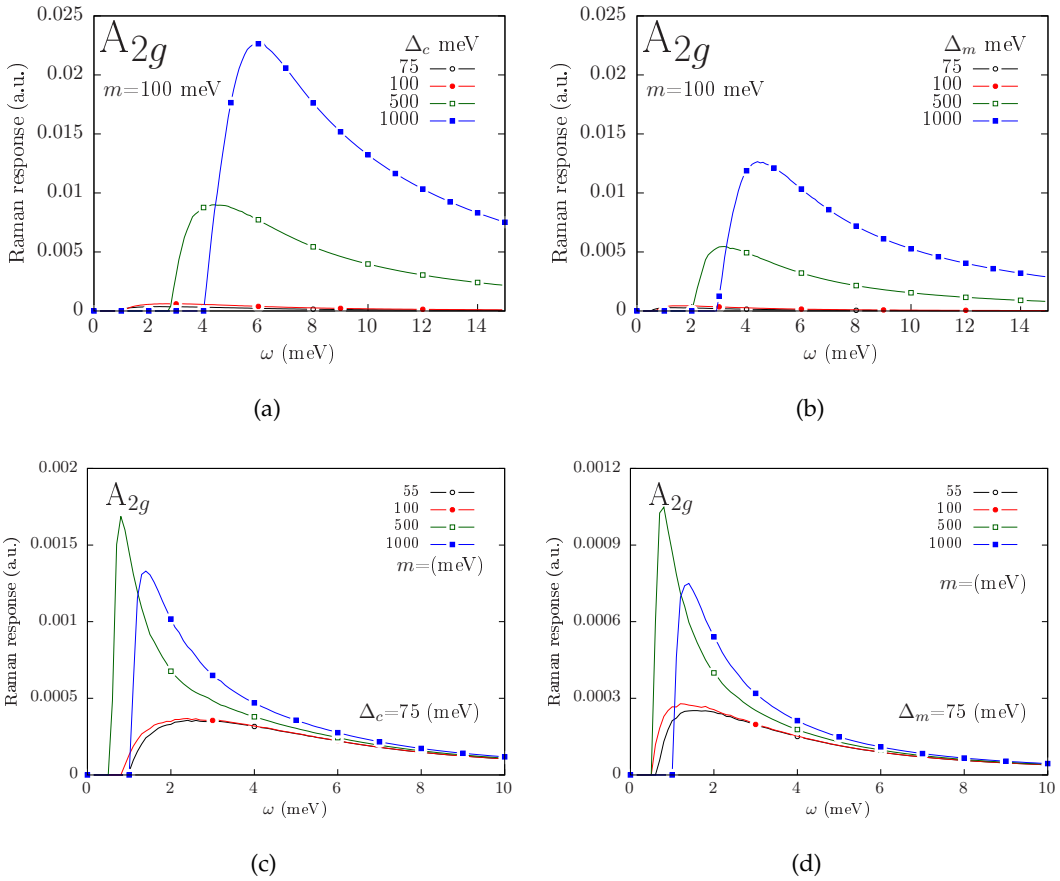

Figure 3.6: Raman response in the spinon current sector for A_{2g}. Figures **(a)-(b)** display the Raman signal when we increase the values of Δ_c and Δ_m, while keeping m fixed. As soon as the values of Δ's are increased above 0.5 eV, the intensity os the signal raises and the gap is enhanced. Figures **(c)-(d)** display the Raman signal when we increase the value of m, while keeping Δ_c and Δ_m fixed. No significant change in the gap is observed even though the maximum is raised for m equals to 0.5 eV and 1.0 eV. We set $t_1 = 1.0$ eV and use a small scattering rate $\Sigma = 3.5$ meV.

In Figs.(3.6(a)) and (3.6(b)), we fixed the value of m while varying the Δ's. Note that, since the space groups No 128 and No 126 are sub-groups of the No 123, the coexistence between the parameter m with a non-zero Δ_m or Δ_c still corresponds to the particular groups No 126 or No 138, respectively. By increasing the values of Δ_m or Δ_c, in both cases, both the peak and the magnitude of the gap increase. This opens the possibility for either the modulated SL phase, connected with space group No 126 ($P4/nnc$), or the chiral SL phase, connected with the space group No 128 ($P4/mnc$). However, we cannot distinguish between these two states because the Raman signal appears to be the same in the two cases. We also verify the effect of varying m for both Δ_m and Δ_c fixed. The results are shown in

Fig.(3.6(c)-3.6(d)). Inthis situation, the value of the gap does not change with m and the intensity of the signal decreases as m increases. We also check the effect of activating t_1 either together with t_2 or t_3, for the A_{2g} symmetry. In the first case, t_1 together with t_2, the gap is still present, whereas, for t_1 together with t_3, it disappears completely, giving way to a quasielastic response.

The A_{2g} symmetry case clearly shows the presence of a gap when both m and one of the Δ's are activated. This result open the possibility for the two spin liquid states: the modulated SL with space symmetry group No 126 ($P4/nnc$) and the CSL, with point symmetry space No 128 ($P4/mnc$). However, we cannot distinguish with exactitude which one is the most appropriate because the Raman signatures look the same for the two cases. We must consider other properties, like the point group symmetry, in order to make predictions bout the HO in URu_2Si_2. Our results show clearly that there is always the presence of a gap, that is associated with an state that breaks the lattice translation symmetry.

3.4 Discussion of the results and connection with Raman experiments in URu_2Si_2.

The main result for the spinon density sector is the appearance of a gap that manifests itself in the Raman signal for the specific A_{1g} and B_{2g} symmetries. Similar responses were observed by Raman scattering in the iron-based superconductor materials [Yang 2014], though this time for different symmetries (B_{1g} and B_{2g}). The spectra of those materials displays many spin density-wave gaps as expected in a band-folding itinerant picture of multiband systems. Here the gap is clearly related with the folding of the Brillouin zone that results from the breaking of lattice translation symmetry from a BCT to simple tetragonal structure. Still in the spinon density sector, for the B_{1g} case, we have observed a Raman signal. However, this signal does not present any considerable difference no matter what parameter we tune. It suggests that with the symmetry B_{1g} we cannot discriminate between any ordered states that considered here.

We then turn our attention to the spinon current sector. The Raman signatures for the associated PM phase, with the space group No 139 ($I4/mmm$), are very similar to the ones obtained in the spinon density sector. Hence, the dispersion of the two bands displays the same nesting feature with $\varepsilon_{\mathbf{k}+\mathbf{Q}} = -\varepsilon_{\mathbf{k}}$, when only t_1 is present. The Raman signatures for the phase in which m takes place, having space group No 123 ($P4/mmm$), are displayed in the A_{1g}, B_{1g} and B_{2g} symmetries. They show the presence of the gap, and a decrease of the corresponding Raman signal as m is increased. This can be associated, again, with

an spin density wave instability. For $m = 0$, the chiral SL and the modulates SL phases do not display any gap either in A_{1g} or B_{1g} symmetries. The only result is present in B_{2g} symmetry, which displays a gap for these two specific orders.

The recently Raman experiments performed in the heavy-fermion compound URu_2Si_2 [Buhot 2014] in the HO regime show the presence of a gap in this particular phase associated precisely with the symmetry A_{2g}. This gap is related with an electron-hole continuum of excitations that is expected if there is a reconstruction of Fermi surface and it is compatible with what was predict by other experimental techniques like inelastic neutron scattering [Villaume 2008] and ARPES [Santander-Syro 2009]. A recent theoretical proposition for the signal in A_{2g} suggested that it is a result of local interactions and the crystal-field splitting of degenerate many-body local multiplet of the U $5f^2$ electronic states [Haule 2009, Kung 2015]. Without taking these scenarios into account, our simple model can predict the signal at A_{2g} symmetry by considering a effective tight-binding model that involves only first neighbors on the BCT lattice.

Our results reproduce the gap that appears in the A_{2g} symmetry, in the spinon current sector. Among the states that we assume to characterize HO, the signal manifests itself for modulated SL and chiral SL at the same time as we keep one small values of m. The particularity arises from the fact that we must consider both the m and one Δ at the same time. This feature suggests the interplay between the the phase discriminated by m parameter and hidden order phase [Chandra 2013]. The gap at hidden order does not mean that this transition is a density wave transition. In terms of space group, or point group symmetry, this feature of having the two parameters activated means that the system lower its symmetry.

Regarding the question of the space group symmetry, it seems clear that there is a phase transition associated with the change in the lattice structure, in both sectors. The paramagnetic order is displayed when we activate any of the homogeneous hopping t_1, t_2 or t_3, and it corresponds to a state with space group No 139 ($I4/mmm$). When activating one of the parameters that break the lattice translation symmetry, we observed a clear change in the Raman response that translates itself into a gap opening, reinforcing the idea of a change in the lattice structure.

The phases in which a non-zero m coexists with the Δ's, where we observed the A_{2g} symmetry, are determined by the particular choice of Δ. If Δ_c is present, the state with the space group No 128 $P4/mnc$ manifests and it is known as a chiral SL phase. On the other hand, if Δ_m takes place, the state is related to the space group No 126 $P4/nnc$ and it is defined as a modulated SL phase. Indications, on the framework of cuprates systems

[Liu 1993], seem to indicate that the A_{2g} symmetry may account for the appearance of one excitation where quantum fluctuations destroy the Néel order, and hence the elementary excitations have a fractional character with a chiral nature [Khveshchenko 1994, Wen 2002, Wen 1989]. This may favor the choice of chiral SL as responsible for the appearance of such excitations.

However, in their analysis, Harima-Miyake-Flouquet rejected this idea based on the fact that the space group No 128 $P4/mnc$ is incompatible with the nuclear quadrupole resonance experiments for URu_2Si_2 [Harima 2010]. Therefore, such phase with this particular symmetry would not account for HO. Another constraint to reject the chiral SL state is the breaking of time-reversal symmetry that is presented by this phase since, at the HO, no evidence for this violation has been reported so far [Das 2013]. Therefore, our results suggest that among the two spin liquid states the modulated SL is the most probable state for the HO phase.

Chapter 4

Conclusions and Perspectives.

The most noticeable result emerging from this thesis is that the hidden order phase can indeed be seen as a modulated spin liquid state. This conclusion was build upon the study of two different models that are used to investigate the HO phase in URu_2Si_2. In the first of them, we investigated the $J_1 - J_2 - J_3$ Heisenberg model for the BCT lattice structure and its relation with the HO and the antiferromagnetism of URu_2Si_2. In the second model, we elaborate on the possible existing non-conventional spin states and use it to explore the recent results from Raman spectroscopy in URu_2Si_2. Motivated by great amount of experimental information of URu_2Si_2, we provided new theoretical elements to investigate the hidden order phase.

In chapter 2, we applied the $J_1 - J_2 - J_3$ Heisenberg model to the BCT lattice. We made use of linear spin wave theory to test the stabilities of the existing magnetic orderings. The magnetic orders derived for this model comprises two commensurate antiferromagnetic phases labeled by the antiferromagnetic wave vectors $\mathbf{Q}^{\mathrm{I}}_{\mathrm{AF}} = (1,1,1)$ and $\mathbf{Q}^{\mathrm{II}}_{\mathrm{AF}} = (1/2,1/2,0)$, with $\mathbf{Q}^{\mathrm{II}}_{\mathrm{AF}}$ being selected by the "order by disorder" mechanism. We also confirmed the existence two *incommensurate* orders, characterized by the vectors $\mathbf{Q}^{\mathrm{II}}_{\mathrm{inc}}$ and $\mathbf{Q}^{\mathrm{III}}_{\mathrm{inc}}$. Then, we checked the stability of the magnons excitations for each of this phases. The linear spin wave theory showed that there are instabilities of these excitation modes associated with the particular *incommensurate* AF orderings, even though the three-dimensionality character of the system allows only small fluctuations.

It became clear that the spin wave approach is too approximate and as a result it is unable to predict spin liquid states. For this reason, we carried out an SU(n) symmetric generalization of the Heisenberg model. The physical motivations for this study were again the unusual phenomena exhibited by URu_2Si_2. They are connected with the fact that the magnetic degrees of freedom seem to be deconfined into fermionic modes and may con-

tribute to the formation of the Fermi surface [Pépin 2011]. We found that it is possible, with this SU(n) approach, to stabilize the spin liquid phases when n is larger than a critical value. Three spin liquid phases emerged naturally from our analysis. Two of those SL are the analogous of the RVB states [Anderson 1973] in a 3d system. We also find the presence of a modulated spin liquid (MSL), with wave vector $\mathbf{Q}_{\mathrm{AF}}^{\mathrm{I}}$. This MSL phase was recently suggested as a candidate to describe the hidden order phase in URu_2Si_2 [Pépin 2011]. This particular modulated state can be verified experimentally by inelastic neutron or Raman scattering experiments or any other experimental techniques based on the orientation dependencies, which are initially set by in the experiment [Thomas 2013]. Such an MSL phase might be responsible also for a commensurately ordered pairing that breaks the BCT symmetry down to the simple tetragonal lattice structure. Moreover, it might also be related to the superconducting instability observed in URu_2Si_2 inside the HO phase.

Secondly, motivated by the result that it is possible to stabilize both the spin liquid phase together with an AF order in a BCT lattice, we turn to chapter 3, where we presented a two band non-interacting effective theory, which is used to explain recent Raman scattering experiments performed at the HO phase of URu_2Si_2 [Buhot 2014]. This new model deals with the same possible electronic states predicted in the framework of Heisenberg $J_1 - J_2 - J_3$ model. Using the space group and point group symmetry arguments of Harima-Miyake-Flouquet [Harima 2010], we made a space group analysis by checking the spin liquid scenarios that results from our effective tight-binding Hamiltonian. We regrouped the spin liquid phases into two different classes of space groups plus two other classes of space groups, one for a metallic state and another one to describe an ordering phase that is characteristic to some phenomena that is common in heavy fermion systems. In the later, if the charge degrees of freedom were considered explicitly in the model, this ordered phase would represent the local Kondo Hybridization or a charge-density wave phase and even it can account to some small magnetic moment.

The first space group under investigation is No 139, with full BCT lattice symmetry, that might describe the high-temperature paramagnetic metallic phase. The other three space groups break the BCT lattice translation symmetry down to the simple tetragonal lattice structure. This change of the lattice space groups also imply a change in point group symmetry. However all the possible candidates still belong to the same tetragonal class of space group. The group No 123, that happens to be the most symmetric one, describes the possibility of a local Kondo Hybridization or a charge density wave phase in a scenario where we could take into account charge degrees of freedom or in the last case a staggered magnetic moment of the localized spin. We justify this assumption by assuming that our

model describe a phenomenological theory for this particular system of URu_2Si_2 and we may proceed with the analysis without take this ingredients explicitly into account and consider as if they were presented since the beginning. The other two space group that we consider is the space group No 126 that favors the modulated SL phase and the space group No 128 represents the chiral SL order.

In the detailed point group symmetry analysis of Harima-Miyake-Flouquet [Harima 2010], they presented a systematic study considering various scattering experiments to investigate the compatibility of the point groups symmetries which could be associated with the candidates to describe the hidden order. Among the space groups they analyzed, three of them are precisely the No 123 ($I4/mmm$) , No 126 ($P4/nnc$) and No 128 ($P4/mnc$). The other point groups considered by them were the No 129, No 131, No 134, No 136 and the No 137. In the end, they concluded that the point group No 136 should characterize the HO phase. However, if we take into account the new experimental results from Raman, we can demonstrate instead that there are clear signatures of the four groups that might be associated with the paramagnetic, antiferromagnetic, modulated SL and chiral SL phases.

Our results reproduces the gap opening in the Raman response for particular symmetries and for a given choice of parameters that describe these phases. This gap is a consequence of the breaking of lattice translation symmetry and is compatible with what happens in the phase transition from PM to HO phase of URu_2Si_2. The Raman scattering measurements for URu_2Si_2 establish strong constraints for the A_{2g} symmetry. This is in agreement with our results which favors a modulated spin liquid phase scenario for HO. The modulated spin liquid phase, with space group No 126 is, in this way, compatible with the Raman experiments invoking the A_{2g} symmetry at HO. The alternative chiral SL is rejected because it automatically results into the breaking of time-reversal symmetry, that it is not observed in the HO phase. In this way, we demonstrate that our relatively simple two-band effective model which take into account bond orderings defined for first neighbors is compatible with Raman scattering signatures at the A_{2g} symmetry.

Future perspectives for this work would be to investigate a two band model with interactions to see how the correlations modify the calculated Raman signatures. Such a model should preserve the features stressed here at HO phase: the breaking of lattice translation symmetry and the preservation of the time reversal symmetry, as well as the direct link of the Fermi surface with the nesting condition for two bands, as recently proposed through the spin-orbit coupling mechanism [Das 2014]. Among these interactions, we could consider for example the interplay between the spin liquid and Kondo physics [Zhu 2008],

since in URu_2Si_2 the charges degrees of freedom coexist with the magnetic correlations.

In this context, the Kondo lattice models should be appropriate to describe on the same footing local and non-local degrees of freedom. There are experimental pieces of evidence that there two kinds of gaps may be revealed in URu_2Si_2. One pseudo-gap signaling the Kondo effect in temperatures $T_K \approx 70$ K which is inferred by spectroscopy measurements [Lobo 2015] and another gap which results as consequence of the folding of the Fermi Surface in temperatures below $T_0 = 17.5$ K, precisely at HO phase, that is detected by angle resolved photoemission spectroscopy (ARPES) [Santander-Syro 2009] and inelastic neutron [Bourdarot 2010]. A recent theoretical approach using the Kondo lattice model [Montiel 2014] shows the coexistence between the Kondo effect and the modulated SL phase. It states that both gaps appearing in URu_2Si_2 can occur at different temperatures, and the HO phase is seen as a modulated SL. In this way, for future investigations, it is important that the Kondo effect is present in our model because since this is a well known mechanism to "deconfine" the local magnetic degrees of freedom into Abrikosov fermions which are partially responsible for the spin liquid states.

Appendix A

Detailed calculations for chapter 2.

A.1 The saddle point equation for the Classical phase diagram.

In this appendix, we will derive here the saddle point equations that minimize the dispersion $J(\mathbf{q})$ presented in the section 2.1. By writing the derivatives of the classical energy

$$J(\mathbf{q}) = 8J_1\gamma_1(\mathbf{q}) + 2J_2\gamma_2(\mathbf{q}) + 4J_3\gamma_3(\mathbf{q}), \tag{A.1}$$

We end up with the following system of equations

$$\frac{\partial J(\mathbf{q})}{\partial q_x} = -4J_1 \sin\left(\frac{q_x}{2}\right)\cos\left(\frac{q_y}{2}\right)\cos\left(\frac{q_z}{2}\right) - 2J_2\sin(q_x) - 4J_3\sin(q_x)\cos(q_y), \tag{A.2}$$

$$\frac{\partial J(\mathbf{q})}{\partial q_y} = -4J_1 \cos\left(\frac{q_x}{2}\right)\sin\left(\frac{q_y}{2}\right)\cos\left(\frac{q_z}{2}\right) - 2J_2\sin(q_y) - 4J_3\cos(q_x)\sin(q_y), \tag{A.3}$$

$$\frac{\partial J(\mathbf{q})}{\partial q_z} = -4J_1 \cos\left(\frac{q_x}{2}\right)\cos\left(\frac{q_y}{2}\right)\sin\left(\frac{q_z}{2}\right) = 0. \tag{A.4}$$

The next step is to solve this system of equations and to do so, we have to take into account the possible cases for q_z.

If we have $q_z = 0$ or $q_z = 2\pi$, we see that eq.(A.4) is automatically satisfied and we end up with two equations for k_x and k_y

$$\pm 4J_1 \sin\left(\frac{q_x}{2}\right)\cos\left(\frac{q_y}{2}\right) - 2J_2\sin(q_x) - 4J_3\sin(q_x)\cos(q_y) = 0, \tag{A.5}$$

$$\pm 4J_1 \cos\left(\frac{q_x}{2}\right)\sin\left(\frac{q_y}{2}\right) - 2J_2\sin(q_y) - 4J_3\cos(q_x)\sin(q_y) = 0. \tag{A.6}$$

These two equations can be factorized as

$$\sin\left(\frac{q_x}{2}\right)\left[\pm\cos\left(\frac{q_y}{2}\right) - p_2\cos\left(\frac{q_x}{2}\right) - 2p_3\cos\left(\frac{q_x}{2}\right)\cos(q_y)\right] = 0, \tag{A.7}$$

and

$$\sin\left(\frac{q_y}{2}\right)\left[\pm\cos\left(\frac{q_x}{2}\right)-p_2\cos\left(\frac{q_y}{2}\right)-2p_3\cos\left(q_x\right)\cos\left(\frac{q_y}{2}\right)\right]=0. \tag{A.8}$$

We introduce the notation where $p_2 = J_2/J_1$ and $p_3 = J_3/J_1$ as the dimensionless parameters. We can consider the trivial solutions when we have q_x and q_y equal to zero or 2π. This give us the first commensurate state, $\mathbf{Q}^{\mathrm{I}}_{\mathrm{AF}} = (0,0,0)$ or $\mathbf{Q}^{\mathrm{I}}_{\mathrm{AF}} = (1,1,1)$. The second trivial solution is obtained for $q_x = \pi$ and $q_y = \pi$. In this case, it does not matter what values q_z takes, because the cosine function vanishes, which means that we have a degeneracy for this wave vector. Therefore the second trivial solution is $\mathbf{Q}^{\mathrm{II}}_{\mathrm{AF}} = (1/2, 1/2, \nu)$.

On the other hand, if $q_x = 0$ or $q_x = 2\pi$ and since $\sin\left(\frac{q_y}{2}\right) \neq 0$, we end up with the first incommensurate wave vector $\mathbf{Q}_{\mathrm{inc}}$, with the condition that

$$\cos\left(\frac{q_y}{2}\right) = \pm\left(\frac{1}{p_2+2p_3}\right). \tag{A.9}$$

In reduced notation we can write this incommensurate wave vector as $\mathbf{Q}^{\mathrm{III}}_{\mathrm{inc}} = (0, \Upsilon_3, 0)$ degenerated with $\mathbf{Q}^{\mathrm{III}}_{\mathrm{inc}} = (1, \Upsilon_3, 1)$, where $\Upsilon_3 = \frac{1}{\pi}\arccos\left(\pm\frac{1}{p_2+2p_3}\right)$. This is completely analogous to the case where we consider now $q_y = 0$ or $q_y = 2\pi$ and $\sin\left(\frac{q_x}{2}\right) \neq 0$. Now we have as the incommensurate state $\mathbf{Q}^{\mathrm{III}}_{\mathrm{inc}} = (\Upsilon_3, 0, 0)$ or $\mathbf{Q}^{\mathrm{III}}_{\mathrm{inc}} = (\Upsilon_3, 1, 1)$. All this states are degenerated in a sense that they reproduce the same classical energy $J(\mathbf{q})$.

If we do not consider the trivial case, which means $\sin\left(\frac{q_x}{2}\right) \neq 0$ and $\sin\left(\frac{q_y}{2}\right) \neq 0$, we have to solve the following system of equations

$$\begin{cases} \mp\cos\left(\frac{q_y}{2}\right)+p_2\cos\left(\frac{q_x}{2}\right)+2p_3\cos\left(\frac{q_x}{2}\right)\cos\left(q_y\right) &= 0 \\ \mp\cos\left(\frac{q_x}{2}\right)+p_2\cos\left(\frac{q_y}{2}\right)+2p_3\cos\left(q_x\right)\cos\left(\frac{q_y}{2}\right) &= 0 \end{cases} \tag{A.10}$$

We perform a change of variables as

$$X = \cos\left(\frac{q_x}{2}\right) \tag{A.11}$$

$$Y = \cos\left(\frac{q_y}{2}\right). \tag{A.12}$$

We end up with a new systems of equations

$$\begin{cases} \mp Y + p_2 X + 2p_3 X(2Y^2-1) &= 0 \\ \mp X + p_2 Y + 2p_3 Y(2X^2-1) &= 0 \end{cases}. \tag{A.13}$$

Summing and subtracting these two equations and making one more change of variables, where we define

$$S = X + Y, \tag{A.14}$$

$$D = X - Y, \tag{A.15}$$

we end up with a new system of equation that in order to solve we have to define some possibilities

$$\begin{cases} \pm S + p_2 S - 2p_3 S + p_3 S(S^2 - D^2) & = 0 \\ \pm D + p_2 D - 2p_3 D - p_3 D(S^2 - D^2) & = 0 \end{cases} \tag{A.16}$$

We consider four different possibilities,

1. $S \neq 0$ and $D = 0$, where $\cos\left(\frac{q_x}{2}\right) = \cos\left(\frac{q_y}{2}\right)$, with $\cos\left(\frac{q_x}{2}\right) = \pm\sqrt{\frac{2p_3 - p_2 \mp 1}{4p_3}}$. This implies that $\mathbf{Q}^{\text{II}}_{\text{inc}} = (\Upsilon_2, \Upsilon_2, 0)$ or $\mathbf{Q}^{\text{II}}_{\text{inc}} = (\Upsilon_2, \Upsilon_2, 1)$.

2. $D \neq 0$ and $S = 0$, where $\cos\left(\frac{q_x}{2}\right) = \cos\left(\frac{q_y}{2} \pm \pi\right)$, with $\cos\left(\frac{q_x}{2}\right) = \pm\sqrt{\frac{2p_3 - p_2 \pm 1}{4p_3}}$. This implies that $\mathbf{Q}^{\text{II}}_{\text{inc}} = (\Upsilon_2, -\Upsilon_2, 0)$ or $\mathbf{Q}^{\text{II}}_{\text{inc}} = (\Upsilon_2, -\Upsilon_2, 1)$.

3. $S = 0$ and $D = 0$, we recover the commensurate phases. Note that if this occurs, we have a degeneracy in k_z for $\mathbf{Q}^{\text{II}}_{\text{AF}}$. This degeneracy can be characterized by the wave vector $\mathbf{Q}^{\text{II}}_{\text{AF}}$ =$(1/2, 1/2, \nu)$ that was introduced before. The argument discussed in the section of order by disorder shows that the most preferred phase is the one that selects $\nu = 0$.

4. $S \neq 0$ and $D \neq 0$, where we can find the constraint for p_3 and p_2 where $p_3 = p_2/2$.

The first two possibilities give us the second incommensurate wave vector $\mathbf{Q}^{\text{II}}_{\text{inc}}$. However, we have to choose the sign inside the square root based on the argument of stability for this state. The next step is to check if our results truly correspond to stable states ordered accordingly to the $\mathbf{Q}$'s wave vectors that we derived. We have to analyze the stability of these two new incommensurate phases.

Since our cosines functions should run between zero until one, which means that the components of the vector $\mathbf{q}$ must lie in the interval $0 < q_i < 2\pi$, we state that what is inside the square roots should be a positive quantities. This means that

$$0 < 2p_3 - p_2 \pm 1 < 1. \tag{A.17}$$

With this last inequality, we found four lines defined by the following equations

$$\frac{p_2 + 1}{2} < p_3 < 1 + \frac{p_2}{2} \tag{A.18}$$

and

$$\frac{p_2 - 1}{2} < p_3 < \frac{p_2}{2}. \tag{A.19}$$

These equations define the regions of the existence of the two incommensurate phases in the phase diagram, as show in Fig.(A.1)

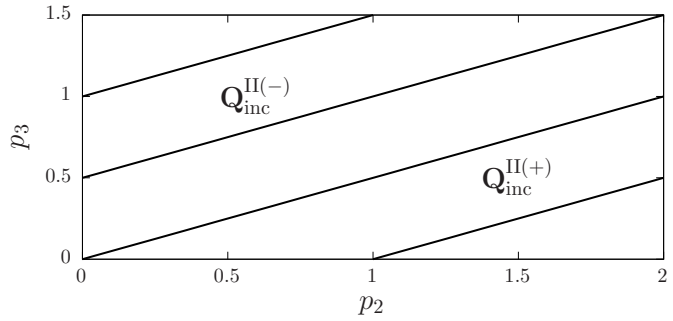

Figure A.1: The regions of existence for $\mathbf{Q}_{\text{inc}}^{\text{II}}$. The expression inside the square root $(2p_3 - p_2 \pm 1)$ choose the value of k_z that give us the sign plus. This will be clear when we comparing the criteria for the stability of the incommensurate phases. We underlined the regions for $\mathrm{Q}_{\text{inc}}^{\text{II}(+)}$ and $\mathbf{Q}_{\text{inc}}^{\text{II}(-)}$.

The next step is comparing the stability between the new incommensurate phases $\mathbf{Q}_{\text{inc}}^{\text{II}(+)}$ and $\mathbf{Q}_{\text{inc}}^{\text{II}(-)}$ with the $Q_{\text{AF}}^{\text{III}}$ and also with the two commensurate $\mathbf{Q}_{\text{AF}}^{\text{I}}$, and $\mathbf{Q}_{\text{AF}}^{\text{II}}$. We can summarize the results for the dispersions relations in the table A.1

By using the expressions for each classical energy, we compared each of this energy against the other in order to establish the critical lines in the phase diagram. We have the following cases:

1. When $E(\mathbf{Q}_{\text{AF}}^{\text{II}}) < E(\mathbf{Q}_{\text{inc}}^{\text{II}(+)})$, it results in the following equation

$$p_3 < \frac{p_2 - 1}{2}. \tag{A.20}$$

2. $E(\mathbf{Q}_{\text{AF}}^{\text{I}}) < E(\mathbf{Q}_{\text{inc}}^{\text{II}(+)})$, that give us another equation

$$p_3 < \frac{1 - p_2}{2}. \tag{A.21}$$

Ordering wave vector	$J_{\mathbf{Q}_{\text{AF}}}$
$\mathbf{Q}_{\text{AF}}^{\text{I}} = (1,1,1)$	$-1 + \frac{p_2}{2} + \frac{p_3}{2}$
$\mathbf{Q}_{\text{AF}}^{\text{II}} = \left(\frac{1}{2}, \frac{1}{2}, 0\right)$	$-\frac{p_2}{2} + \frac{p_3}{2}$
$\mathbf{Q}_{\text{inc}}^{\text{III}} = (1, M, 1)$	$-\frac{1}{2(p_2+2p_3)} - \frac{p_3}{2}$
$\mathbf{Q}_{\text{inc}}^{\text{II}(-)} = (q_x, q_y, 1)$, $\mathbf{Q}_{\text{inc}}^{\text{II}(-)} = (q_x, q_y, 0)$	$-\frac{c_1^2}{8p_3} - \frac{p_2}{2} + \frac{p_3}{2}$, $c_1 = 2p_3 - p_2 - 1$
$\mathbf{Q}_{\text{inc}}^{\text{II}(+)} = (q_x, q_y, 0)$, $\mathbf{Q}_{\text{inc}}^{\text{II}(+)} = (q_x, q_y, 1)$	$-\frac{c_2^2}{8p_3} - \frac{p_2}{2} + \frac{p_3}{2}$, $c_2 = 2p_3 - p_2 + 1$

Table A.1: Ordering wave vectors for each antiferromagnetic state and its respective classical energy.

3. When $E(\mathbf{Q}_{\text{inc}}^{\text{II}(+)}) < E(\mathbf{Q}_{\text{inc}}^{\text{II}})$, we end up with the equation

$$p_3^3 + \left(\frac{p_2}{2} - 1\right) p_3^2 + \left(\frac{1 - p_2^2}{4}\right) p_3 - \left(\frac{p_2 \left(p_2 - 1\right)^2}{8}\right) < 0, \tag{A.22}$$

which has the trivial solution

$$p_3 < \frac{p_2}{2}. \tag{A.23}$$

4. When $E(\mathbf{Q}_{\text{AF}}^{\text{II}}) < E(\mathbf{Q}_{\text{inc}}^{\text{II}(-)})$ we have the following result

$$p_3 < \frac{p_2 + 1}{2} \tag{A.24}$$

5. If we have $E(\mathbf{Q}_{\text{inc}}^{\text{II}(-)}) < E(\mathbf{Q}_{\text{inc}}^{\text{III}})$, we find the equation

$$p_3^3 + \left(\frac{p_2}{2} + 1\right) p_3^2 - \left(\frac{p_2^2 - 1}{4}\right) p_3 - \left(\frac{p_2 \left(p_2 + 1\right)^2}{8}\right) > 0. \tag{A.25}$$

with the trivial solution

$$p_3 > \frac{p_2}{2} \tag{A.26}$$

6. The last case is when $E(\mathbf{Q}_{\text{AF}}^{\text{I}}) < E(\mathbf{Q}_{\text{inc}}^{\text{II}(-)})$. It give us the result

$$p_3 < \frac{3 - p_2 \pm \sqrt{8\left(1 - p_2\right)}}{2}. \tag{A.27}$$

By comparing each of these cases, we can conclude that the ordering vector $\mathbf{Q}_{\text{inc}}^{\text{II}(-)}$ is not stable against the other phases. With the equations above we can predict that the shape of the phase diagram is like the Fig.(2.2). By this point end on we should always use $\mathbf{Q}_{\text{inc}}^{\text{II}}$ instead of $\mathbf{Q}_{\text{inc}}^{\text{II}(+)}$.

A.2 Continuous versus discontinuous transitions lines.

Another simple check that we can make is to test if the wave vectors are continuous in each critical line of the phase diagram. This is a crucial point in order to investigate the $1/S$ corrections in the framework of spin wave calculations, since we have already had some results for the commensurate phases.

First, let us test the continuity of $\mathbf{Q}_{\text{inc}}^{\text{II}}$ when we approaching to the critical lines that delimits $\mathbf{Q}_{\text{AF}}^{\text{I}}$ end $\mathbf{Q}_{\text{AF}}^{\text{III}}$. For $\mathbf{Q}_{\text{inc}}^{\text{II}}$, we have the condition

$$\cos\left(\frac{q_x}{2}\right) = -\cos\left(\frac{q_y}{2}\right) = \pm\sqrt{\frac{2p_2 - p_2 + 1}{4p_3}}, \tag{A.28}$$

that can be written as

$$\cos\left(\frac{q_x}{2}\right) = \cos\left(\frac{q_y}{2} + \pi\right). \tag{A.29}$$

Therefore, we have the relation between q_x and q_y

$$q_x = \pm q_y \pm 2\pi + 4n\pi. \tag{A.30}$$

When we approach to the critical line defined by $p_3^c = \frac{p_2-1}{2}$, that is the critical line that delimits the phase transition between $\mathbf{Q}_{\text{inc}}^{\text{II}}$ and $\mathbf{Q}_{\text{AF}}^{\text{II}}$, we end up with the following condition for q_x

$$\cos\left(\frac{q_x}{2}\right) = 0. \tag{A.31}$$

This implies that $q_x = \pm\pi + 2n\pi$ and $q_y = \pm\pi$. This is the limit of wave-vector $\mathbf{Q}_{\text{AF}}^{\text{II}} = (\pi, \pi, 0)$ and we conclude that $\mathbf{Q}_{\text{inc}}^{\text{inc}}$ is continuous in this critical line.

If we approach to the line between $\mathbf{Q}_{\text{inc}}^{\text{II}}$ and $\mathbf{Q}_{\text{AF}}^{\text{I}}$, $p_3^c = \frac{1-p_2}{2}$, we end up with

$$\cos\left(\frac{q_x}{2}\right) = \pm 1 \tag{A.32}$$

which means $q_x = \pm 2\pi + 2n\pi$ and $q_y = \pm 2\pi$. This is the limit of wave-vector $\mathbf{Q}_{\text{AF}}^{\text{I}} = (2\pi, 2\pi, 0)$ and we conclude that $\mathbf{Q}_{\text{inc}}^{\text{II}}$ is also continuous in this critical line.

On the other hand, if we approach to the line between $\mathbf{Q}_{\text{inc}}^{\text{II}}$ and $\mathbf{Q}_{\text{inc}}^{\text{III}}$, $p_3^c = \frac{p_2}{2}$, we end up with the condition

$$\cos\left(\frac{q_x}{2}\right) = \pm\frac{1}{\sqrt{2p_2}} \tag{A.33}$$

This does not correspond to the limit when we take the relations of cosines for $\mathbf{Q}_{\text{inc}}^{\text{III}}$ and this tells that the wave vector is not continuous at this critical line. Although, in the limit of $p_2 \to \infty$, we have $\mathbf{Q}_{\text{inc}}^{\text{III}} \to \mathbf{Q}_{\text{AF}}^{\text{III}}$ and $\mathbf{Q}_{\text{inc}}^{\text{II}} \to \mathbf{Q}_{\text{AF}}^{\text{II}}$, which corresponds to the limit of an antiferromagnetic in 2D case, with $\mathbf{Q}_{\text{AF}}^{\text{III}} = (0, \pi)$ and $\mathbf{Q}_{\text{AF}}^{\text{II}} = (\pi, \pi)$.

A.3 The mean field decoupling of SU(n) Heisenberg model.

We are going to explain the procedure of mean field decoupling that led to definitions in eq.(2.32) and eq.(2.33). For this aim, we use one generalization of the Abrikosov fermionic representation of the spin operators

$$\mathbf{S}_i = \frac{1}{n}\sum_{\alpha\beta} \chi_{i\alpha}^\dagger \vec{\sigma}_{\alpha\beta} \chi_{i\beta} \tag{A.34}$$

where, $\chi_{i\alpha}^\dagger(\chi_{i\alpha})$ is the creation (destruction) operator for fermions at site i and the index α specifies the spin, where $\alpha = 1, ..., n$. The operators satisfy the local constraint

$\sum_\sigma \chi^\dagger_{i,\sigma}\chi_{i,\sigma} = n/2$, with $n/2$ fermions on each site, each one with a different flavour due to the Pauli exclusion principle [Affleck 1988a, Marston 1989]. As n increases from 2 to larger values, quantum spin fluctuations are enhanced, weakening any spin order.

Let us use this in the Heisenberg Hamiltonian

$$\hat{H} = \frac{1}{n^2}\sum_{\langle i,j\rangle} J_{i,j} \sum_{\alpha\beta,\alpha'\beta'} \chi^\dagger_{i\alpha}\chi_{j\beta}\chi^\dagger_{j\alpha'}\chi_{i\beta'}\left(n\delta_{\alpha\beta'}\delta_{\alpha'\beta} - \delta_{\alpha\beta}\delta_{\alpha'\beta'}\right) \tag{A.35}$$

$$\hat{H} = \frac{J}{n}\sum_{\langle i,j\rangle}\sum_{\alpha\beta} \chi^\dagger_{i\alpha}\chi_{j\beta}\chi^\dagger_{j\beta}\chi_{i\alpha} - \frac{J}{n^2}\sum_{\langle i,j\rangle}\sum_{\alpha,\alpha'} \chi^\dagger_{i\alpha}\chi_{i\alpha}\chi^\dagger_{j\alpha'}\chi_{j\alpha'} \tag{A.36}$$

If $J = J_{Weiss} + J_{SL}$, applying the mean field theory, we have

$$\begin{aligned}\hat{H} =& -\frac{J^{Weiss}_{(l)}}{n}\sum_{\langle i,j\rangle}\sum_{\alpha\beta}[\langle\chi^\dagger_{i\alpha}\chi_{i\alpha}\rangle\chi^\dagger_{j\beta}\chi_{j\beta} + \chi^\dagger_{i\alpha}\chi_{i\alpha}\langle\chi^\dagger_{j\beta}\chi_{j\beta}\rangle + \langle\chi^\dagger_{i\alpha}\chi_{i\alpha}\rangle\langle\chi^\dagger_{j\beta}\chi_{j\beta}\rangle] \\ & -\frac{J^{SL}_{(l)}}{n}\sum_{\langle i,j\rangle}\sum_{\alpha}[\langle\chi^\dagger_{i\alpha}\chi_{j\alpha}\rangle\chi^\dagger_{j\alpha}\chi_{i\alpha} + \chi^\dagger_{i\alpha}\chi_{j\alpha}\langle\chi^\dagger_{j\alpha}\chi_{i\alpha}\rangle + \langle\chi^\dagger_{i\alpha}\chi_{j\alpha}\rangle\langle\chi^\dagger_{j\alpha}\chi_{i\alpha}\rangle]\end{aligned} \tag{A.37}$$

Here we do not take into account the second term in eq.(A.36) because it is of second order in large n expansion. In eq.(A.37) we wrote the products of fermionic operators like in mean field formalism. Here we consider the couplings $J_{Weiss} > 0$ and $J_{SL} > 0$. The interactions in a 3-d BCT Lattice are J_1-J_2-J_3,

$$\begin{aligned}\hat{H} =& -\frac{J^{SL}_{(l)}}{n}\sum_{\langle i,j\rangle}\sum_{\alpha}[\langle\chi^\dagger_{i\alpha}\chi_{j\alpha}\rangle\chi^\dagger_{j\alpha}\chi_{i\alpha} + \chi^\dagger_{i\alpha}\chi_{j\alpha}\langle\chi^\dagger_{j\alpha}\chi_{i\alpha}\rangle + \langle\chi^\dagger_{i\alpha}\chi_{j\alpha}\rangle\langle\chi^\dagger_{j\alpha}\chi_{i\alpha}\rangle] \\ & + \frac{J^{Weiss}_{(l)}}{n}\sum_{\langle i,j\rangle}\sum_{\alpha}[\langle\chi^\dagger_{i\alpha}\chi_{i\alpha}\rangle\chi^\dagger_{j\alpha}\chi_{j\alpha} + \chi^\dagger_{i\alpha}\chi_{i\alpha}\langle\chi^\dagger_{j\alpha}\chi_{j\alpha}\rangle - \langle\chi^\dagger_{i\alpha}\chi_{i\alpha}\rangle\langle\chi^\dagger_{j\alpha}\chi_{j\alpha}\rangle]\end{aligned} \tag{A.38}$$

Now we defined three kinds of fields $\tilde{\varphi}^1_{i,j}$,$\tilde{\varphi}^2_{i,j}$ and $\tilde{\varphi}^3_{i,j}$ by

$$\tilde{\varphi}^{(l)}_{i,j} = -\sum_\alpha \langle\chi^\dagger_{i\alpha}\chi_{j\alpha}\rangle \tag{A.39}$$

That are associated with each coupling constant J_1, J_2 and J_3 respectively. The magnetization is defined by

$$m_{\vec{R}_i} = \frac{1}{n}\sum_\alpha \langle\chi^\dagger_{i\alpha}\chi_{i\alpha}\rangle \tag{A.40}$$

Appendix B

Detailed calculations for chapter 3

B.1 The structure factors γ_k.

In this section we present the derivations for the relation that were presented in the section 3 for the structure factors γ_k associated with the hoping $t_{i,j}$. First, let us write down the Hamiltonian from the real to k-space, by using the Fourier transforms of the creation destruction operators. Remembering the Hamiltonian

$$H = \sum_i (E_0 + me^{i\mathbf{Q}\cdot\mathbf{R}_i}) c_i^\dagger c_i + \sum_{\langle i,j\rangle} t_{ij} c_i^\dagger c_j, \tag{B.1}$$

with the respective definitions for the hoping terms that specify the point group symmetries in eq.(3.2), (3.3) and (3.4). We highlight that the sing $\pm$ in (3.3) and (3.4), means that the it is alternating between two sites. By making use of the Fourier transforms of the c's operators

$$c_i^\dagger = \frac{1}{\sqrt{N}} \sum_{\mathbf{k}}^{BCT-BZ} e^{-i\mathbf{k}\cdot\mathbf{R}_i} c_{\mathbf{k}}^\dagger \tag{B.2}$$

$$c_{\mathbf{k}}^\dagger = \frac{1}{\sqrt{N}} \sum_{\mathbf{R}}^{BCT-Lattice} e^{i\mathbf{k}\cdot\mathbf{R}_i} c_i^\dagger \tag{B.3}$$

The sum in sites are related with the BCT lattice. The Hamiltonian can be seen as a sum $H = H_0 + H_t$, where $H_0 = \sum_i (E_o + me^{i\mathbf{Q}\cdot\mathbf{R}_i}) c_i^\dagger c_i$ and $H_1 = \sum_{\langle i,j\rangle} t_{ij} c_i^\dagger c_j$. Let us concentrate on the hopping term

$$H_1 = \sum_{\langle i,j\rangle} t_{ij} c_i^\dagger c_j, \tag{B.4}$$

since is this part that gives rise the factor's structure γ.

We developed the calculation for a general hopping $t_{i,j}$ and at the end we will concentrate only in the first neighbours inter-plane, since the in-plane relations can be derived in the same fashion as for square lattice. For the hopping inter-plane, we have

$$t_{ij} \quad = \quad t_1 \pm i\Delta_c. \tag{B.5}$$

and

$$t_{ij} \quad = \quad t_1 \pm \Delta_M. \tag{B.6}$$

For the CSL case, the sign plus means that the link is oriented in the incoming direction of the central site, otherwise is minus. On the other hand, for the MSL case the sign plus means a bonding (full line) between one site at corner and central site, otherwise is an anti-boding (dashed line), as showed in fig(3.1).

By using the Fourier transforms in (B.3), we rewrite the Hamiltonian and we end up with

$$H_1 = \frac{1}{N}\sum_{\mathbf{k},\mathbf{k'}} c^{\dagger}_{\mathbf{k}} c_{\mathbf{k'}} \sum_{\mathbf{i}} e^{-i(\mathbf{k}-\mathbf{k'})\cdot\mathbf{R_i}} E_{\mathbf{R}_i}(\mathbf{k'}) \tag{B.7}$$

Where we defined $E_{\mathbf{R}_i}(\mathbf{k'}) = \sum_{\delta} t_{i,i+\delta} e^{i\mathbf{k'}\cdot\delta}$ and the sum is k runs over the first Brillouin zone of BCT. The next step is to split the sum in the BCT-Brillouin zone as being a sum of two tetragonal lattices, where we use the fact that the BCT is bipartite in two simple tetragonal sub-lattices A and B. We end up with four terms

$$\begin{aligned} H_1 = \frac{1}{N}\sum_{\mathbf{k},\mathbf{k'}} c^{\dagger}_{\mathbf{k}} c_{\mathbf{k'}} \sum_{i} e^{-i(\mathbf{k}-\mathbf{k'})\cdot\mathbf{R}_i} E_{\mathbf{R}_i}(\mathbf{k'}) \\ + \frac{1}{N}\sum_{\mathbf{k},\mathbf{k'}} c^{\dagger}_{\mathbf{k}} c_{\mathbf{k'}+\mathbf{Q}} \sum_{i} e^{-i(\mathbf{k}-\mathbf{k'}-\mathbf{Q})\cdot\mathbf{R_i}} E_{\mathbf{R}_i}(\mathbf{k'}+\mathbf{Q}) \\ + \frac{1}{N}\sum_{\mathbf{k},\mathbf{k'}} c^{\dagger}_{\mathbf{k}+\mathbf{Q}} c_{\mathbf{k'}} \sum_{i} e^{-i(\mathbf{k}+\mathbf{Q}-\mathbf{k'})\cdot\mathbf{R}_i} E_{\mathbf{R}_i}(\mathbf{k'}) \\ + \frac{1}{N}\sum_{\mathbf{k},\mathbf{k'}} c^{\dagger}_{\mathbf{k}+\mathbf{Q}} c_{\mathbf{k'}+\mathbf{Q}} \sum_{i} e^{-i(\mathbf{k}-\mathbf{k'})\cdot\mathbf{R}_i} E_{\mathbf{R}_i}(\mathbf{k'}+\mathbf{Q}). \end{aligned}$$

Now the sums in k run over the T-lattice. But the sums in i run over the BCT lattice.

We can also split the sum in the BCT-Lattice in a sum for sub-lattice A and B. This requires that $t_{i,i+\delta} = t^A_{\delta}$ if $R_i \in$ A or $t_{i,i+\delta} = t^B_{\delta}$ if $R_i \in$ B. The condition $t^B_{\delta} = \left(t^A_{\delta}\right)^*$ preserves the hermiticity of the Hamiltonian. Which gives the relation between $E(\mathbf{k}) \equiv E_{\mathbf{B}}(\mathbf{k'}) = (E_{\mathbf{A}}(\mathbf{k'}))^*$. We know that $\frac{1}{N}\sum_{\mathbf{R}} e^{-i(\mathbf{k}-\mathbf{k'})\cdot\mathbf{R}} = \frac{1}{2}\delta_{\mathbf{k}\mathbf{k'}}$ and $e^{-i\mathbf{Q}\cdot\mathbf{R}} = \pm 1$ if $\mathbf{R}$

belongs to A or B, respectively. Then,

$$H = \frac{1}{2}\sum_{\mathbf{k}} c^{\dagger}_{\mathbf{k}} c_{\mathbf{k}}[E(\mathbf{k}) + E^{*}(\mathbf{k})] + \frac{1}{2}\sum_{\mathbf{k}} c^{\dagger}_{\mathbf{k}+\mathbf{Q}} c_{\mathbf{k}+\mathbf{Q}}\left[E\left(\mathbf{k}+\mathbf{Q}\right) + E^{*}\left(\mathbf{k}+\mathbf{Q}\right)\right]$$
$$+\frac{1}{2}\sum_{\mathbf{k}} c^{\dagger}_{\mathbf{k}+\mathbf{Q}} c_{\mathbf{k}}\left[E\left(\mathbf{k}\right) - E^{*}\left(\mathbf{k}\right)\right] + \frac{1}{2}\sum_{\mathbf{k}} c^{\dagger}_{\mathbf{k}} c_{\mathbf{k}+\mathbf{Q}}[E\left(\mathbf{k}+\mathbf{Q}\right) - E^{*}\left(\mathbf{k}+\mathbf{Q}\right)] \tag{B.8}$$

We can write the Hamiltonian in a matrix representation, as follows

$$H=\sum_{\mathbf{k}} \Psi^{\dagger}_{\mathbf{k}} h'_{\mathbf{k}} \Psi_{\mathbf{k}}. \tag{B.9}$$

With the definition of $\Psi_{\mathbf{k}}$ given by eq.(3.8) and

$$h'_{\mathbf{k}}=\begin{pmatrix} \frac{E(\mathbf{k})+E^{*}(\mathbf{k})}{2} & \frac{E(\mathbf{k}+\mathbf{Q})-E^{*}(\mathbf{k}+\mathbf{Q})}{2} \\ \frac{E(\mathbf{k})-E^{*}(\mathbf{k})}{2} & \frac{E(\mathbf{k}+\mathbf{Q})+E^{*}(\mathbf{k}+\mathbf{Q})}{2} \end{pmatrix}. \tag{B.10}$$

With the definition of $E(\mathbf{k})$, the hopping $t_{i,j}$ and taking the wave vector $\mathbf{Q} = (1,1,1)$ we can recognize the following terms when doing the sum in the neighbours vectors δ.

$$\frac{E(\mathbf{k}) + E^{*}(\mathbf{k})}{2} = t_1\gamma^1_k + t_2\gamma^2_k + t_3\gamma^3_k \tag{B.11}$$

$$\frac{E\left(\mathbf{k}+\mathbf{Q}\right) + E^{*}\left(\mathbf{k}+\mathbf{Q}\right)}{2} = -t_1\gamma^1_k + t_2\gamma^2_k + t_3\gamma^3_k \tag{B.12}$$

$$\frac{E\left(\mathbf{k}+\mathbf{Q}\right) - E^{*}\left(\mathbf{k}+\mathbf{Q}\right)}{2} = i8\Delta_{SL}\gamma^{SL}_k \tag{B.13}$$

$$\frac{E(\mathbf{k}) - E^{*}(\mathbf{k})}{2} = i8\Delta_{SL}\gamma^{SL}_k \tag{B.14}$$

If we add the contribution from m and E_0 we recover the $h_{\mathbf{k}}$ matrix defined in section (**??**).

We would like to highlight the derivation of the k dependent term in V_k, which came from the Δ in $t_{i,j}$. Considering the first neighbours inter-plane. In this case, the sum in δ take in to account the eight different neighbours inter-plane. They are respectively

$$\delta=(x,y,z) \tag{B.15}$$
$$\delta_1=(a/2,a/2,c/2) \tag{B.15a}$$
$$\delta_2=(-a/2,a/2,c/2) \tag{B.15b}$$
$$\delta_3=(-a/2,-a/2,c/2) \tag{B.15c}$$
$$\delta_4=(a/2,-a/2,c/2) \tag{B.15d}$$
$$\delta_5=(-a/2,-a/2,-c/2) \tag{B.15e}$$
$$\delta_6=(a/2,-a/2,-c/2) \tag{B.15f}$$
$$\delta_7=(a/2,a/2,-c/2) \tag{B.15g}$$
$$\delta_8=(-a/2,a/2,-a/2) \tag{B.15h}$$

The first sum in δ taking the t_1 term produce the γ_k^1 and the second sum give us γ_k^{SL}. This last terms can be γ_k^c or γ_k^m depending on the definition of t_{ij} (eq.(3.3) and eq.(3.4)). This complete our demonstration of the relation that have been presented so far in that section.

B.2 Diagonalisation of the Hamiltonian.

The procedure for diagonalizing the Hamiltonian in k-space use a general representation of Bogoliubov transformations. The Hamiltonian in eq(3.1) must be in a diagonal form and in order to do that we invoke a unitary transformation matrix that makes

$$\Psi_{\mathbf{k}} = \hat{P}_k \Psi_k^{diag} \tag{B.16}$$

Where, as introduced before, the matrix for the spin component is

$$\Psi_{\mathbf{k}} = \begin{pmatrix} c_{\mathbf{k}} \\ c_{\mathbf{k}+\mathbf{Q}} \end{pmatrix} \tag{B.17}$$

While in the diagonal basis is

$$\Psi_{\mathbf{k}}^{diag} = \begin{pmatrix} c_{+,\mathbf{k}} \\ c_{-,\mathbf{k}} \end{pmatrix} \tag{B.18}$$

The unitary matrix transformation is

$$\hat{P}_k = \begin{pmatrix} \cos\theta_k & e^{i\varphi}\sin\theta_k \\ -e^{-i\varphi}\sin\theta_k & \cos\theta_k \end{pmatrix} \tag{B.19}$$

Which allow us to write

$$h_{\mathbf{k}} = \hat{P}_k h_{\mathbf{k}}^{dia} \hat{P}_k^{-1}. \tag{B.20}$$

Where $h_{\mathbf{text}}$ is the matrix in (3.9) and $h_{\mathbf{k}}^{dia}$ is the matrix of the Hamiltonian written down in the diagonal basis with the diagonal terms being the eigenvalues of H. Consequently, the Hamiltonian in the diagonal basis is

$$\hat{H} = \sum_{\mathbf{k}}^{T-BZ} \begin{pmatrix} c_{+,\mathbf{k}}^\dagger & c_{-,\mathbf{k}}^\dagger \end{pmatrix} \begin{pmatrix} E_{\mathbf{k}}^+ & 0 \\ 0 & E_{\mathbf{k}}^- \end{pmatrix} \begin{pmatrix} c_{+,\mathbf{k}} \\ c_{-,\mathbf{k}} \end{pmatrix} \tag{B.21}$$

Where the dispersions are given by

$$E_{\mathbf{k}}^{\pm} = \frac{\varepsilon(k)+\varepsilon(k+Q)}{2} \pm \sqrt{|V(k)|^2 + \left(\frac{\varepsilon(k)-\varepsilon(k+Q)}{2}\right)^2} \tag{B.22}$$

We have to solve the matrix equation (B.20) that leads to the following linear systems of equations.

$$\varepsilon_{\mathbf{k}} = E^{+}_{\mathbf{k}} \cos^2\theta_k + E^{-}_{\mathbf{k}} \sin^2\theta_k \tag{B.23}$$

$$\varepsilon_{\mathbf{k}+\mathbf{Q}} = E^{+}_{\mathbf{k}} \sin^2\theta_k + E^{-}_{\mathbf{k}} \cos^2\theta_k \tag{B.24}$$

$$V_{\mathbf{k}} = (E^{-}_{\mathbf{k}} - E^{+}_{\mathbf{k}})\, e^{-i\phi} \sin\theta_k \cos\theta_k \tag{B.25}$$

$$V^{*}_{\mathbf{k}} = (E^{-}_{\mathbf{k}} - E^{+}_{\mathbf{k}})\, e^{i\phi} \sin\theta_k \cos\theta_k \tag{B.26}$$

the equation (B.26) and (B.26) are linearly dependants since one is the conjugate of the other. The relations for $\cos\theta_k$ and $\sin\theta_k$. By summing and subtracting B.24 and B.25, we have

$$\varepsilon_{\mathbf{k}} + \varepsilon_{\mathbf{k}+\mathbf{Q}} = E^{+}_{\mathbf{k}} + E^{-}_{\mathbf{k}} \tag{B.27}$$

$$\varepsilon_{\mathbf{k}} - \varepsilon_{\mathbf{k}+\mathbf{Q}} = (E^{+}_{\mathbf{k}} - E^{-}_{\mathbf{k}}) \cos 2\theta_k \tag{B.28}$$

From the second equation we easily obtain the condition of θ_k by

$$\cos 2\theta_k = \frac{\varepsilon_{\mathbf{k}} - \varepsilon_{\mathbf{k}+\mathbf{Q}}}{\sqrt{|V_k|^2 + \left(\frac{\varepsilon_{\mathbf{k}} - \varepsilon_{\mathbf{k}+\mathbf{Q}}}{2}\right)^2}}. \tag{B.29}$$

$$\sin 2\theta_k = \frac{|V_k|}{\sqrt{|V_k|^2 + \left(\frac{\varepsilon_k - \varepsilon_{k+Q}}{2}\right)^2}} \tag{B.30}$$

$$\tag{B.31}$$

The condition for φ_k is extract from (B.26), written in the polar form for a complex number. Therefore,

$$\varphi_k = -(\arg(V_k) \pm \pi). \tag{B.32}$$

This complete our demonstration of the relation in eq.(3.21) and (3.22).

B.3 The density-density correlation function.

Let us derive the result for the density-density correlation function in eq.(3.27). The procedure is analogous for the current-current correlation in eq.(**??**).

Recall that the dynamical effective density-density correlation function or Raman response $\tilde{S}$ can be written in terms of a dynamical effective density susceptibility $\tilde{\chi}$ via the fluctuation dissipation theorem Recall the effective density operator $\hat{\tilde{\rho}}(\mathbf{q}, \tau)$,

$$\hat{\tilde{\rho}}^{\lambda}(\mathbf{q}, \tau) = \sum_{\mathbf{k},\alpha,\alpha'} \gamma^{\lambda}_{\alpha,\alpha'}(\mathbf{k}) c^{\dagger}_{\mathbf{k}+\mathbf{q}/2,\alpha}(\tau) c_{\mathbf{k}-\mathbf{q}/2\alpha'}(\tau) \tag{B.33}$$

The operators $c^{\dagger}_{\mathbf{k}+\mathbf{q}/2,\alpha}(\tau)$ and $c_{\mathbf{k}-\mathbf{q}/2,\alpha'}(\tau)$ are time dependent, as in the Heisenberg representation, and they are related with the creation and destruction of electrons, respectively.

We can work out the correlation function in 3.25, just inserting the definition of $\hat{\tilde{\rho}}^{\lambda}(\mathbf{q},\tau)$ on it. In this way,

$$\tilde{\chi}^{\lambda}(\mathbf{q},i\omega) = -\frac{1}{\mathcal{V}}\int_0^{\beta} d\tau e^{i\omega\tau} \sum_{\mathbf{k}_1,\mathbf{k}_2} \sum_{\alpha_1,\alpha_1'\alpha_2,\alpha_2'} \gamma^{\lambda}_{\alpha_1\alpha_1'}(\mathbf{k}_1)\gamma^{\lambda}_{\alpha_2\alpha_2'}(\mathbf{k}_2) \\ \times \langle T_{\tau}(c^{\dagger}_{\mathbf{k}_1+\frac{\mathbf{q}}{2},\alpha_1}(\tau)c_{\mathbf{k}_1-\frac{\mathbf{q}}{2},\alpha_1'}(\tau)c^{\dagger}_{\mathbf{k}_2-\frac{\mathbf{q}}{2},\alpha_2}(0)c_{\mathbf{k}_2+\frac{\mathbf{q}}{2},\alpha_2'}(0))\rangle \quad \text{(B.34)}$$

Using the Wick's theorem in $\langle ...\rangle$, we arrive into a product of two Green Functions

$$\langle ...\rangle = \langle c_{\mathbf{k}_1-\frac{\mathbf{q}}{2},\alpha_1'}(\tau)c^{\dagger}_{\mathbf{k}_1+\frac{\mathbf{q}}{2},\alpha_1}(\tau)\rangle\langle c_{\mathbf{k}_2+\frac{\mathbf{q}}{2},\alpha_2'}(0)c^{\dagger}_{\mathbf{k}_2-\frac{\mathbf{q}}{2},\alpha_2}(0)\rangle \\ - \langle c_{\mathbf{k}_1-\frac{\mathbf{q}}{2},\alpha_1'}(\tau)c^{\dagger}_{\mathbf{k}_2-\frac{\mathbf{q}}{2},\alpha_2}(0)\rangle\langle c_{\mathbf{k}_2+\frac{\mathbf{q}}{2},\alpha_2'}(0)c^{\dagger}_{\mathbf{k}_1+\frac{\mathbf{q}}{2},\alpha_1}(\tau)\rangle \quad \text{(B.35)}$$

The definition of Green's function is $G^{\alpha\alpha'}_{kk'}(\tau) = -\langle c_{k,\alpha}(\tau)c^{\dagger}_{k',\alpha'}(0)\rangle$ for $\tau > 0$, where α are eigenumbers for $\hat{H}$. Then

$$\langle ...\rangle = G^{\alpha_1\alpha_1'}_{\mathbf{k}_1-\frac{\mathbf{q}}{2},\mathbf{k}_1+\frac{\mathbf{q}}{2}}(0)G^{\alpha_2\alpha_2'}_{\mathbf{k}_2+\frac{\mathbf{q}}{2},\mathbf{k}_2-\frac{\mathbf{q}}{2}}(0) - G^{\alpha_1',\alpha_2}_{\mathbf{k}_1-\frac{\mathbf{q}}{2},\mathbf{k}_2-\frac{\mathbf{q}}{2}}(\tau)G^{\alpha_1\alpha_2'}_{\mathbf{k}_2+\frac{\mathbf{q}}{2},\mathbf{k}_1+\frac{\mathbf{q}}{2}}(-\tau) \quad \text{(B.36)}$$

We can write down the Fourier transform for the Green's function as

$$G_{\mathbf{k}}(\tau) = \frac{1}{\beta}\sum_n e^{-i\omega_n\tau}G_{\mathbf{k}}(i\omega_n) \quad \text{(B.37)}$$

We end up,

$$\langle ...\rangle = \frac{1}{\beta^2}\sum_{n_1,n_2} G^{\alpha_1\alpha_1'}_{\mathbf{k}_1-\frac{\mathbf{q}}{2},\mathbf{k}_1+\frac{\mathbf{q}}{2}}(i\omega_{n_1})G^{\alpha_2\alpha_2'}_{\mathbf{k}_2+\frac{\mathbf{q}}{2},\mathbf{k}_2-\frac{\mathbf{q}}{2}}(i\omega_{n_2}) \quad \text{(B.38)} \\ -\frac{1}{\beta^2}\sum_{n_3,n_4} e^{-i\omega_{n_3}\tau}\, e^{i\omega_{n_4}\tau}G^{\alpha_1\alpha_2'}_{\mathbf{k}_2+\frac{\mathbf{q}}{2},\mathbf{k}_1+\frac{\mathbf{q}}{2}}(i\omega_{n_4})G^{\alpha_1',\alpha_2}_{\mathbf{k}_1-\frac{\mathbf{q}}{2},\mathbf{k}_2-\frac{\mathbf{q}}{2}}(i\omega_{n_3})$$

Therefore,

$$\tilde{\chi}^{\lambda}(\mathbf{q},i\omega) = \frac{1}{\mathcal{V}}\int_0^{\beta} d\tau e^{i\omega\tau} \sum_{\mathbf{k}_1,\mathbf{k}_2} \sum_{\alpha_1,\alpha_1'\alpha_2,\alpha_2'} \gamma^{\lambda}_{\alpha_1\alpha_1'}(\mathbf{k}_1)\gamma^{\lambda}_{\alpha_2\alpha_2'}(\mathbf{k}_2) \\ \times \left[\frac{1}{\beta^2}\sum_{n_3,n_4} e^{-i\omega_{n_3}\tau}\, e^{i\omega_{n_4}\tau}G^{\alpha_1\alpha_2'}_{\mathbf{k}_2+\frac{\mathbf{q}}{2},\mathbf{k}_1+\frac{\mathbf{q}}{2}}(i\omega_{n_4})G^{\alpha_1',\alpha_2}_{\mathbf{k}_1-\frac{\mathbf{q}}{2},\mathbf{k}_2-\frac{\mathbf{q}}{2}}(i\omega_{n_3}) \right. \\ \left. -\frac{1}{\beta^2}\sum_{n_1,n_2} G^{\alpha_1\alpha_1'}_{\mathbf{k}_1-\frac{\mathbf{q}}{2},\mathbf{k}_1+\frac{\mathbf{q}}{2}}(i\omega_{n_1})G^{\alpha_2\alpha_2'}_{\mathbf{k}_2+\frac{\mathbf{q}}{2},\mathbf{k}_2-\frac{\mathbf{q}}{2}}(i\omega_{n_2})\right] \quad \text{(B.39)}$$

The integrals in imaginary time give $\int_0^{\beta} d\tau\, e^{i\omega\tau} = \beta\delta_{-\omega,0}$ and $\int_0^{\beta} d\tau\, e^{-i(\omega_{n_3}-\omega-\omega_{n_4})\tau} = \beta\delta_{\omega_{n_3},\omega_{n_4}+\omega}$. We remark that all ω_n are fermionic Matsubara frequencies and that ω is a

bosonic one. The Green function for the Hamiltonian in a diagonalized form is $G^{\alpha\alpha'}_{\mathbf{k}\mathbf{k}'}(i\omega_n) = \delta_{\alpha\alpha'}\delta_{\mathbf{k}\mathbf{k}'}G_{\mathbf{k}}(i\omega_n)$. Then, the final result is

$$\tilde{\chi}^{\lambda}(\mathbf{q}=0,i\omega) = \frac{1}{\mathcal{V}}\sum_{\mathbf{k}}\sum_{\alpha_1,\alpha_2}\gamma^{\lambda}_{\alpha_1\alpha_2}(\mathbf{k})\gamma^{\lambda}_{\alpha_2\alpha_1}(\mathbf{k})\frac{1}{\beta}\sum_{n}G_{\mathbf{k}}(i\omega_n)G_{\mathbf{k}}(i\omega_n+i\omega) - \frac{1}{\mathcal{V}}\sum_{\mathbf{k}_1,\mathbf{k}_2}\sum_{\alpha_1\alpha_2}\gamma^{\alpha_1\alpha_1}_{\mu}(\mathbf{k}_1)\gamma^{\alpha_2\alpha_2}_{\nu}(\mathbf{k}_2)\frac{1}{\beta}\sum_{n_1,n_2}G_{\mathbf{k}_1}(i\omega_{n_1})G_{\mathbf{k}_2}(i\omega_{n_2})\delta_{\omega,0} \tag{B.40}$$

We have the following dynamical part

$$\tilde{\chi}^{\lambda}(i\omega) = \frac{1}{\mathcal{V}}\sum_{\mathbf{k}}\frac{1}{\beta}\sum_{n}\mathbf{Tr}\left[\gamma^{\lambda}(\mathbf{k})G_{\mathbf{k}}(i\omega_n+i\omega)\gamma^{\lambda}(\mathbf{k})G_{\mathbf{k}}(i\omega_n)\right], \tag{B.41}$$

that provides the signal at the charge channel. The next step is to compute the trace in this expression and the sums in Matsubara fermionic frequency. Finally, we perform the numerical integration over k space in the first Brillouin zone of Simple T-lattice by replacing the sum into an integral as

$$\frac{1}{\mathcal{V}}\sum_{\mathbf{k}} \rightarrow \int_{TBZ}\frac{d^3k}{(2\pi)^3}. \tag{B.42}$$

B.4 Matsubara sums.

In the correlation functions on eq.(3.27) and (**??**), after write down the trace for each od this correlations, we must to perform the Matsubara's sum over the fermionic frequency ω_n. It can be done analytically, since they are of the kind

$$S = \frac{1}{\beta}\sum_{n}G^{\alpha}(\mathbf{k},i\omega_n+i\omega_m)G^{\alpha}(\mathbf{k},i\omega_n) \tag{B.43}$$

Where the Green's functions are $G^{\alpha}(\mathbf{k},i\omega_n) = 1/(i\omega_n - E^{\alpha}_{\mathbf{k}})$, α is $\pm$ related to the eigenvalue $E^{\pm}_{\mathbf{k}}$. We rewrite the product of these two green functions as

$$G^{\alpha}(\mathbf{k},i\omega_n+i\omega_m)G^{\alpha'}(\mathbf{k},i\omega_n) = \frac{1}{i\omega_m + E^{\alpha'}_{\mathbf{k}} - E^{\alpha}_{\mathbf{k}}}[G^{\alpha'}(\mathbf{k},i\omega_n) - G^{\alpha}(\mathbf{k},i\omega_n+i\omega_m)] \tag{B.44}$$

If we place this last expression inside the sum S and have in mind the usual result [Mahan 2000],

$$\frac{1}{\beta}\sum_{n}G^{\alpha}(\mathbf{k},i\omega_n) = n_F(E^{\alpha}_{\mathbf{k}}), \tag{B.45}$$

in which $n_F(E^{\alpha}_{\mathbf{k}})$ is the Fermi distribution, with energy $E^{\pm}_{\mathbf{k}}$. Finally, we get the following result

$$S = \frac{1}{i\omega_m + E^{\alpha'}_{\mathbf{k}} - E^{\alpha}_{\mathbf{k}}}(n_F(E^{\alpha'}_{\mathbf{k}}) - n_F(E^{\alpha}_{\mathbf{k}})) \tag{B.46}$$

References

[Affleck 1988a] Ian Affleck and J. Brad Marston. *Large- n limit of the Heisenberg-Hubbard model: Implications for high-T_c superconductors*. Phys. Rev. B, vol. 37, pages 3774–3777, Mar 1988. (Cited on pages 15, 16, 41, 42 and 77.)

[Affleck 1988b] Ian Affleck, Z. Zou, T. Hsu and P. W. Anderson. *SU(2) gauge symmetry of the large-U limit of the Hubbard model*. Phys. Rev. B, vol. 38, pages 745–747, Jul 1988. (Cited on page 15.)

[Anderson 1952] P. W. Anderson. *An Approximate Quantum Theory of the Antiferromagnetic Ground State*. Phys. Rev., vol. 86, pages 694–701, Jun 1952. (Cited on pages 10 and 11.)

[Anderson 1973] P.W. Anderson. *Resonating valence bonds: A new kind of insulator?* Materials Research Bulletin, vol. 8, no. 2, pages 153 – 160, 1973. (Cited on pages 7, 8, 10, 14, 37, 38 and 68.)

[Anderson 1987] P. W. Anderson, G. Baskaran, Z. Zou and T. Hsu. *Resonating – valence-bond theory of phase transitions and superconductivity in La_2CuO_4-based compounds*. Phys. Rev. Lett., vol. 58, pages 2790–2793, Jun 1987. (Cited on pages 8, 14, 40 and 44.)

[Andreev 1984] A.F. Andreev and I.A. Grishchuk. *Spin nematics*. Journal of Experimental and Theoretical Physics, vol. 60, no. 2, page 267, 1984. (Cited on page 7.)

[Ashcroft 1976] N.W. Ashcroft and N.D. Mermin. Solid state physics. Science: Physics. Saunders College,Orlando-FL., 1976. (Cited on page 1.)

[Balents 2010] Leon Balents. *Spin liquids in frustrated magnets*. Nature, vol. 464, pages 199–208, Mar 2010. (Cited on pages 7 and 14.)

[Bareille 2014] C. Bareille, F. L. Boariu, H. Schwab, P. Lejay, F. Reinert and A. F. Santander-Syro. *Momentum-resolved hidden-order gap reveals symmetry breaking and origin of entropy loss in URu_2Si_2*. Nature Communications, vol. 5, pages 1–11, July 2014. (Cited on page 49.)

[Baskaran 1987] G. Baskaran, Z. Zou and P.W. Anderson. *The resonating valence bond state and high-Tc superconductivity - A mean field theory*. Solid State Communications, vol. 63, no. 11, pages 973–976, 1987. (Cited on page 44.)

[Baskaran 1988] G. Baskaran and P. W. Anderson. *Gauge theory of high-temperature superconductors and strongly correlated Fermi systems*. Phys. Rev. B, vol. 37, pages 580–583, Jan 1988. (Cited on page 15.)

[Bauer 2014] B. Bauer, L. Cincio, B.P. Keller, M. Dolfi, G. Vidal, S. Trebst and A.W.W. Ludwig. *Chiral spin liquid and emergent anyons in a Kagome lattice Mott insulator*. Nature Communications, vol. 5, pages 1–8, Oct 2014. (Cited on page 16.)

[Baym 1990] G. Baym. Lectures on quantum mechanics. Advanced book program. Addison-Wesley, 1990. (Cited on page 18.)

[Bloch 1930] F. Bloch. *Zur Theorie des Ferromagnetismus*. Zeitschrift für Physik, vol. 61, no. 3, pages 206–219, 1930. (Cited on page 10.)

[Boariu 2013] F. L. Boariu, C. Bareille, H. Schwab, A. Nuber, P. Lejay, T. Durakiewicz, F. Reinert and A. F. Santander-Syro. *Momentum-Resolved Evolution of the Kondo Lattice into "Hidden Order" in* $\mathrm{URu_2Si_2}$. Phys. Rev. Lett., vol. 110, page 156404, Apr 2013. (Cited on pages 4 and 48.)

[Bogoljubov 1958] N. N. Bogoljubov. *On a new method in the theory of superconductivity*. Il Nuovo Cimento (1955-1965), vol. 7, no. 6, pages 794–805, 1958. (Cited on page 12.)

[Bourdarot 2010] Frederic Bourdarot, Elena Hassinger, Stephane Raymond, Dai Aoki, Valentin Taufour, Louis-Pierre Regnault and Jacques Flouquet. *Precise Study of the Resonance at* $\mathbf{Q}_0 = (1, 0, 0)$ *in* URu_2Si_2. Journal of the Physical Society of Japan, vol. 79, no. 6, page 064719, 2010. (Cited on pages 51 and 70.)

[Bourges 1996] P. Bourges, L. P. Regnault, Y. Sidis and C. Vettier. *Inelastic-neutron-scattering study of antiferromagnetic fluctuations in* $\mathrm{YBa_2Cu_3O_{6.97}}$. Phys. Rev. B, vol. 53, pages 876–885, Jan 1996. (Cited on page 17.)

[Bramwell 2001] Steven T. Bramwell and Michel J. P. Gingras. *Spin Ice State in Frustrated Magnetic Pyrochlore Materials*. Science, vol. 294, no. 5546, pages 1495–1501, 2001. (Cited on page 7.)

[Bramwell 2011] Steven T. Bramwell. Neutron scattering and highly frustrated magnetism, pages 45–78. Springer Berlin Heidelberg, Berlin, Heidelberg, 2011. (Cited on page 17.)

[Broholm 1987] C. Broholm, J. K. Kjems, W. J. L. Buyers, P. Matthews, T. T. M. Palstra, A. A. Menovsky and J. A. Mydosh. *Magnetic excitations and ordering in the heavy-electron superconductor* URu_2Si_2. Phys. Rev. Lett., vol. 58, pages 1467–1470, Apr 1987. (Cited on page 2.)

[Broholm 1991] C. Broholm, H. Lin, P. T. Matthews, T. E. Mason, W. J. L. Buyers, M. F. Collins, A. A. Menovsky, J. A. Mydosh and J. K. Kjems. *Magnetic excitations in the heavy-fermion superconductor* URu_2Si_2. Phys. Rev. B, vol. 43, pages 12809–12822, Jun 1991. (Cited on page 45.)

[Buhot 2014] J. Buhot, M.-A. Méasson, Y. Gallais, M. Cazayous, A. Sacuto, G. Lapertot and D. Aoki. *Symmetry of the Excitations in the Hidden Order State of* URu_2Si_2. Phys. Rev. Lett., vol. 113, page 266405, Dec 2014. (Cited on pages 4, 26, 47, 48, 65 and 68.)

[Buhot 2015] Jonathan Buhot. *Hidden orders and magnetism studied by Raman spectroscopy under extreme conditions*. Theses, Université Paris Diderot-Paris 7 Sorbonne Paris Cité, April 2015. (Cited on pages 26 and 27.)

[Buhrandt 2014] S. Buhrandt and L. Fritz. *Spin-liquid phase and order by disorder of classical Heisenberg spins on the swedenborgite lattice*. prb, vol. 90, no. 2, page 020403, July 2014. (Cited on pages 12 and 36.)

[Castro 2006] Eduardo V. Castro, N. M. R. Peres, K. S. D. Beach and Anders W. Sandvik. *Site dilution of quantum spins in the honeycomb lattice*. Phys. Rev. B, vol. 73, page 054422, Feb 2006. (Cited on page 10.)

[Chandra 1988] P. Chandra and B. Doucot. *Possible spin-liquid state at large S for the frustrated square Heisenberg lattice*. Phys. Rev. B, vol. 38, pages 9335–9338, Nov 1988. (Cited on pages 7, 10, 12, 13, 38 and 39.)

[Chandra 1990] P. Chandra, P. Coleman and A. I. Larkin. *Ising transition in frustrated Heisenberg models*. Phys. Rev. Lett., vol. 64, pages 88–91, Jan 1990. (Cited on page 13.)

[Chandra 2013] P. Chandra, P. Coleman and R. Flint. *Hastatic order in the heavy-fermion compound URu2Si2*. Nature, vol. 493, pages 0028–0836, 01 2013. (Cited on pages 3 and 65.)

[Chubukov 1984] A V Chubukov. *On the quantum effects in helimagnets*. Journal of Physics C: Solid State Physics, vol. 17, no. 36, page L991, 1984. (Cited on page 32.)

[Chubukov 1994] A V Chubukov, S Sachdev and T Senthil. *Large-S expansion for quantum antiferromagnets on a triangular lattice*. Journal of Physics: Condensed Matter, vol. 6, no. 42, page 8891, 1994. (Cited on pages 11 and 32.)

[Cooper 1987] S. L. Cooper, M. V. Klein, M. B. Maple and M. S. Torikachvili. *Magnetic excitations and phonon anomalies in U$\mathrm{Ru_2Si_2}$*. Phys. Rev. B, vol. 36, pages 5743–5746, Oct 1987. (Cited on page 26.)

[Custers 2003] J. Custers, P. Gegenwart, H. Wilhelm, K. Neumaier, Y. Tokiwa, O. Trovarelli, C. Geibel, F. Steglich, C. Pepin and P. Coleman. *The break-up of heavy electrons at a quantum critical point*. Nature, vol. 424, no. number, pages 524– 527, July 2003. (Cited on page 1.)

[Dagotto 1988] Elbio Dagotto, Eduardo Fradkin and Adriana Moreo. *SU(2) gauge invariance and order parameters in strongly coupled electronic systems*. Phys. Rev. B, vol. 38, pages 2926–2929, Aug 1988. (Cited on page 15.)

[Danu 2016] Bimla Danu, Gautam Nambiar and R. Ganesh. *Extended degeneracy and order by disorder in the square lattice $J_1 - J_2 - J_3$ model*. Phys. Rev. B, vol. 94, page 094438, Sep 2016. (Cited on page 13.)

[Das 2012] Tanmoy Das. *Spin-orbit density wave induced hidden topological order in URu2Si2*. Scientific Reports, vol. 2, no. 596, pages 1–5, 2012. (Cited on page 47.)

[Das 2013] P Das, R E Baumbach, K Huang, M B Maple, Y Zhao, JÂ S Helton, J W Lynn, E D Bauer and M Janoschek. *Absence of a static in-plane magnetic moment in the hidden-order phase of URu_2Si_2*. New Journal of Physics, vol. 15, no. 5, page 053031, 2013. (Cited on page 66.)

[Das 2014] Tanmoy Das. *Spin-orbit density wave: a new phase of matter applicable to the hidden order state of URu2Si2*. Philosophical Magazine, vol. 94, no. 32-33, pages 3838–3862, 2014. (Cited on pages 47, 49 and 69.)

[de Oliveira 1991] Mário J. de Oliveira. *Phase diagram of the spin-1/2 Heisenberg antiferromagnet on a square lattice with nearest- and next-nearest-neighbor couplings*. Phys. Rev. B, vol. 43, pages 6181–6183, Mar 1991. (Cited on page 10.)

[Devereaux 1997] Thomas Peter Devereaux and Arno Paul Kampf. *Raman Scattering in Cuprate Superconductors*. International Journal of Modern Physics B, vol. 11, no. 18, pages 2093–2118, 1997. (Cited on pages 19 and 25.)

[Devereaux 1999] T. P. Devereaux and A. P. Kampf. *Theory of electronic Raman scattering in nearly antiferromagnetic Fermi liquids*. Phys. Rev. B, vol. 59, pages 6411–6420, Mar 1999. (Cited on page 25.)

[Devereaux 2007] Thomas P. Devereaux and Rudi Hackl. *Inelastic light scattering from correlated electrons*. Rev. Mod. Phys., vol. 79, pages 175 –233, Jan 2007. (Cited on pages 18, 19, 24, 48, 53 and 54.)

[Diep 1989] H. T. Diep. *Low-temperature properties of quantum Heisenberg helimagnets*. Phys. Rev. B, vol. 40, pages 741–744, Jul 1989. (Cited on page 32.)

[Duyne 2003] R.P. Van Duyne and C.L. Haynes. *Raman Spectroscopy*. In Robert A. Meyers, editor, Encyclopedia of Physical Science and Technology (Third Edition), pages 845 – 866. Academic Press, New York, third edition édition, 2003. (Cited on page 18.)

[Elgazzar 2009] S. Elgazzar, J. Rusz, M. Amft, P. M. Oppeneer and J. A. Mydosh. *Hidden order in URu2Si2 originates from Fermi surface gapping induced by dynamic symmetry breaking*. Nature Materials, vol. 8, pages 337–341, Apr 2009. (Cited on pages 4 and 48.)

[Farias 2016] Carlene Farias, Christopher Thomas, Catherine Pépin, Alvaro Ferraz, Claudine Lacroix and Sébastien Burdin. *Spin liquid versus long-range magnetic order in the frustrated body-centered-tetragonal lattice*. Phys. Rev. B, vol. 94, page 134420, Oct 2016. (Cited on pages 29 and 40.)

[Farnell 2016] D. J. J. Farnell, O. Götze and J. Richter. *Ground-state ordering of the J_1-J_2 model on the simple cubic and body-centered cubic lattices*. Phys. Rev. B, vol. 93, page 235123, Jun 2016. (Cited on page 45.)

[Fazekas 1974] P. Fazekas and P. W. Anderson. *On the ground state properties of the anisotropic triangular antiferromagnet*. Philosophical Magazine, vol. 30, no. 2, pages 423–440, 1974. (Cited on pages 7, 40 and 44.)

[Fazekas 1999] Patrik Fazekas. Lecture notes on electron correlation and magnetism. Mod. Condensed Matter Phys. World Scientific, Singapore, 1999. (Cited on page 8.)

[Foulkes 2001] W. M. C. Foulkes, L. Mitas, R. J. Needs and G. Rajagopal. *Quantum Monte Carlo simulations of solids*. Rev. Mod. Phys., vol. 73, pages 33–83, Jan 2001. (Cited on page 14.)

[Freericks 2001] J. K. Freericks and T. P. Devereaux. *Raman scattering through a metal-insulator transition*. Phys. Rev. B, vol. 64, page 125110, Sep 2001. (Cited on page 25.)

[Friedemann 2009] S. Friedemann, T. Westerkamp, M. Brando, N. Oeschler, S. Wirth, P. Gegenwart, C. Krellner, C. Geibel and F. Steglich. *Detaching the antiferromagnetic quantum critical point from the Fermi-surface reconstruction in $YbRh_2Si_2$*. Nat Phys, vol. 5, pages 465– 469, July 2009. (Cited on page 1.)

[Garmire 2013] E. Garmire, M. Cardona, J.M. Hammer, H. Kogelnik, T. Tamir and F. Zernike. Light scattering in solids 1. Topics in Applied Physics. Springer Berlin Heidelberg, 2013. (Cited on page 19.)

[Gingras 2009] M. J. P. Gingras. *Spin Ice*. ArXiv e-prints, pages 1–33, March 2009. (Cited on page 7.)

[Goldstone 1962] J. Goldstone, A. Salam and S. Weinberg. *Broken Symmetries*. Physical Review, vol. 127, pages 965–970, August 1962. (Cited on page 11.)

[Han 2012] Tian-Heng Han, Joel S. Helton, Shaoyan Chu, Daniel G. Nocera, Jose A. Rodriguez-Rivera, Collin Broholm and Young S. Lee. *Fractionalized excitations in the spin-liquid state of a kagome-lattice antiferromagnet*. Nature, vol. 492, pages 406–410, Dec 2012. (Cited on page 7.)

[Harima 2010] Hisatomo Harima, Kazumasa Miyake and Jacques Flouquet. *Why the Hidden Order in URu_2Si_2 Is Still Hidden-One Simple Answer*. Journal of the Physical Society of Japan, vol. 79, no. 3, page 033705, 2010. (Cited on pages 3, 4, 47, 48, 49, 66, 68 and 69.)

[Hassinger 2008] E. Hassinger, G. Knebel, K. Izawa, P. Lejay, B. Salce and J. Flouquet. *Temperature-pressure phase diagram of URu_2Si_2 from resistivity measurements and ac calorimetry: Hidden order and Fermi-surface nesting*. Phys. Rev. B, vol. 77, page 115117, Mar 2008. (Cited on page 2.)

[Hassinger 2010] E. Hassinger, G. Knebel, T. D. Matsuda, D. Aoki, V. Taufour and J. Flouquet. *Similarity of the Fermi Surface in the Hidden Order State and in the Antiferromag-*

netic State of URu_2Si_2. Phys. Rev. Lett., vol. 105, page 216409, Nov 2010. (Cited on pages 4 and 48.)

[Haule 2009] Kristjan Haule and Gabriel Kotliar. *Arrested Kondo effect and hidden order in* URu_2Si_2. Nat Phys, vol. 5, pages 796–799, Nov 2009. (Cited on pages 3 and 65.)

[Hayes 2012] W. Hayes and R. Loudon. Scattering of light by crystals. Dover Books on Physics. Dover Publications, 2012. (Cited on pages 23 and 24.)

[He 2015] Yin-Chen He, Subhro Bhattacharjee, Frank Pollmann and R. Moessner. *Kagome Chiral Spin Liquid as a Gauged* $U(1)$ *Symmetry Protected Topological Phase*. Phys. Rev. Lett., vol. 115, page 267209, Dec 2015. (Cited on page 16.)

[Heisenberg 1928] W. Heisenberg. *Zur Theorie des Ferromagnetismus*. Zeitschrift für Physik, vol. 49, no. 9, pages 619–636, 1928. (Cited on page 8.)

[Helton 2007] J. S. Helton, K. Matan, M. P. Shores, E. A. Nytko, B. M. Bartlett, Y. Yoshida, Y. Takano, A. Suslov, Y. Qiu, J.-H. Chung, D. G. Nocera and Y. S. Lee. *Spin Dynamics of the Spin-*$1/2$ *Kagome Lattice Antiferromagnet* $ZnCu_3(OH)_6Cl_2$. Phys. Rev. Lett., vol. 98, page 107204, Mar 2007. (Cited on page 7.)

[Holstein 1940] T. Holstein and H. Primakoff. *Field Dependence of the Intrinsic Domain Magnetization of a Ferromagnet*. Phys. Rev., vol. 58, pages 1098–1113, Dec 1940. (Cited on page 11.)

[Hutchings 1972] M. T. Hutchings and E. J. Samuelsen. *Measurement of Spin-Wave Dispersion in NiO by Inelastic Neutron Scattering and Its Relation to Magnetic Properties*. Phys. Rev. B, vol. 6, pages 3447–3461, Nov 1972. (Cited on page 17.)

[Igarashi 2005] Jun-ichi Igarashi and Tatsuya Nagao. *1/S-expansion study of spin waves in a two-dimensional Heisenberg antiferromagnet*. Phys. Rev. B, vol. 72, page 014403, Jul 2005. (Cited on page 40.)

[Iqbal 2012] Y. Iqbal, F. Becca and D. Poilblanc. *Valence-bond crystals in the kagomé spin-1/2 Heisenberg antiferromagnet: a symmetry classification and projected wave function study*. New Journal of Physics, vol. 14, no. 11, page 115031, November 2012. (Cited on page 7.)

[Khveshchenko 1994] D. V. Khveshchenko and P. B. Wiegmann. *Raman scattering and anomalous current algebra in Mott insulators*. Phys. Rev. Lett., vol. 73, pages 500–503, Jul 1994. (Cited on pages 16, 54 and 66.)

[Kitaev 2006] Alexei Kitaev. *Anyons in an exactly solved model and beyond*. Annals of Physics, vol. 321, no. 1, pages 2 – 111, 2006. January Special Issue. (Cited on page 50.)

[Kubo 1952] Ryogo Kubo. *The Spin-Wave Theory of Antiferromagnetics*. Phys. Rev., vol. 87, pages 568–580, Aug 1952. (Cited on page 10.)

[Kung 2015] H.-H. Kung, R. E. Baumbach, E. D. Bauer, V. K. Thorsmølle, W.-L. Zhang, K. Haule, J. A. Mydosh and G. Blumberg. *Chirality density wave of the "hidden order" phase in URu2Si2*. Science, pages 1339–1342, 2015. (Cited on pages 27 and 65.)

[Kusunose 2011] Hiroaki Kusunose and Hisatomo Harima. *On the Hidden Order in URu2Si2 - Antiferro Hexadecapole Order and Its Consequences*. Journal of the Physical Society of Japan, vol. 80, no. 8, page 084702, 2011. (Cited on page 3.)

[Kusunose 2012] Hiroaki Kusunose. *Magnetic Exciton Mediated Superconductivity in the Hidden-Order Phase of URu2Si2*. Journal of the Physical Society of Japan, vol. 81, no. 2, page 023704, 2012. (Cited on page 45.)

[Lacroix 2011] C. Lacroix, P. Mendels and F. Mila. Introduction to frustrated magnetism: Materials, experiments, theory. Springer Series in Solid-State Sciences. Springer Berlin Heidelberg, 2011. (Cited on pages 7 and 43.)

[Lampakis 2006] D. Lampakis, D. Palles, E. Liarokapis and J.A. Mydosh. *Raman study of the heavy fermion system URu2Si2 at low temperatures and high hydrostatic pressures*. Physica B: Condensed Matter, vol. 378-380, pages 578–580, 2006. Proceedings of the International Conference on Strongly Correlated Electron SystemsSCES 2005Proceedings of the International Conference on Strongly Correlated Electron Systems. (Cited on page 26.)

[Laubach 2016] Manuel Laubach, Darshan G. Joshi, Johannes Reuther, Ronny Thomale, Matthias Vojta and Stephan Rachel. *Quantum disordered insulating phase in the frustrated cubic-lattice Hubbard model*. Phys. Rev. B, vol. 93, page 041106, Jan 2016. (Cited on page 45.)

[Laughlin 1988] R. B. Laughlin. *Superconducting Ground State of Noninteracting Particles Obeying Fractional Statistics*. Phys. Rev. Lett., vol. 60, pages 2677–2680, Jun 1988. (Cited on page 54.)

[Lee 2000] S.-H. Lee, C. Broholm, T. H. Kim, W. Ratcliff and S-W. Cheong. *Local Spin Resonance and Spin-Peierls-like Phase Transition in a Geometrically Frustrated Antiferromagnet*. Phys. Rev. Lett., vol. 84, pages 3718–3721, Apr 2000. (Cited on page 17.)

[Liu 1970] S. H. Liu. *Inelastic Neutron Scattering from Itinerant Electron Antiferromagnets: Theory*. Phys. Rev. B, vol. 2, pages 2664–2674, Oct 1970. (Cited on page 17.)

[Liu 1993] Ran Liu, D. Salamon, M. V. Klein, S. L. Cooper, W. C. Lee, S-W. Cheong and D. M. Ginsberg. *Novel Raman-active electronic excitations near the charge-transfer gap in insulating cuprates*. Phys. Rev. Lett., vol. 71, pages 3709–3712, Nov 1993. (Cited on pages 54 and 66.)

[Lobo 2015] R. P. S. M. Lobo, J. Buhot, M. A. Méasson, D. Aoki, G. Lapertot, P. Lejay and C. C. Homes. *Optical conductivity of* $\mathrm{URu_2Si_2}$ *in the Kondo liquid and hidden-order phases*. Phys. Rev. B, vol. 92, page 045129, Jul 2015. (Cited on page 70.)

[Mahan 2000] Gerald D. Mahan. Many particle physics. Physics of Solids and Liquids. Springer, 3nd édition, 2000. (Cited on page 85.)

[Manousakis 1991] Efstratios Manousakis. *The spin-*$\frac{1}{2}$ *Heisenberg antiferromagnet on a square lattice and its application to the cuprous oxides*. Rev. Mod. Phys., vol. 63, pages 1–62, Jan 1991. (Cited on pages 9 and 11.)

[Maple 1986] M. B. Maple, J. W. Chen, Y. Dalichaouch, T. Kohara, C. Rossel, M. S. Torikachvili, M. W. McElfresh and J. D. Thompson. *Partially gapped Fermi surface in the heavy-electron superconductor* $\mathrm{URu_2Si_2}$. Phys. Rev. Lett., vol. 56, pages 185–188, Jan 1986. (Cited on pages 1, 2, 3, 4 and 48.)

[Marston 1989] J. Brad Marston and Ian Affleck. *Large-n limit of the Hubbard-Heisenberg model*. Phys. Rev. B, vol. 39, pages 11538–11558, Jun 1989. (Cited on pages 15 and 77.)

[Mathur 1998] N. D. Mathur, F. M. Grosche, S. R. Julian, I. R. Walker, D. M. Freye, R. K. W. Haselwimmer and G. G. Lonzarich. *Magnetically mediated superconductivity in heavy fermion compounds*. Nature, vol. 394, pages 39–43, july 1998. (Cited on page 2.)

[Mirebeau 2014] Isabelle Mirebeau and Sylvain Petit. *Magnetic frustration probed by inelastic neutron scattering: Recent examples*. Journal of Magnetism and Magnetic Materials, vol. 350, pages 209 – 216, 2014. (Cited on page 17.)

[Moessner 2011] Roderich Moessner and Kumar S. Raman. Quantum dimer models, chapter 17, pages 437–479. Springer Series in Solid-State Sciences. Springer Berlin Heidelberg, 2011. (Cited on page 14.)

[Montiel 2014] X. Montiel, S. Burdin, C. Pépin and A. Ferraz. *Modulated spin-liquid and magnetic order from a Kondo-Heisenberg model applied to* URu_2Si_2. Phys. Rev. B, vol. 90, page 045125, Jul 2014. (Cited on page 70.)

[Mucciolo 2004] Eduardo R. Mucciolo, A. H. Castro Neto and Claudio Chamon. *Excitations and quantum fluctuations in site-diluted two-dimensional antiferromagnets*. Phys. Rev. B, vol. 69, page 214424, Jun 2004. (Cited on page 10.)

[Mydosh 2011] J. A. Mydosh and P. M. Oppeneer. *Colloquium : Hidden order, superconductivity, and magnetism: The unsolved case of* URu_2Si_2. Rev. Mod. Phys., vol. 83, pages 1301–1322, Nov 2011. (Cited on pages 1 and 45.)

[Nambu 1960] Yoichiro Nambu. *Quasi-Particles and Gauge Invariance in the Theory of Superconductivity*. Phys. Rev., vol. 117, pages 648–663, Feb 1960. (Cited on page 11.)

[Nolting 2009] W. Nolting and A. Ramakanth. Quantum theory of magnetism. Springer Berlin Heidelberg, 2009. (Cited on page 30.)

[Oguchi 1960] Takehiko Oguchi. *Theory of Spin-Wave Interactions in Ferro- and Antiferromagnetism*. Phys. Rev., vol. 117, pages 117–123, Jan 1960. (Cited on page 10.)

[Oguchi 1990] Takehiko Oguchi and Hidetsugu Kitatani. *Spin Wave Theory for a Frustrated Antiferromagnetic Heisenberg Model on a Square Lattice*. Journal of the Physical Society of Japan, vol. 59, no. 9, pages 3322–3330, 1990. (Cited on pages 10 and 11.)

[Ohara 1989] Keiichi Ohara and Kei Yosida. *A Modified Spin-Wave Theory of the Square-Lattice Antiferromagnet*. Journal of the Physical Society of Japan, vol. 58, no. 7, pages 2521–2530, 1989. (Cited on page 12.)

[Okazaki 2011] R. Okazaki, T. Shibauchi, H. J. Shi, Y. Haga, T. D. Matsuda, E. Yamamoto, Y. Onuki, H. Ikeda and Y. Matsuda. *Rotational Symmetry Breaking in the Hidden-Order Phase of URu2Si2*. Science, vol. 331, no. 6016, pages 439–442, 2011. (Cited on page 3.)

[Oppeneer 2011] P. M. Oppeneer, S. Elgazzar, J. Rusz, Q. Feng, T. Durakiewicz and J. A. Mydosh. *Spin and orbital hybridization at specifically nested Fermi surfaces in* URu_2Si_2. Phys. Rev. B, vol. 84, page 241102, Dec 2011. (Cited on pages 47, 49 and 60.)

[Palstra 1985] T. T. M. Palstra, A. A. Menovsky, J. van den Berg, A. J. Dirkmaat, P. H. Kes, G. J. Nieuwenhuys and J. A. Mydosh. *Superconducting and Magnetic Transitions in the Heavy-Fermion System U*$\mathrm{Ru_2Si_2}$. Phys. Rev. Lett., vol. 55, pages 2727–2730, Dec 1985. (Cited on pages 1, 2, 3 and 45.)

[Pépin 2011] C. Pépin, M. R. Norman, S. Burdin and A. Ferraz. *Modulated Spin Liquid: A New Paradigm for URu$_2$Si$_2$*. Phys. Rev. Lett., vol. 106, page 106601, Mar 2011. (Cited on pages 3, 15, 16, 29, 41 and 68.)

[Perkins 2013] Natalia B. Perkins, Gia-Wei Chern and Wolfram Brenig. *Raman scattering in a Heisenberg $S = \frac{1}{2}$ antiferromagnet on the anisotropic triangular lattice*. Phys. Rev. B, vol. 87, page 174423, May 2013. (Cited on page 25.)

[Ramirez 1994] A. P. Ramirez. *Strongly Geometrically Frustrated Magnets*. Annual Review of Materials Science, vol. 24, no. 1, pages 453–480, 1994. (Cited on page 7.)

[Rastelli 1987] E Rastelli and A Tassi. *Order produced by quantum disorder in the Heisenberg rhombohedral antiferromagnet*. Journal of Physics C: Solid State Physics, vol. 20, no. 15, page L303, 1987. (Cited on pages 7, 12, 13 and 36.)

[Rastelli 1989] E Rastelli, S Sedazzari and A Tassi. *Long-range order in tetragonal antiferromagnets supported by quantum fluctuations*. Journal of Physics: Condensed Matter, vol. 1, no. 28, page 4735, 1989. (Cited on page 13.)

[Rastelli 1990] E Rastelli, S Sedazzari and A Tassi. *Frustration and zero-point motion in Heisenberg body-centred tetragonal antiferromagnets*. Journal of Physics: Condensed Matter, vol. 2, no. 45, page 8935, 1990. (Cited on page 7.)

[Ren 2014] Yong-Zhi Ren, Ning-Hua Tong and Xin-Cheng Xie. *Cluster mean-field theory study of J_1-J_2 Heisenberg model on a square lattice*. Journal of Physics: Condensed Matter, vol. 26, no. 11, page 115601, 2014. (Cited on page 10.)

[Riseborough 2012] Peter S. Riseborough, B. Coqblin and S. G. Magalhães. *Phase transition arising from the underscreened Anderson lattice model: A candidate concept for explaining hidden order in URu$_2$Si$_2$*. Phys. Rev. B, vol. 85, page 165116, Apr 2012. (Cited on page 3.)

[Saitoh 2005] Satoru Saitoh, Shigeru Takagi, Makoto Yokoyama and Hiroshi Amitsuka. *101Ru NQR and Hidden Order in URu2Si2*. Journal of the Physical Society of Japan, vol. 74, no. 8, pages 2209–2213, 2005. (Cited on page 4.)

[Santander-Syro 2009] Andres F. Santander-Syro, Markus Klein, Florin L. Boariu, Andreas Nuber, Pascal Lejay and Friedrich Reinert. *Fermi-surface instability at the /'hidden-order/' transition of URu_2Si_2*. Nature Physics, vol. 5, pages 637– 641, Feb 2009. (Cited on pages 65 and 70.)

[Santos 2003] Raimundo R. dos Santos. *Introduction to quantum Monte Carlo simulations for fermionic systems*. Brazilian Journal of Physics, vol. 33, pages 36 – 54, 03 2003. (Cited on page 14.)

[Schollwöck 2005] U. Schollwöck. *The density-matrix renormalization group*. Rev. Mod. Phys., vol. 77, pages 259–315, Apr 2005. (Cited on page 43.)

[Shastry 1990] B. Sriram Shastry and Boris I. Shraiman. *Theory of Raman Scattering in Mott-Hubbard Systems*. Phys. Rev. Lett., vol. 65, pages 1068–1071, Aug 1990. (Cited on page 24.)

[Shender 1982] E.F. Shender. *Antiferromagnetic garnets with fluctuationally interacting sublattices*. Sovietic Phys, vol. 56, no. 1, page 178, July 1982. (Cited on page 12.)

[Sinkovicz 2016] Péter Sinkovicz, Gergely Szirmai and Karlo Penc. *Order by disorder in a four-flavor Mott insulator on the fcc lattice*. Phys. Rev. B, vol. 93, page 075137, Feb 2016. (Cited on page 13.)

[Sokoloff 1969] J. B. Sokoloff. *Theory of Inelastic Neutron Scattering in the Itinerant Model Antiferromagnetic Metals. I.* Phys. Rev., vol. 185, pages 770–782, Sep 1969. (Cited on page 17.)

[Starykh 2015] Oleg A Starykh. *Unusual ordered phases of highly frustrated magnets: a review*. Reports on Progress in Physics, vol. 78, no. 5, page 052502, 2015. (Cited on page 7.)

[Steglich 1979] F. Steglich, J. Aarts, C. D. Bredl, W. Lieke, D. Meschede, W. Franz and H. Schäfer. *Superconductivity in the Presence of Strong Pauli Paramagnetism: $CeCu_2Si_2$*. Phys. Rev. Lett., vol. 43, pages 1892–1896, Dec 1979. (Cited on page 2.)

[Stewart 1984] G. R. Stewart. *Heavy-fermion systems*. Rev. Mod. Phys., vol. 56, pages 755–787, Oct 1984. (Cited on page 1.)

[Sugiyama 1990] Kiyohiro Sugiyama, Hiroyuki Fuke, Koichi Kindo, Kenji Shimohata, Alois A. Menovsky, John A. Mydosh and Muneyuki Date. *Field-Induced Destruction of Heavy Fermion State in URu2Si2*. Journal of the Physical Society of Japan, vol. 59, no. 9, pages 3331–3339, 1990. (Cited on page 31.)

[Thomas 2013] Christopher Thomas, Sébastien Burdin, Catherine Pépin and Alvaro Ferraz. *Three-dimensional modulated spin liquid model applied to URu_2Si_2*. Phys. Rev. B, vol. 87, page 014422, Jan 2013. (Cited on pages 3, 29, 41, 45, 57 and 68.)

[Tonegawa 2012] S. Tonegawa, K. Hashimoto, K. Ikada, Y.-H. Lin, H. Shishido, Y. Haga, T. D. Matsuda, E. Yamamoto, Y. Onuki, H. Ikeda, Y. Matsuda and T. Shibauchi. *Cyclotron Resonance in the Hidden-Order Phase of* $\mathrm{URu_2Si_2}$. Phys. Rev. Lett., vol. 109, page 036401, Jul 2012. (Cited on pages 4 and 48.)

[Troyer 2005] Matthias Troyer and Uwe-Jens Wiese. *Computational Complexity and Fundamental Limitations to Fermionic Quantum Monte Carlo Simulations*. Phys. Rev. Lett., vol. 94, page 170201, May 2005. (Cited on page 14.)

[Valenzuela 2013] B. Valenzuela, M. J. Calderón, G. León and E. Bascones. *Optical conductivity and Raman scattering of iron superconductors*. Phys. Rev. B, vol. 87, page 075136, Feb 2013. (Cited on page 53.)

[Ványolos 2005] András Ványolos and Attila Virosztek. *Electronic Raman scattering in unconventional density waves*. Phys. Rev. B, vol. 72, page 115119, Sep 2005. (Cited on page 51.)

[Villain 1980] J. Villain, R. Bidaux, J.-P. Carton and R. Conte. *Order as an effect of disorder*. Journal Phys. France, vol. 41, no. 11, pages 1263–1272, novembre 1980. (Cited on page 12.)

[Villaume 2008] A. Villaume, F. Bourdarot, E. Hassinger, S. Raymond, V. Taufour, D. Aoki and J. Flouquet. *Signature of hidden order in heavy fermion superconductor URu_2Si_2: Resonance at the wave vector $Q_0 = (1, 0, 0)$*. Phys. Rev. B, vol. 78, page 012504, Jul 2008. (Cited on pages 2, 4, 48 and 65.)

[Wen 1989] X. G. Wen, Frank Wilczek and A. Zee. *Chiral spin states and superconductivity*. Phys. Rev. B, vol. 39, pages 11413–11423, Jun 1989. (Cited on pages 16, 57 and 66.)

[Wen 1996] Xiao-Gang Wen and Patrick A. Lee. *Theory of Underdoped Cuprates*. Phys. Rev. Lett., vol. 76, pages 503–506, Jan 1996. (Cited on pages 15 and 40.)

[Wen 2002] Xiao-Gang Wen. *Quantum orders and symmetric spin liquids*. Phys. Rev. B, vol. 65, page 165113, Apr 2002. (Cited on pages 15 and 66.)

[Wen 2004] X.G. Wen. Quantum field theory of many-body systems: From the origin of sound to an origin of light and electrons. Oxford Graduate Texts. OUP Oxford, 2004. (Cited on page 16.)

[Wessel 2005] Stefan Wessel and Igor Milat. *Quantum fluctuations and excitations in antiferromagnetic quasicrystals*. Phys. Rev. B, vol. 71, page 104427, Mar 2005. (Cited on page 10.)

[Xu 1991] J. H. Xu and C. S. Ting. *Modified spin-wave theory of low-dimensional quantum spiral magnets*. Phys. Rev. B, vol. 43, pages 6177–6180, Mar 1991. (Cited on page 10.)

[Yang 2014] Y.-X. Yang, Y. Gallais, F. Rullier-Albenque, M.-A. Méasson, M. Cazayous, A. Sacuto, J. Shi, D. Colson and A. Forget. *Temperature-induced change in the Fermi surface topology in the spin density wave phase of* $Sr(Fe_{1-x}Co_x)_2As_2$. Phys. Rev. B, vol. 89, page 125130, Mar 2014. (Cited on pages 49, 51 and 64.)

[Zhu 2008] Jian-Xin Zhu, I. Martin and A. R. Bishop. *Kondo Stripes in an Anderson-Heisenberg Model of Heavy Fermion Systems*. Phys. Rev. Lett., vol. 100, page 236403, Jun 2008. (Cited on page 69.)